[redacted]

D-3

UNCLASSIFIED

LA-5238

~~AFATL-TR-79-61~~

C. 3

Evaluation of Depleted-Uranium Alloys for Use in Armor-Piercing Projectiles (U)

los alamos
scientific laboratory
of the University of California
LOS ALAMOS, NEW MEXICO 87544

[redacted]

UNCLASSIFIED

[redacted]

1143-1340

[redacted]

Classified by J. L. Watts,
ISD-6 Staff Member.

[redacted]

[redacted]

[redacted]

LA-5238
AFATL-TR-73-61
SPECIAL DISTRIBUTION
ISSUED: June 1973

UNCLASSIFIED

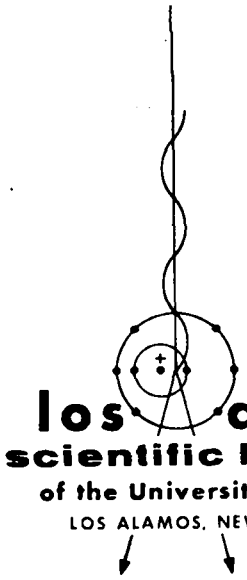

los alamos
scientific laboratory
of the University of California
LOS ALAMOS, NEW MEXICO 87544

Evaluation of Depleted-Uranium Alloys for Use in Armor-Piercing Projectiles (U)

by

John W. Hopson
Lawrence W. Hantel
Donald J. Sandstrom

This work supported by Air Force Armament Laboratory, Air Force Systems Command, Eglin Air Force Base, Florida.

[redacted]

UNCLASSIFIED

[redacted]

CONTENTS

[redacted]

EVALUATION OF DEPLETED-URANIUM ALLOYS FOR USE IN ARMOR-PIERCING PROJECTILES

by

John W. Hopson, Lawrence W. Hantel, and Donald J. Sandstrom

ABSTRACT (U)

Several depleted-uranium alloys were evaluated for use as the penetrator core of armor-piercing projectiles. From a large number of previously studied alloys, four basic systems were chosen for detailed evaluation: U-0.75 wt% Ti, U-2 wt% Mo, U-4.5 wt% Nb, and U-2 wt% Nb-1 wt% Ti. Various heat treatments were tested, and the composition of the U-Ti system was varied, producing a total of 16 materials. Each material was characterized by complete metallographic analysis as well as normal corrosion tests, static mechanical tests, plane-wave impact tests, and sound-velocity measurements. Protection ballistic limits were determined at 0, 30, and 60° obliquity against rolled homogeneous, steel armor plate using .50-cal and 30-mm projectiles containing AP cores fabricated from candidate alloys. The interaction between the uranium alloy penetrator and the armor was studied using high-speed photography, flash radiography, and post-impact metallography of penetrators and armor. From these data, it was concluded that within a certain hardness range most uranium alloys are ballistically equivalent. On the basis of estimated manufacturing cost, reasonable corrosion resistance, and ballistic performance, the U-0.75 wt% Ti alloy system was recommended as the best penetrator material.

I. INTRODUCTION

The Armed Services have considered using depleted uranium in the penetrator core of armor-piercing (AP) projectiles for many years. Depleted uranium is an attractive material for many reasons. Its density is more than twice that of steel, making it easy to produce a penetrator with high sectional density which delivers its momentum and kinetic energy to a small volume of the target armor. In addition, uranium is highly pyrophoric. Impact velocities as low as 100 ft/sec against steel targets are known to produce burning fragments that can ignite flammables, such as gasoline, diesel fuel, and propellants, producing severe secondary damage.[1] Depleted uranium is also readily available in the large quantities necessary to meet the Service's munitions requirements. Some 80,000 metric tons are currently available from AEC stockpile, and the continued yearly production rate is approximately 20,000 metric tons per year. In contrast, tungsten carbide and other tungsten alloys, the only high-density materials currently used in AP cores, must be obtained largely from sources outside the continent and, furthermore, are much more expensive than depleted uranium.

[redacted]

One disadvantage of depleted uranium as compared with other penetrator materials is that it is more reactive. This greater reactivity causes potential incompatibility with other projectile materials, and, during exposure to air, causes high corrosion rates. In addition, some uranium alloys are known to be susceptible to stress-corrosion cracking, to the point that cracks may result from the residual stresses induced by fabrication and heat treatment of parts. Any consideration of the use of uranium in actual munitions that must be stored for long periods must take these potential difficulties into account.

There are many alloys of uranium which, because of their much greater strength and hardness are more attractive penetrator materials than the pure metal. The quasi-static mechanical properties of these alloys have already been studied in considerable detail. However, selection of an alloy for optimum penetrator performance is made difficult by the following considerations. First, it is not clear that the results of low-strain-rate tests can be extrapolated to the very high strain rates associated with projectile impact. Second, the relationship among penetrator performance and the usual parameters useful in characterizing a structural material (for example, compressive strength, modulus, hardness, and ductility) is not well understood.

The project described in this report was designed to evaluate several depleted-uranium alloys specifically for use in AP cores. The intention was to arrive at an alloy that would provide maximum penetrability, be economical to produce in large quantities, and not pose a severe storage problem due to surface oxidation or cracking. The work was performed and funded under an agreement with the Air Force Armament Laboratory, Eglin Air Force Base, Florida. The objective of the project was to provide the Air Force an optimum alloy for use in a new 30-mm gun system now being developed.

The initial problem was to select, from the many alloys previously studied, a reasonable number of promising systems for thorough testing and evaluation. The four alloys chosen were uranium-titanium, with titanium contents ranging from 0.6 to 1.2 wt%; uranium-2 wt% molybdenum; uranium-4.5 wt% niobium; and a ternary alloy, uranium-2 wt% niobium-1 wt% titanium. These are certainly not the only alloys that are potentially good penetrator materials. However, these four systems can be heat-treated to have nearly the full range of mechanical properties possible with uranium alloys, and each has one or more additional features (for example, low cost, fabricability, corrosion resistance) that make it an attractive candidate.

Before the alloys were tested for penetration performance, the composition, microstructure, hardness, density, and elastic moduli of each were thoroughly characterized. In addition, a plane-wave impact test was used to determine the dynamic compressive and tensile strengths at high strain rates ($\sim 10^4$ to 10^5/sec). Early in the project, several different heat treatments were tried for each alloy, and the results of physical testing were used to select the most promising ones for ballistic evaluation. These data were also necessary for quality-control in the future production of the selected alloy, and we hoped to establish some correlation between these results and penetration performance. The metallurgy and mechanical properties of the candidate alloys are discussed in Sec. II. The casting and fabrication is described in detail in Appendix B.

Section III is concerned with the corrosion resistance of the candidate alloys. Several samples of each alloy, in the various heat-treated conditions, were subjected to a straightforward accelerated-corrosion test. This consisted of placing the samples in a 165°F, 75% relative-humidity, atmosphere for over 4 months. The rate of sample weight gain due to oxidation was used as a measure of susceptibility to general corrosion.

[redacted]

Although the Air Force intends to use the selected alloy in the core of 30-mm projectiles, most of the penetration performance tests for each alloy were performed with a scaled-down, .50-caliber projectile. The relatively low cost of the smaller projectile allowed us to fire many more test shots and thus more thoroughly evaluate each alloy. The size difference should not affect the relative performance, but we tested the two most promising alloys in full-scale projectiles to add confidence to this assumption. Penetration performance was determined by firing the test projectiles at sections of military-specification, rolled, homogeneous, steel armor plate. Ballistic limits for all of the alloys were obtained for both 0° and 60° angles of impact, and some of the full-scale tests were also conducted at 30° obliquity. The general results of the penetration tests are discussed in Sec. IV, and a complete presentation of the data is found in Appendix A.

In addition to determining ballistic limits, we studied the phenomenology of penetrator-armor interaction. In particular, we fired a number of shots using the PHERMEX flash x-ray facility to obtain high-speed radiographs of the penetration process. It was possible to resolve a 30-mm projectile core through several inches of armor and thus determine the core deformation at several stages of penetration. High-speed conventional photographs of projectile impact and post-impact metallography of the test armor and core fragments were also useful in understanding the penetration mechanism. The results of these studies are presented in Sec. V.

II. PHYSICAL METALLURGY AND SELECTION OF CANDIDATE ALLOYS

A. Alloy Selection

Determination of an optimum penetrator alloy is a monumental task because there are an almost infinite number of alloying combinations that might provide good penetrator performance. Several groups both within and outside of the United States have studied uranium alloys extensively. References 2-23 constitute a bibliography of the work reviewed for the purpose of selecting candidate alloys.

The material properties that appear to contribute to the performance of armor-piercing penetrators in general are: hardness, density, modulus of elasticity, and dynamic compressive and tensile strength. For alloy selection, the Rockwell 'C' hardness has been designated as having to exceed 45, the density should be greater than 18 g/cm^3, the modulus of elasticity should be greater than 20 x 10^6 psi, and there should be some dynamic ductility to prevent premature shattering of the penetrator. The pyrophoricity of the uranium alloys also is extremely important for this application. However, all of the uranium alloys are pyrophoric at moderate impact velocities against steel armor, and differences among alloys may be too subtle to distinguish. Since the actual penetrators may be subjected to a variety of storage environments in the field, corrosion resistance was also a criterion in the initial alloy selection.

The choice of alloys to evaluate was largely based on past experience with structural uranium alloys at Los Alamos Scientific Laboratory (LASL). The LASL Materials Technology Group has over 25 years of experience in melting, casting, and fabricating uranium and uranium alloys. References 24-27 are a partial bibliography of this work. Our experience with these alloys has led us to believe that alloy simplicity is very important from the standpoint of manufacture and economy. Use of polynary alloys of uranium does not seem entirely justifiable on the basis of cost and increased complexity of manufacture. Any possible advantage these more complex alloys might have in penetration performance must be carefully balanced against the increased processing costs. Therefore, our choice of alloys for this

program was limited to simple binary systems in all but one case.

The following alloy systems have been evaluated:

1. uranium-titanium over the range of titanium content from ~ 0.6 to 1.2 wt%.
2. uranium-2 wt% molybdenum.
3. uranium-4.5 wt% niobium.
4. uranium-2 wt% niobium-1 wt% titanium.

All these alloys can be heat treated to have the required mechanical properties, except the U-4.5 wt% Nb system which is slightly low in density and elastic modulus. We included this alloy in the program because of its excellent corrosion resistance. In this section, each specific alloy system is treated separately, but some of the data are collected so that certain properties comparisons can be made readily.

B. Uranium-Titanium Alloys

1. General Characteristics. The binary alloy system of uranium-titanium has been the subject of considerable study at LASL for a number of years. This particular alloy is of interest because it can be age hardened by simple heat treatments. It is typical of binary alloys that have complete solute solubility in the high-temperature, body-centered-cubic (bcc) gamma phase. Figure 1 is a constitution diagram of the U-Ti alloy system prepared by Battelle Memorial Institute.[28] This diagram shows that, at the composition studied, the alloy is in the single-phase gamma field at temperatures above 800°C. Quenching from these temperatures produces a two-phase structure of uranium plus δ U_2Ti. Earlier work at LASL demonstrated the effect of titanium content on the hardness of both quenched and aged uranium-titanium alloys. Figures 2-4 clearly illustrate this effect. The "as-quenched" hardness shown on the ordinate of each plot increases with increasing titanium content. The exact mechanism of hardening has been studied in detail by Ammons[29] at the Y-12 Plant of Union Carbide Corporation at Oak Ridge, Tennessee.

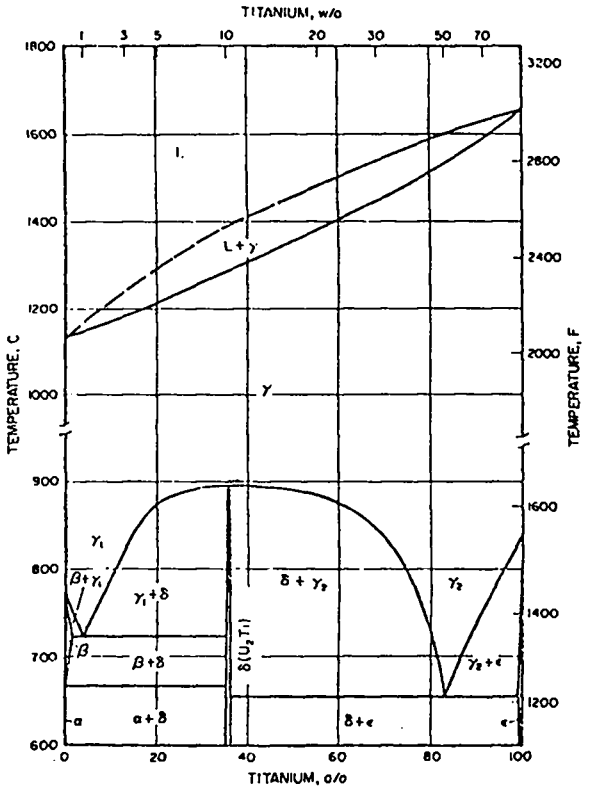

Fig. 1. Constitution diagram for uranium-titanium alloys.

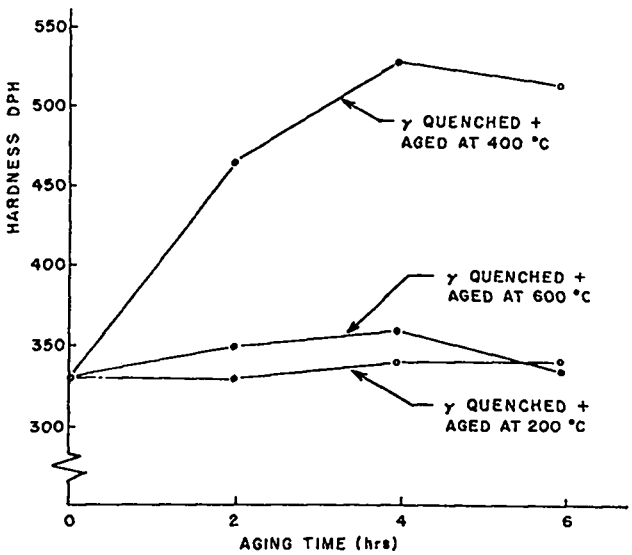

Fig. 2. A U-0.5 wt% Ti alloy's hardness variation with aging treatment.

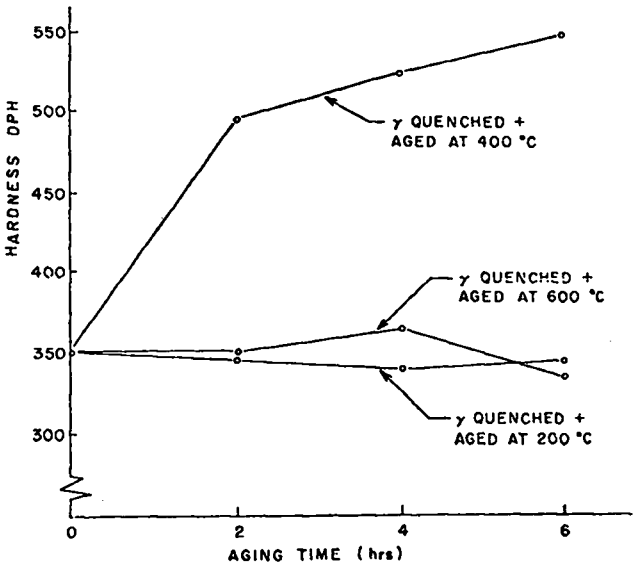

Fig. 3. A U-0.8 wt% Ti alloy's hardness variation with aging treatment.

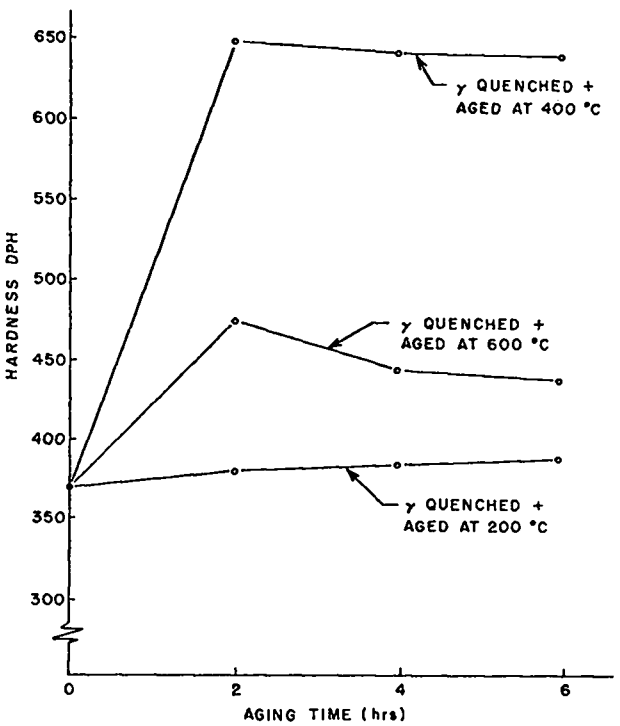

Fig. 4. A U-1.5 wt% Ti alloy's hardness variation with aging treatment.

His results have established that the hardness of the quenched material is due to solid-solution hardening effects. The subsequent hardening developed when the material is artificially aged after gamma quenching is attributed to precipitation of the very finely divided delta phase, which is U_2Ti. The increased hardness with increasing titanium content can be easily rationalized on the basis that increasing the solute content causes higher concentration of the precipitating phase. This work substantiates earlier work by the British investigators Harding, Waldron, and Knight[4] who established that the primary hardening effect was due to precipitation of the submicroscopic hexagonal phase, U_2Ti.

2. Chemical Analyses. In the course of developing the optimum alloy composition for this penetrator work, we studied alloy compositions in the 0.6 to 1.2 wt% titanium range. For convenience, we divided these alloys into four groups. The groups are separated on the basis of chemical analysis, and include samples with less than 0.64 wt% titanium, 0.65 to 0.74 wt% titanium, 0.75 to 0.84 wt% titanium, and more than 0.85 wt% titanium. We subjected all of these compositions to heat treatments designed to produce penetrator hardnesses greater than 45 Rockwell 'C' (R_c). For some plane-wave experiments, the material was studied in the "gamma-quenched" condition which yields a softer material. This condition was used only to establish base-line information on the alloys.

Chemical analyses of all samples were performed by the Analytical Chemistry Group at LASL. All the analyses consisted of wet analytical procedures to determine the concentrations of the principal alloying elements, titanium, molybdenum, or niobium, and a quantitative spectrographic analysis to determine the trace-element concentrations. Concentrations of carbon and the interstitial impurities, nitrogen and hydrogen, were measured by the fusion technique, which was used only on selected samples. Table I shows the results of chemical analyses of some representative heats

TABLE I

CHEMICAL ANALYSIS OF REPRESENTATIVE HEATS OF U-Ti ALLOYS

Element	Heat Numbers 498	510	493	499
Ti	0.62 wt%	0.73 wt%	0.84 wt%	1.17 wt%
C		50		5
H_2	20[a,b]	3[c]	15[b]	17[b]
Li	<0.2	<0.2	<0.2	<0.5
Be	<0.2	<0.2	<0.2	<0.5
B	<0.2	<0.2	<0.2	<0.5
Na	<1	1	1	<1
Mg	3	1	1	<2
Al	15	5	5	25
Si	100	50	50	100
P	<50	<50	<50	<50
Ca	<5	<5	<5	<5
V	<3	<1	<1	<50
Cr	3	1	1	<5
Mn	10	4	4	3
Fe	100	50	50	40
Ni	50	50	50	25
Cu	30	30	30	30
Zn	<25	<25	<25	<25
Sr	<20	<5	<5	<20
Mo	100	25	25	25
Ag	1	<1	<1	<1
Cd	<1	<1	<1	<1
Sn	1	<1	<1	<2
Sb	<5	<5	<5	<5
Ba	<5	<2	<5	<5
Pb	7	2	2	25
Bi	<2	<2	<2	<2

a. All values are in ppm unless otherwise noted.
b. Analysis was of samples used in plane-wave impact experiments on heat-treated 1.5-in.-diam disks.
c. Analysis was of heat-treated tensile-specimen remnants.

of the various uranium-titanium alloy compositions. Gross alloy chemistry and casting conditions for all the alloys tested are tabulated in Appendix B.

Early investigators[30] showed that the hydrogen content of uranium has a pronounced effect on the ductility of the material as measured in a standard tensile test. The results of the dynamic tests and penetrator performance indicate that this effect does not carry over to high strain rates. This is very significant because it simplifies the manufacturing procedures required to heat treat these alloys. The hydrogen analyses in Table I are representative of the samples used in the plane-wave impact experiments. The "as cast" hydrogen content of these penetrator alloys was always less than 5.0 ppm. Subsequent extrusion and heat treatment, increased the hydrogen content. The increased hydrogen content now seems to be primarily a surface phenomenon, since the hydrogen content of the samples from heat number 510 was less than 3 ppm and this was the only sample all of whose surfaces were machined before chemical analysis. The samples for heats 493, 498, and 499 were as-extruded bar stock, and, though they were aged in vacuum before chemical analysis, we made no attempt to remove the oxidized surface layer. The other noteworthy feature of the analyzed material is the general trace-element content of the penetrator stock. This material is the standard depleted-uranium alloy feed stock that can be obtained commercially. The material used throughout was procured from the Y-12 plant of the Union Carbide Nuclear Corporation. The master-alloy buttons from which the alloys were prepared were produced by the bomb-reduction process.

3. Heat Treatments. Heat treatment of all U-Ti alloys for this program involved one or the other of two basic techniques. In both cases, the material is first solution heat treated to a temperature in the gamma-phase region of the constitution diagram. This is always done in a protective atmosphere of flowing argon gas. After the material has equilibrated at the solution-annealing or gamma-phase temperature, (~ 850°C) it is either quenched in water at room temperature (gamma quenched) and subsequently aged at some intermediate temperature, or quenched directly in a salt bath at the desired aging temperature. The latter technique is known as isothermal quenching.

Experiments by Eckelmeyer and Zanner[31] at Sandia Laboratories have shown that the critical cooling rate for quenching U-Ti alloys is < 30°C/sec, which corresponds to a moderate oil quench.

Their result has been substantiated by the experience gained in this project. Note, however, that the material produced for this project was heat treated in the form of 2-in.-diam by 3/8-in.-thick disks or 19/32-in.-diam rods. The effect of heat treatment in larger pieces was not determined.

The U-Ti alloys were aged either in a vacuum furnace, in molten lead, or in a KCO_3-$LiCO_3$ salt bath. The aging was necessary to produce the hardness required for the penetrator. The Air Force required that the penetrator have a hardness of 44-60 Rockwell 'C' (R_c). Previous work at LASL[25] had clearly demonstrated the practicality of producing this hardness by aging treatments. Figures 2-4 show the effect of aging temperature and time on the hardness developed in three different alloy compositions. Peak hardness appeared to be developed after two to six hours at 400° C, depending on the alloy composition. Aging the samples at 600° C caused severe overaging, and aging at 200° C gave no age hardening even after six hours. Using these data, we decided to evaluate U-Ti alloys in the following three heat-treatment conditions: (1) Gamma quenched and aged at 450° C to produce material with near maximum hardness, (2) Gamma quenched and aged at 550° C to produce an overaged material that might have greater ductility at high strain rates, and (3) Isothermally quenched and aged at 500° C, this being the simplest heat treatment that can develop the desired hardness.

The resulting hardnesses are shown in Fig. 5. These data clearly demonstrate the high reproducibility of hardness in this alloy system. The exact titanium content is apparently not critical from 0.62 to 1.17 wt% Ti, so U-0.75 wt% Ti is an ideal nominal composition that lends itself to simple processing and fabrication.

It is worth noting that only very simple equipment is required to heat treat these alloys. Figure 6 shows the kind of equipment used for all of the heat treating. The alloys were gamma

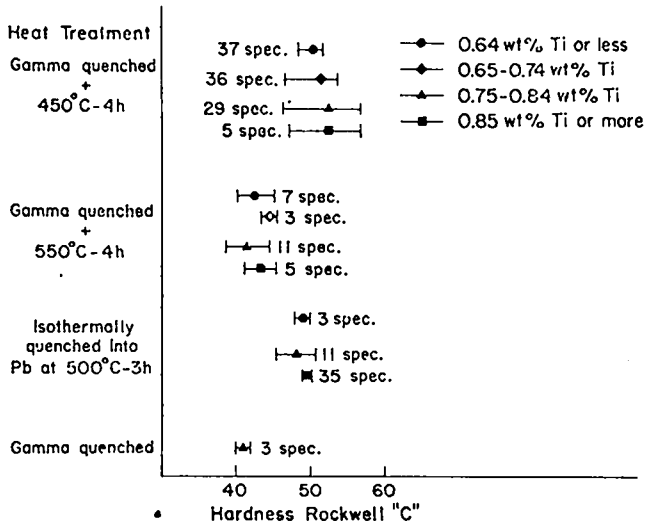

Fig. 5. Rockwell hardness developed in candidate uranium-titanium alloys.

Fig. 6. Equipment used to heat treat candidate uranium alloys.

quenched out of a simple muffle furnace into water. Aging was done in a resistance-heated multipurpose furnace equipped with interchangeable pots that the user can simply change for various heat-treating media. The lead bath was used for samples aged at 450° C and for the 500°C aging treatments. Samples were also heat treated in a vacuum furnace, but no improvement in properties was noted. For simplicity and economy of production, we recommend the lead-bath aging treatment.

4. Microstructures Developed in Heat-Treated U-Ti Alloy Penetrator Stock. The microstructures developed in the various U-Ti alloys were studied throughout the program. The casting and fabrication techniques used in preparing all the uranium alloy stock, including the microstructure samples, are described in detail in Appendix B. Since all extrusion was at a temperature well within the gamma region (~ 900° C) and at an extrusion ratio of 4 to 1 that completely "breaks up" the cast structure, we expected uniform grain size in the bar stock. After the initial ingot breakdown from the cast 4.0-in.-diam ingot to the 2.0-in.-diam rod, samples were abstracted for sound-velocity and dynamic compressive- and tensile-strength measurements. Samples of the extrusion were examined for microstructure at this time and also corrosion tested. These samples had essentially the same structure and hardness as the re-extruded 19/32-in.-diam penetrator stock.

Figure 7 is a series of photomicrographs of a U-0.84 wt% Ti alloy used for plane-wave impact experiments. The "as-gamma-quenched" sample exhibits the classical basket weave or Widmanstätten structure produced in heat-treated U-Ti alloys. Also there is no "decoration" of the grain boundaries with the U_2Ti phase. The hardness in the quenched condition is still high at 40.5 R_c.

The microstructure of the sample that was gamma quenched and aged at 450° C in vacuum for four hours is shown in Fig. 7A. It shows strongly decorated grain boundaries where precipitation has occurred. There is also some evidence of coalescence of the precipitate within the grains themselves.

The microstructure developed in the sample aged at 550° C shows that it is severely overaged, with excessive etching of the precipitated phase and a corresponding decrease in hardness down to 39.0 R_c. The microstructure developed in an isothermally quenched sample of U-0.84 wt% Ti does not show the degree of grain-boundary precipitate observed in the 450° C aged specimen; also, the hardness at 50 R_c is somewhat reduced compared to that of the 450° C aged material.

Figure 8 is a series of photomicrographs of microstructures developed in three different compositions of U-Ti by two different heat treatments. All samples aged at 450° C were aged in a molten-lead bath, and the samples aged at 550° C were aged in molten carbonate salt. The samples aged at 450° C show a marked decrease in U_2Ti precipitate at the grain boundaries with decreasing titanium content. However, there is no significant decrease in gross hardness. This strongly suggests that the grain-boundary precipitate is noncoherent and does not significantly strengthen the heat-treated alloy.

The samples aged at 550° C have extremely dark structures indicating excessive precipitation and coalescence of the U_2Ti. The hardness variation in these three samples is inconsequential, again suggesting that the precipitate is incoherent with the matrix. The "ghost structure" observed in the U-0.75 wt% Ti sample aged at 550° C has not been identified.

Figure 9 is included simply to show that aging in a lead bath or in vacuum produces no significant difference in structure. The lead-bath-aged sample appears to have heavier grain-boundary precipitate, but this is probably due to quenching, rather than the aging treatment. The hardness values obtained are independent of heat-treating media, and analyses of samples for H_2 content

Fig. 7A. γ-quench from 850°C, 40.5 R_c.

Fig. 7B. γ-quench + age 450°C, 4 h, vac. 54.0 R_c

Fig. 7C. γ-quench + age 550°C, 4 h, vac. 39.0 R_c.

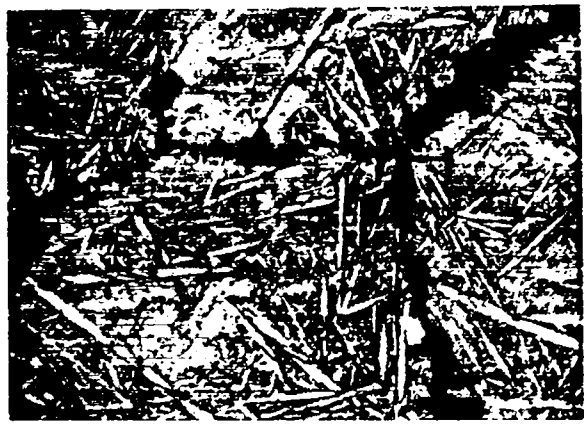

Fig. 7D. Isothermal quench at 500°C, 3 h, in lead, 50.0 R_c.

Fig. 7. Microstructures developed in a U-0.84 wt% Ti alloy by various heat treatments.

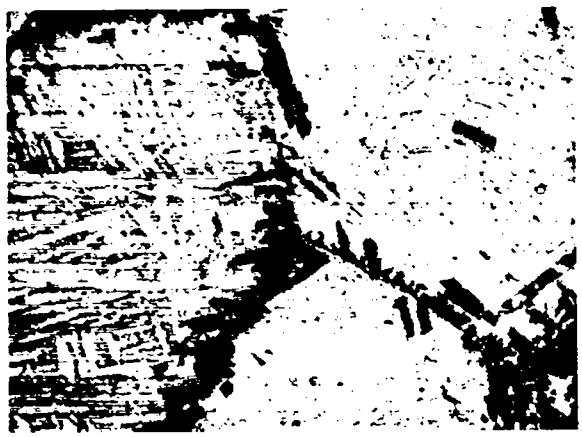

Fig. 8A. U-0.62 wt% Ti. γ-quench + age 450°C, 4 h, in lead, 51.4 R_c

Fig. 8B. U-0.62 wt% Ti. γ-quench + age 550°C, 4 h, in salt, 42.0 R_c.

Fig. 8C. U-0.75 wt% Ti. γ-quench + age 450°C. 4 h, in lead, 51.0 R_c.

Fig. 8D. U-0.75 wt% Ti. γ-quench + age 550°C, 4 h, in salt, 42.0 R_c.

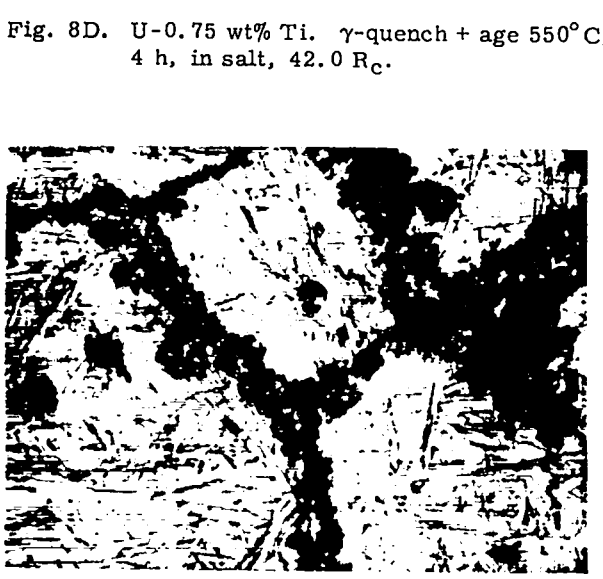

Fig. 8E. U-1.17 wt% Ti. γ-quench + age 450°C, 4 h, in lead, 53.0 R_c.

Fig. 8F. U-1.17 wt% Ti. γ-quench + age 550°C, 4 h, in salt, 43.0 R_c.

Fig. 8. Microstructures developed in candidate U-Ti alloys as a function of composition and heat treatment.

indicate that the lead-bath-aged material does not contain significantly more H_2 than the vacuum-aged material.

5. Static Mechanical Properties. We made very limited measurements of quasi-static tensile and compressive strengths simply to establish base-line data for penetrators. The value of a low-strain-rate tensile, or compressive, test for evaluating a penetrator material is very suspect. We believe that the compressive test can be useful as a process-control technique, but not as a method of defining properties for actual penetrator applications in lieu of more definitive tests.

Tensile tests were performed on standard ASTM 0.252-in.-diam specimens with threaded ends. The compressive-test samples were 0.350 in. diam by 0.700 in. thick. All specimens were fabricated from extruded penetrator stock. Two metal-foil strain gages were cemented diametrically opposite each other at the midpoint of each sample. The strain was taken to be the average of readings from the two gages. All specimens were tested using an Instron testing machine operated at a cross-head speed of 0.005 in./min.

Fig. 9A. γ-quench + age 450° C, 4 h, lead bath, 52.0 R_c.

Fig. 9B. γ-quench + age 450° C, 4 h, vac., 52.0 R_c.

Fig. 9. Microstructures developed in a U-0.74 wt% Ti alloy by vacuum and lead-bath aging.

Two different U-Ti alloy compositions were tested, and the results are summarized in Table II. The material with the highest titanium content seems to have the highest yield strength; however, there is no significant difference in the tensile strength or ductility of these two different alloy compositions. Note that neither of these series of test specimens has any significant ductility. However, this composition and heat treatment gave the best penetrator performance of any alloy and heat treatment evaluated in this program.

6. Plane-Wave Impact Tests. All alloys evaluated in this project were also subjected to ultra-high strain-rate (10^4-10^5/sec) measurements of tensile and compressive strength. These experiments were performed using 1-5/8-in.-diam by 3/8-in.-thick samples of the uranium alloys and striking them with copper disks launched from a compressed-gas gun. Measured free-surface velocities of the specimens produced by the impact-generated stress waves were then used to calculate the material's Hugoniot elastic limit (dynamic compressive strength) and spall strength (dynamic tensile strength).

These calculations require that the density and velocity of sound in each sample be known. Therefore, we measured the ultrasonic longitudinal and shear-wave velocities, the corresponding dynamic moduli, and the density of representative samples of each alloy and heat treatment. Details of the techniques and results of all the dynamic-properties experiments are presented in Appendix C. However, some of the results are summarized here to facilitate comparison with other properties of the alloys.

The Hugoniot elastic limits (dynamic compressive strength) of a number of U-Ti alloy samples are presented in Fig. 10. Note that for the gamma-quenched and aged samples, the heat treatment (450° C aged for four hours) that develops maximum hardness in a standard Rockwell hardness test also produces the highest Hugoniot elastic limit (HEL) by about a factor of two. However, samples that were isothermally quenched had a relatively low HEL, even though their static hardness was quite high (~ 49 R_c). This points up the possible danger in using quasi-statically determined mechanical properties to select a material for high-strain-rate applications. It is also important to note that the HEL is almost independent of titanium content over the range of compositions studied.

1143-1354

TABLE II

MECHANICAL PROPERTIES OF SELECTED U-Ti ALLOY PENETRATOR STOCK GAMMA QUENCHED AND AGED IN MOLTEN LEAD AT 450°C FOR FOUR HOURS

Specimen	Alloy Comp (wt% Ti)	Tensile Str (psi)	Yield[a] Str (psi)	% Elong.	Modulus[b]	Comp Yield Str	Comp Modulus
526-121-1	0.61	201,200	129,400	2	25.9×10^6		
526-121-2	0.61	221,600	132,700	2	25.7×10^6		
526-122-1	0.61	222,700	133,500	2	25.5×10^6		
526-122-2	0.61	223,900	132,400	2	25.6×10^6		
526-123-1	0.61	219,600	132,400	1	25.4×10^6		
526-211-1	0.61					193,300	24.0×10^6
526-211-2	0.61					185,400	23.9×10^6
526-211-3	0.61					169,900	24.2×10^6
526-211-4	0.61					179,200	24.3×10^6
526-211-5	0.61					177,800	25.6×10^6
C1-510-1-2	0.75	210,200	150,300	<2	26.6×10^6		
C1-510-1-2	0.75	209,900	161,800	<2	25.5×10^6		
C1-510-1-2	0.75	212,700	146,100	<2	29.6×10^6		
C1-510-1-2	0.75	232,600	169,400	<2	26.7×10^6		
C1-510-1-1	0.75					181,600	26.8×10^6
C1-510-1-1	0.75					183,900	26.4×10^6
C1-510-1-1	0.75					201,500	25.8×10^6
C1-510-1-1	0.75					196,800	26.9×10^6

a. Based on 0.2% offset from the initial modulus. The proportional limit varied from 31,000 to 62,000 psi for the compression specimens and from 25,000 to 30,000 psi for tension specimens.
b. Based on the best straight-line plot near the origin of a curve plotted using load values and the average strain of the two metal-foil strain gages.

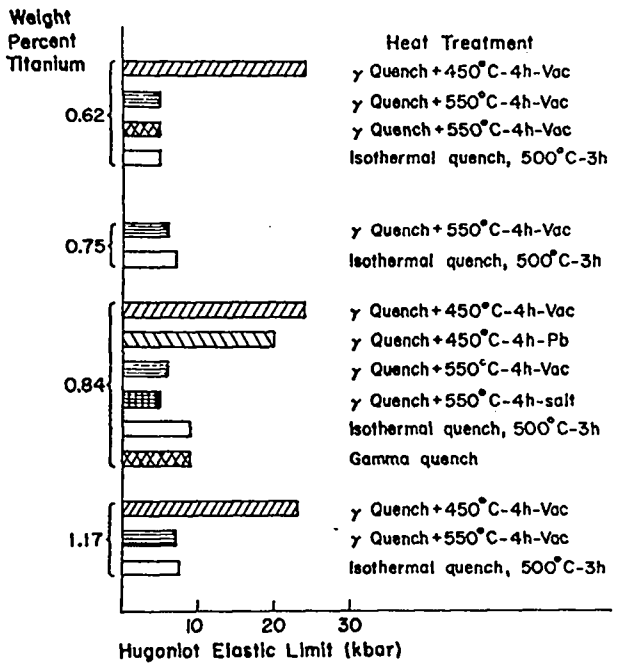

Fig. 10. Hugoniot elastic limit (dynamic compressive strength) of candidate U-Ti alloys.

Fig. 11 is a summary of the spall-strength (dynamic tensile-strength) results for the U-Ti samples. There is little variation of this property with either alloy composition or heat treatment, except that the sample that was gamma quenched only (no subsequent aging) had an appreciably higher spall strength than the aged samples. This is not surprising, since the gamma-quenched material is also much softer and more ductile in static tests than the other samples. The plane-wave impact tests do not provide a direct measure of high-strain-rate ductility. However, most of the U-Ti specimens recovered after impact loading were either intact or broken into relatively large pieces, indicating some degree of dynamic ductility.

In summary, the uranium-titanium binary system is very attractive for penetrator production, because of the simple processing required and the broad range of compositions that can be heat-treated to produce the desired mechanical

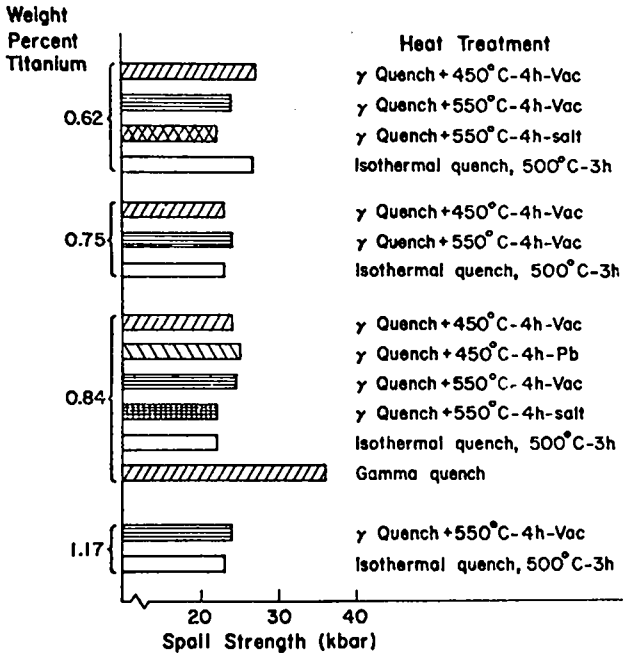

Fig. 11. Spall strength (dynamic tensile strength) of candidate U-Ti Alloys.

properties. On the basis of preliminary mechanical tests and the corrosion-test results discussed in Sec. III, a simple gamma quench and subsequent aging at 450° C is the most promising heat treatment for this system.

C. Uranium-Molybdenum Alloys

1. General Characteristics. The binary system of uranium-molybdenum has been studied extensively throughout the AEC and at other laboratories around the world. This alloy system has been of great interest because increasing the molybdenum content to ~ 8 wt% can produce a gamma-stable alloy. We chose the low alloy, U-2 wt% Mo for this program because it can be heat treated to produce a wide range of mechanical properties much the same as those of the U-Ti alloys. This alloy has already been used in preliminary Armed Forces studies of uranium penetrators and is, therefore, useful as a standard for penetration performance.

Figure 12 is a reproduction of the uranium-molybdenum constitution diagram.[28] The molybdenum alloy is heat treated by first heating it into the high-temperature gamma-phase field. Upon rapid quenching, the material transforms from $\gamma \rightarrow \alpha + \partial$, the α transformation occurring by a shear mechanism, or martensite transformation. The resultant structure is a supersaturated alpha phase. Upon subsequent precipitation heat treatment, the ordered tetragonal delta phase is precipitated out of the saturated alpha solid solution, significantly hardening and strengthening the alloy phase.

2. Chemical Analyses. The chemical-analysis results shown in Table III are largely identical to those for the U-Ti alloys. However, note that the carbon content measured for the U-Mo alloys was appreciably higher than that measured for the U-Ti alloys. Titanium is a stronger carbide former than molybdenum, and, therefore, tends to

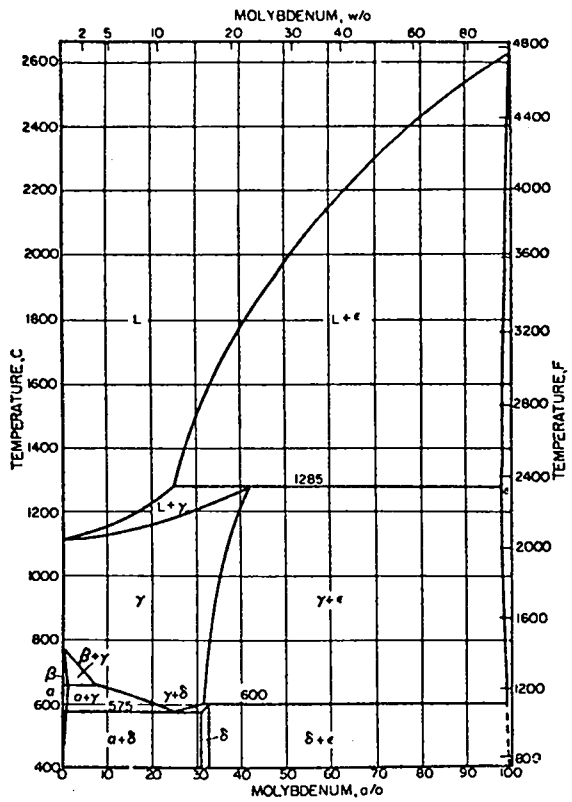

Fig. 12. Constitution diagram for uranium-molybdenum alloys.

TABLE III

CHEMICAL ANALYSES OF REPRESENTATIVE HEATS OF U-2 WT% MO ALLOY

Element	Heat Numbers 496	507
Mo	2.04 wt%	2.04 wt%
C	140[a]	170
H_2	-	10
Li	< 0.5	< 0.5
Be	< 0.5	< 1
B	< 0.5	< 0.5
Na	< 1	< 2
Mg	< 2	2
Al	15	10
Si	50	80
P	< 50	< 100
Ca	< 5	< 5
V	< 50	< 50
Cr	5	5
Mn	< 2	3
Fe	30	60
Ni	20	60
Cu	8	25
Zn	< 25	< 25
Sr	< 40	< 40
Ag	< 1	< 1
Cd	< 5	< 5
Sn	< 2	< 2
Sb	< 3	< 25
Ba	< 5	< 10
Pb	5	2
Bi	< 5	< 1

a. Values are in ppm unless otherwise noted.

lower the alloy's gross carbon content. The lower carbon content may be significant in the improved corrosion resistance noted for U-Ti as opposed to U-Mo.

3. Heat Treatments and Resulting Micro-Structure and Hardness. The heat treatments chosen for the U-2 wt% Mo alloy were designed to produce a material of greater than 45 R_c hardness. Like the U-Ti alloys, the material was heat treated by solution annealing at a temperature in the gamma-phase region of the constitution diagram. The solution annealing treatment was always performed under a flowing argon gas atmosphere, and the samples were generally quenched in water at room temperature.

As was done for U-Ti, we used several different aging media for the U-Mo alloy to try to determine whether they would affect the mechanical properties. Samples were aged by heating at 300° C for four hours in vacuum, at 450° C for four hours in vacuum, at 550° C for four hours in both vacuum and molten salt, and by isothermally quenching directly from 850° C into a molten-lead bath at 500° C for three hours. The hardnesses developed by these heat treatments on the U-Mo alloys are summarized in Fig. 13. The small hardness spread associated with any specific heat treatment gives strong evidence of the alloy's uniformity and reproducible response to heat treatment. Isothermal quenching is the treatment we finally used for production of full-scale armor-piercing penetrators of this particular alloy. This heat treatment was simple and yielded a very uniform and highly reproducible product.

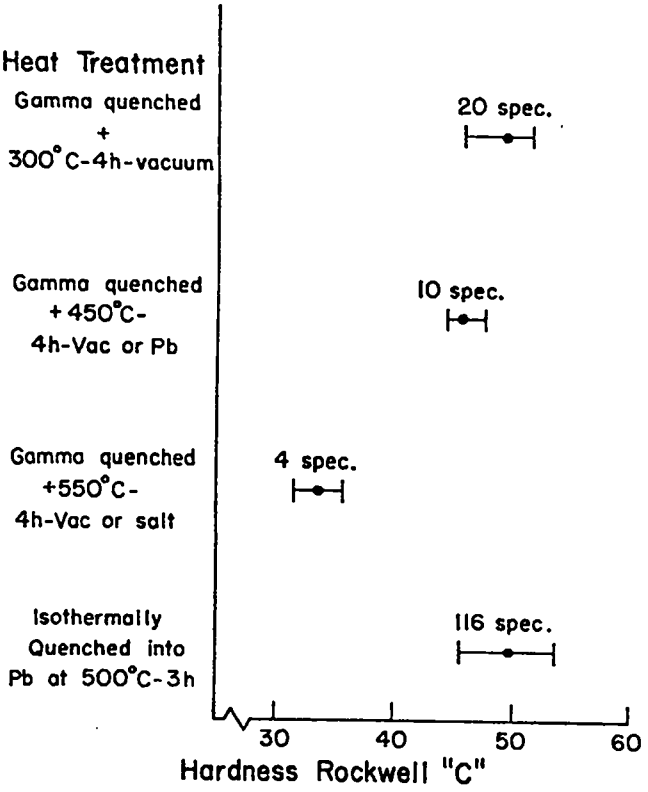

Fig. 13. Rockwell hardness developed in candidate U-2 wt% Mo alloys.

Figure 14 consists of photomicrographs of the structures developed by the two most promising heat treatments. The microstructure of the sample aged at 300°C is characteristic of the underaged condition in this alloy system. The structure consists of gamma-phase grains containing a martensite structure. The precipitation-hardening delta phase has not coalesced enough to be visible.

The microstructure of the material heat treated by isothermally quenching into molten lead at 500°C for three hours is characteristic of an overaged structure. The phase responsible for hardening has coalesced enough to completely etch the sample surface.

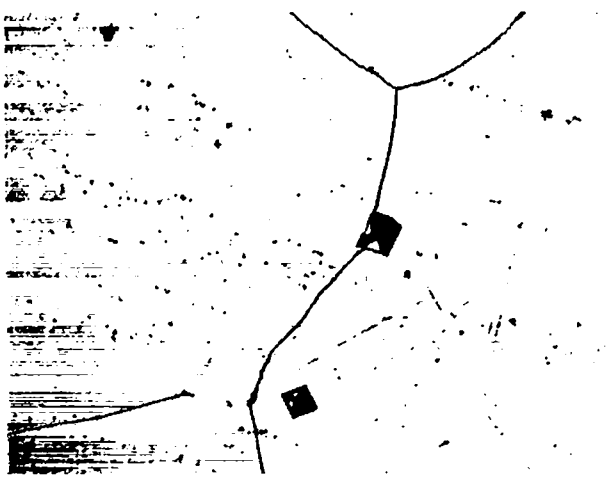

Fig. 14A. γ-quench + age 300°C, 4 h, vac., 46.4 R_C.

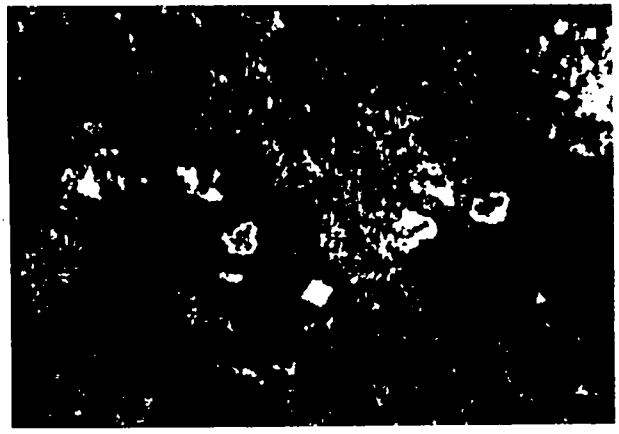

Fig. 14B. Isothermal quench at 500°C, 3 h, 50.0 R_C.

Fig. 14. Microstructures developed in candidate U-2 wt% Mo alloys.

4. Static Mechanical Properties. The mechanical properties of isothermally quenched U-2 wt% Mo alloy were measured and are shown in Table IV. This was one of the two materials finally chosen for production of full-scale 30-mm projectile cores. The tensile results obtained in these tests are strikingly similar to those for the heat-treated U-Ti alloys. The ultimate tensile strength and yield strength are high, but the tensile ductility is low. The compressive yield strength of the U-Mo alloy is high, but not significantly different from that of the U-Ti alloys. Once again, the standard tensile and compressive tests can be used only as techniques for establishing whether a material has been properly heat treated, because, except for hardness, there is little correlation between quasi-statically determined mechanical properties and penetration performance.

5. Plane-Wave Impact Tests. We measured the dynamic compressive strength (HEL) and dynamic tensile (spall) strength of the U-2 wt% Mo alloys in all of the heat-treatment conditions evaluated in this project. Details of the technique and results of these measurements are presented in Appendix C, but Figs. 15 and 16 summarize the important results. Unlike those of the U-Ti alloys, the dynamic compressive strengths determined for the variously heat-treated U-Mo alloys are consistent with static-hardness data. Also, the highest HEL observed for a U-Mo alloy is the same, within experimental error, as that observed for the best U-Ti material.

Spall strengths were somewhat higher for the U-Mo than for the U-Ti alloys. However, the penetration tests (Sec. IV) showed little or no correlation between spall strength and penetrator performance against homogeneous steel armor. Again, the U-Mo alloy specimens were usually recovered intact or in a few large pieces after impact testing, indicating some degree of dynamic ductility.

TABLE IV

TENSILE AND COMPRESSIVE PROPERTIES OF A U-2.04 WT% Mo ALLOY ISOTHERMALLY QUENCHED INTO MOLTEN LEAD AT 500°C

Specimen	Tensile Str (psi)	Yield[a] Str (psi)	% Elong	Modulus[b]	Comp Yield Str	Comp Modulus
523-121-1	206,800	169,100	1	24.3×10^6		
523-121-2	198,100	142,900	1	24.6×10^6		
523-122-1	214,700	152,500	1	23.9×10^6		
523-122-2	225,800	172,100	1	24.1×10^6		
523-123-1	218,200	159,000	1	24.0×10^6		
523-211-1					181,400	25.0×10^6
523-211-2					184,000	24.5×10^6
523-211-3					186,900	25.7×10^6
523-211-4					191,200	24.6×10^6
523-211-5					189,300	23.8×10^6

a. Based on 0.2% offset from the modulus line.
b. Based on the best straight line near the origin of a curve traced from the average of two diametrically opposite strain gages and load values.

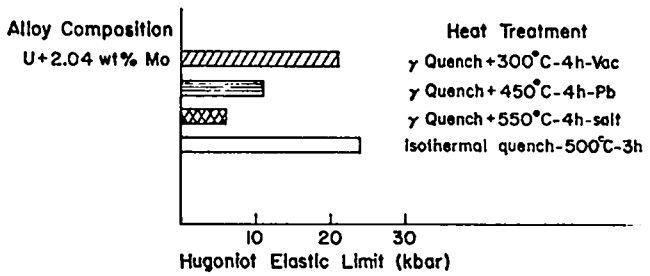

Fig. 15. Hugoniot elastic limit (dynamic compressive strength) of candidate U-2 wt% Mo alloys.

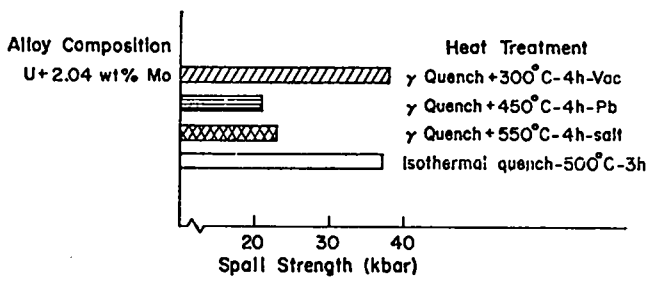

Fig. 16. Spall strength (dynamic tensile strength) of U-2 wt% Mo alloys.

Preliminary mechanical tests on U-2 wt% Mo alloy indicate that its penetration effectiveness should be nearly equivalent to that of U-0.75 wt% Ti. This material's corrosion resistance is not comparable to that of the other candidate alloys, and it also showed a tendency toward stress-corrosion cracking. This makes it a less desirable choice for a penetrator material if it must be subjected to marine environments, or for that matter, to any high-humidity atmospheres.

D. Uranium-Niobium and Uranium-Niobium-Titanium Alloys

1. General Characteristics. The final two alloy systems evaluated were U-4.5 wt% Nb and a nominal U-2 wt% Nb-1 wt% Ti ternary alloy. These two alloys are grouped together because they have some similar physical properties. Both should have better than average corrosion resistance, because the addition of niobium generally imparts high corrosion resistance to uranium alloys. However, they also exhibit a tendency toward stress-corrosion cracking.

Both the U-4.5 wt% Nb and the U-2 wt% Nb-1 wt% Ti alloy can be hardened by simple heat treatments. The hardening mechanisms are,

again, similar to those observed for U-Ti and U-Mo alloys. The material is water quenched from the all-gamma-phase field of the respective constitution diagram. Simple aging treatments after gamma quenching are then applied to produce the hardness and strength required for penetrator applications.

2. Chemical Analyses. Chemical analyses of the U-4.5 wt% Nb binary and U-2 wt% Nb-1 wt% Ti ternary were performed identically to that of the previously described alloys. The compositions of both the U-Nb binary and U-Nb-Ti ternary alloys are much harder to control because of the comparatively low density and high melting point of the niobium. Also, both niobium and titanium have a strong tendency to form carbides and separate out of the melted alloy.

Tables V and VI show typical chemical analyses of these alloys. The results for the U-Nb-Ti ternary alloy point up the difficulty in obtaining castings with reproducible compositions.

3. Heat Treatments and Resulting Microstructures and Hardness. The heat treatments used on these alloy compositions were designed to give a hardness greater that 45 R_c. Those used on the U-4.5 wt% Nb alloy consisted of quenching from the gamma-phase temperature (850 °C) then aging the samples at 300°C for four hours in vacuum, or 500°C for four hours in vacuum. These heat treatments correspond to underaging the 300°C sample, with a resulting hardness of 47.5 R_c, and overaging the 500°C sample with a resulting hardness of 45 R_c (see Fig. 18). Figure 17 illustrates the resulting microstructures. The underaged sample appears to be a fine equiaxed structure with no optically discernible features, other than the grain boundaries. The overaged structure is a mixture of α and γ_2 phases, the latter being very rich in niobium.

The U-Nb-Ti alloy had variable hardness depending strongly upon the chemical composition. This alloy developed the highest hardness of any candidate material. The hardening mechanism is not known, but is probably the combined effect of solid-solution hardening and precipitation hardening, with the precipitating phase(s) being both U_2Ti and the γ_2 phase. The heat treatments on this alloy system included a 450°C age, a 550°C age, and an isothermal quench in molten lead at 500°C. Figure 18 is a plot of the hardnesses of these heat-treated materials.

The microstructure of a U-2.5 wt% Nb-1.25 wt% Ti alloy gamma-quenched and aged at 450°C for four hours is shown in Fig. 19. This structure seems to consist of very heavily decorated gamma grains with course precipitation throughout the grains. This material is extremely

TABLE V

TYPICAL CHEMICAL ANALYSIS OF SEVERAL U-Nb BINARY-ALLOY CASTINGS

	Heat Numbers		
Element	509	518	520
Nb	4.8%	5.2	4.8
C	190[a]	150	120
H_2	-	-	5
Li	<0.2	<0.2	<0.2
Be	<0.2	<0.2	<0.2
B	0.3	0.3	<0.2
Na	<1	2	<1
Mg	<1	<1	<1
Al	<5	<5	<5
Si	100	100	100
P	<50	<50	<50
Ca	<50	<50	<50
V	<200	<200	<200
Cr	<2	<2	<2
Mn	5	5	3
Fe	50	40	30
Ni	15	15	30
Cu	7	7	30
Zn	<25	<25	<25
Mo	<25	<25	<25
Ag	<2	<2	<2
Cd	<1	<1	<1
Sn	<1	<1	<1
Sb	<5	<5	<5
Ba	<100	<100	<100
Pb	<1	<1	<1
Bi	<2	<2	<2

a. All values are in ppm unless otherwise noted.

[redacted]

TABLE VI

TYPICAL CHEMICAL ANALYSIS OF TWO DIFFERENT HEATS OF A U-Nb-Ti ALLOY

Element	Heat Numbers 500	508
Nb	1.25 wtω	2.65 wt%
Ti	1.85 wt%	1.40 wt%
C	120[a]	130
H_2	-	5
Li	<0.1	<0.1
Be	<0.5	<0.5
B	<0.2	0.2
Na	<1	1
Mg	<1	<1
Al	5	<5
Si	50	60
P	<50	<100
Ca	<10	<5
V	<100	<100
Cr	<5	<1
Mn	6	6
Fe	40	50
Ni	40	10
Cu	12	20
Zn	<25	<25
Sr	<40	<20
Mo	<50	<25
Ag	15	3
Cd	<1	<1
Sn	<1	<1
Sb	<3	<5
Ba	<5	<5
Pb	2	3
Bi	<1	<2

a. All values are in ppm unless otherwise noted.

brittle, as would be expected for a structure of this type.

4. Plane-Wave Impact Tests. We measured the dynamic mechanical properties of both the U-Nb binary and U-Nb-Ti ternary alloys by the gun-impact method described in Appendix C. The results are summarized in Figs. 20 and 21. Within each alloy system, the dynamic compressive strength (HEL) correlates well with static Rockwell hardness for different heat treatments. This is not true for comparisons between different alloys. For example, the U-4.65 wt% Nb alloy, γ-quenched and aged at 300°C for four hours, had the highest HEL of any material studied, but both the ternary alloys

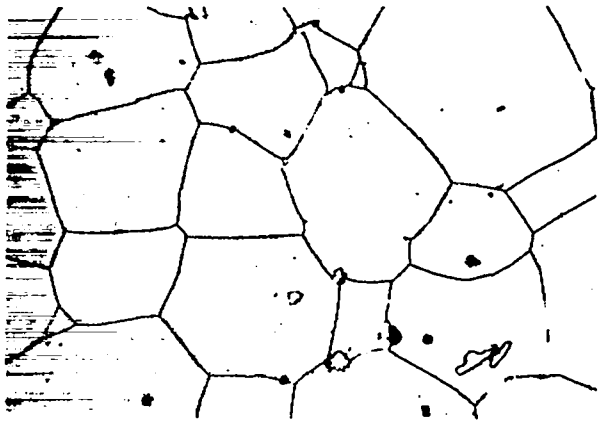

Fig. 17A. γ-quench + age 300°C, 4 h, vac., 47.5 R_c

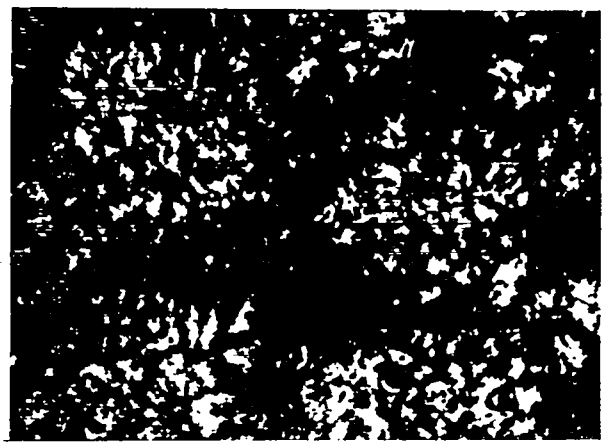

Fig. 17B. γ-quench + age 500°C, 4 h, vac., 45.0 R_c

Fig. 17. Microstructures developed in candidate U-4.65 wt% Nb alloys.

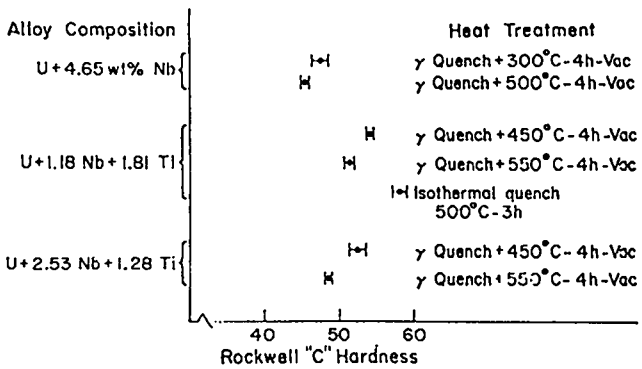

Fig. 18. Rockwell hardness developed in candidate U-Nb and U-Nb-Ti alloys.

[redacted]

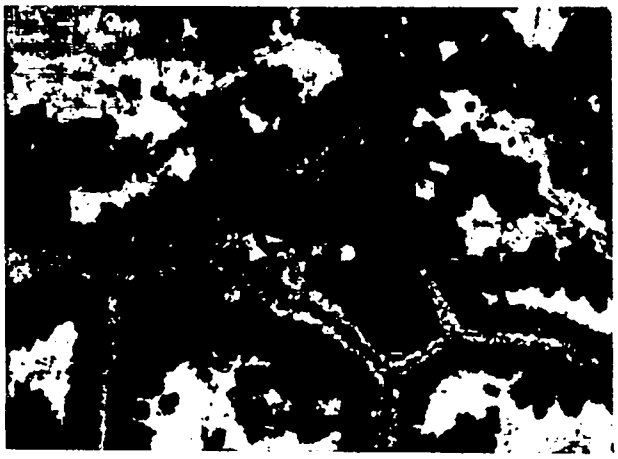

Fig. 19. Microstructure developed in a U. 2.5 wt% Nb-1.25 wt% Ti alloy. Heat treatment: γ-quench + age 450°C, 4 h, vac. Hardness: 52.3 R_c.

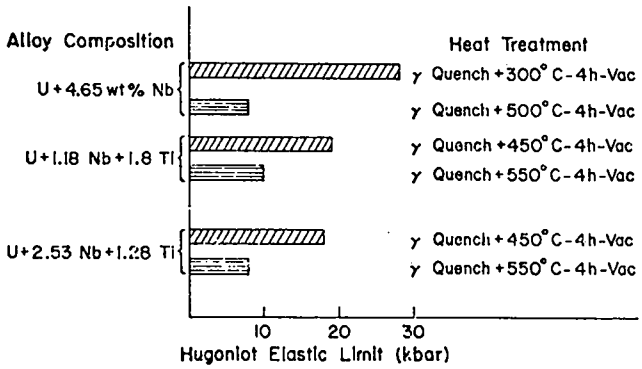

Fig. 20. Hugoniot elastic limit (dynamic compressive strength) of candidate U-Nb and U-Nb-Ti alloys.

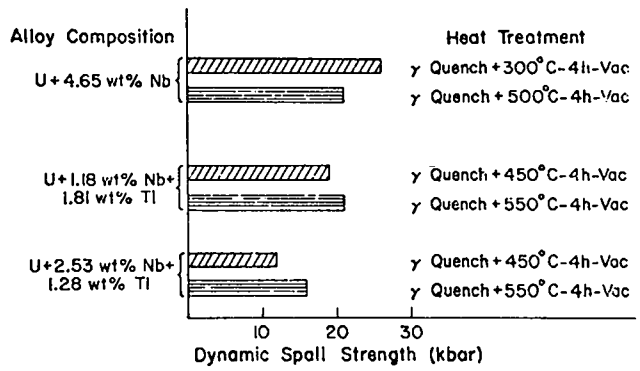

Fig. 21. Spall strength (dynamic tensile strength) of candidate U-Nb and U-Nb-Ti alloys.

had higher static hardness. This, again, points up the value of dynamic testing in selecting materials for high-strain-rate applications.

The spall (dynamic-tensile) strength of the U-Nb alloy was comparable to that of the other alloys studied (U-Ti and U-Mo), but the U-Nb-Ti ternary had somewhat lower spall strength. Also, upon impact loading, the ternary samples tended to shatter into much smaller fragments than the other materials, indicating substantially reduced high-strain-rate ductility.

As the results discussed in this section indicate, the four candidate alloy systems can be heat treated to span a reasonably wide range of microstructures and mechanical properties. Each had potentially useful features. The U-Ti system provided high dynamic strength and ease of fabrication and was remarkably insensitive to precise composition. The U-2 wt% Mo material also had a high dynamic compressive strength and was useful as a reference for penetration performance, since it had been used in previous uranium penetrator tests. The enhanced corrosion resistance of U-4.5 wt% Nb made it attractive if its penetration performance were as good as that of either U-Ti or U-Mo. We chose the U-2 wt% Nb-1 wt% Ti alloy in hopes of obtaining high strength and enhanced corrosion resistance. These four systems should provide a good basis from which to select an optimum penetrator material.

III. CORROSION RESISTANCE

A. Introduction

Uranium and its alloys are notorious for their susceptibility to corrosion, both surface oxidation and stress-corrosion cracking. Any AP projectile actually put into service will have to withstand periods of storage under a variety of environmental conditions. In the final 30-mm projectile design, the uranium alloy core may be totally enclosed; however, a highly reactive metal may also be incompatible with the other projectile

materials. The Air Force and LASL, therefore, decided to use corrosion resistance as a consideration in the initial selection of candidate alloys, and to subject each alloy to a general corrosion test under the most severe conditions set by military ordnance storage requirements, namely 165° F and 75% relative humidity.

B. Test Procedures

Specimens were cut from extruded bar stock that had been handled exactly like the corresponding penetrator stock (see Appendix B). All heat treatments evaluated in the ballistic and mechanical tests also underwent corrosion testing. We ran two series of tests, the first for 147 days and the second for 60 days. The specimens for the second series of tests were cut from the same pieces of extruded bar stock used to fabricate cores for the penetration tests.

Each specimen was degreased and pickled in concentrated nitric acid to remove any oxide layer before it was initially weighed. The samples were then placed in individual glass dishes and suspended over the humidity fluid (30 vol % H_2SO_4) in a sealed battery jar. The battery jar was placed in a circulating-air oven maintained at 165 ± 2° F. The 30 vol % H_2SO_4 solution provides 75% relative humidity at this temperature. The specimens were periodically weighed in their dish on an analytical balance. A simple computer code was used to maintain a tabulation of the total weight gained per unit area (mg/cm^2) and the average rate of weight gain (mg/cm^2/day) for each sample.

C. Results and Discussion

The results are summarized in Tables VII and VIII, and Figs. 22-29 are photographic records of the progress of the tests. In Table VII, the specimens are grouped according to alloy composition and heat treatment. In Table VIII, they are arranged by sample number to provide a key to the pictures that follow. Samples 1 to 21 represent the first test series, and the final results after 147 days exposure are illustrated in Fig. 22. Samples 22 to 47 represent the second series of tests. Photographs (Figs. 23-28) of this series were taken at frequent intervals to illustrate the progress of corrosion. Figure 29 shows the final condition of samples 22 to 47 after 60 days exposure and after the oxide layer was removed with nitric acid.

There was an approximately tenfold variation in corrosion rate for each binary alloy depending on heat treatment, the U-Nb, U-Ti, and U-Nb-Ti alloys were generally considerably superior to the U-Mo alloys, and the worst U-Nb and U-Ti specimens were about equal to the best U-Mo alloys in corrosion resistance. The average rate of weight gain for the U-Nb-Ti alloys was 0.0038 mg/cm^2/day, that for U-Nb alloys 0.0091, for U-Ti alloys 0.0130, and for U-Mo alloys 0.100.

Although we ran no specific stress-corrosion cracking tests on the candidate alloys, a number of the corrosion samples developed cracks simply because of residual stresses caused by heat treatment. The cracked specimens included 2 of 3 U-Nb-Ti samples, 3 of 13 U-Mo, 1 of 5 U-Nb, and 1 of 25 U-Ti. The oxide coating on all specimens in the first test series (samples 1 to 21) began flaking off within the first two months of exposure. Although a number of the second series of specimens had not flaked after 60 days exposure, it seems probable that flaking would always occur on bare metal parts stored under these conditions for as long as three months. The corrosion rates of all specimens were approximately constant in time.

The behavior of the four alloy systems can be summarized as follows:

1. U-Nb Alloys. The U-4.5 wt% Nb alloy specimens gamma quenched and heat treated at 300° C showed the best corrosion resistance of all specimens, a weight gain rate of about 0.002 mg/cm^2/day. Those heat treated at 500 and 550° C showed a tenfold increase in corrosion rate.

[redacted]

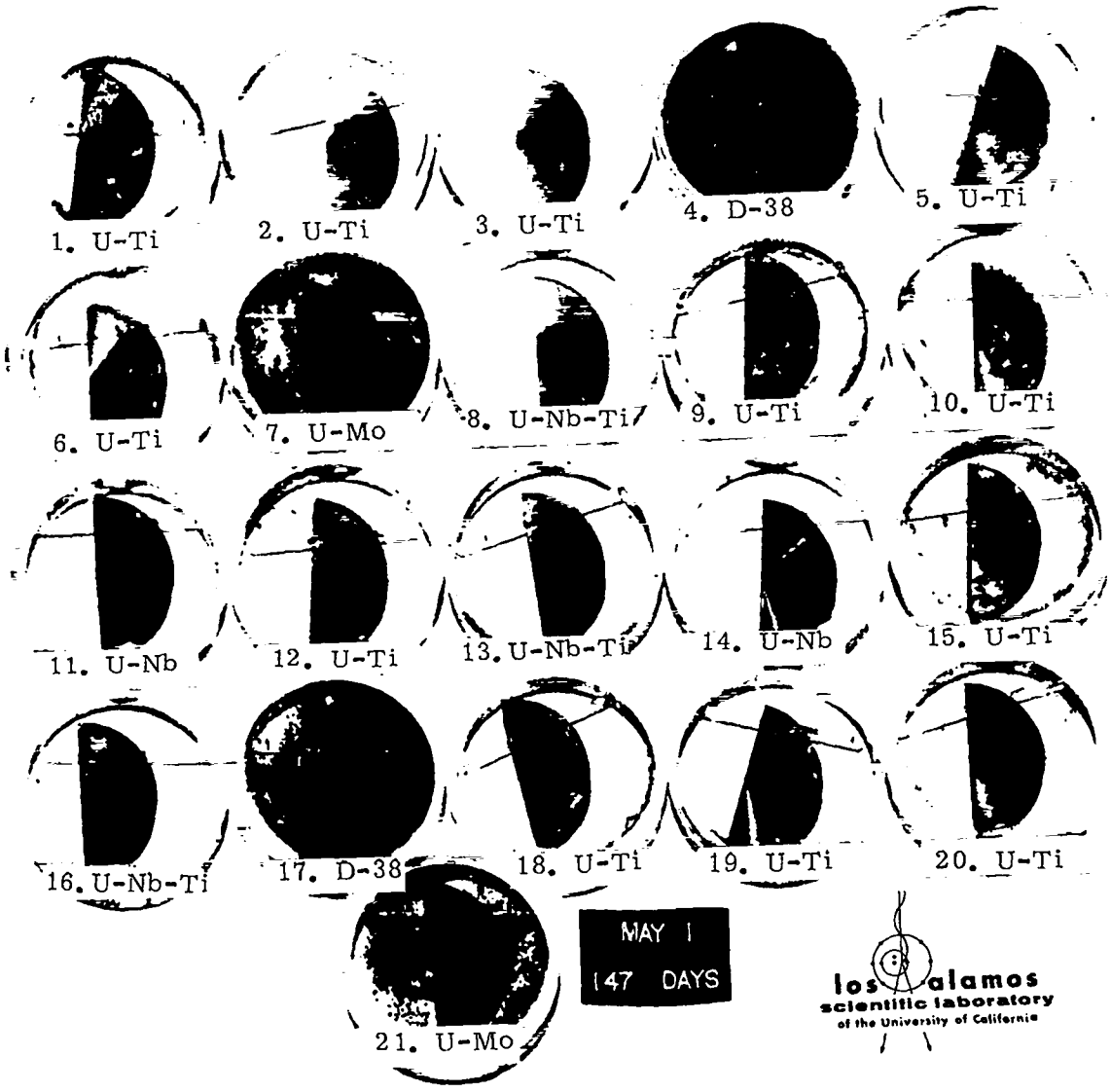

Fig. 22. Corrosion samples 1-21 after 147-day exposure to 165°F and 75% relative humidity.

[redacted]

UNCLASSIFIED

UNCLASSIFIED

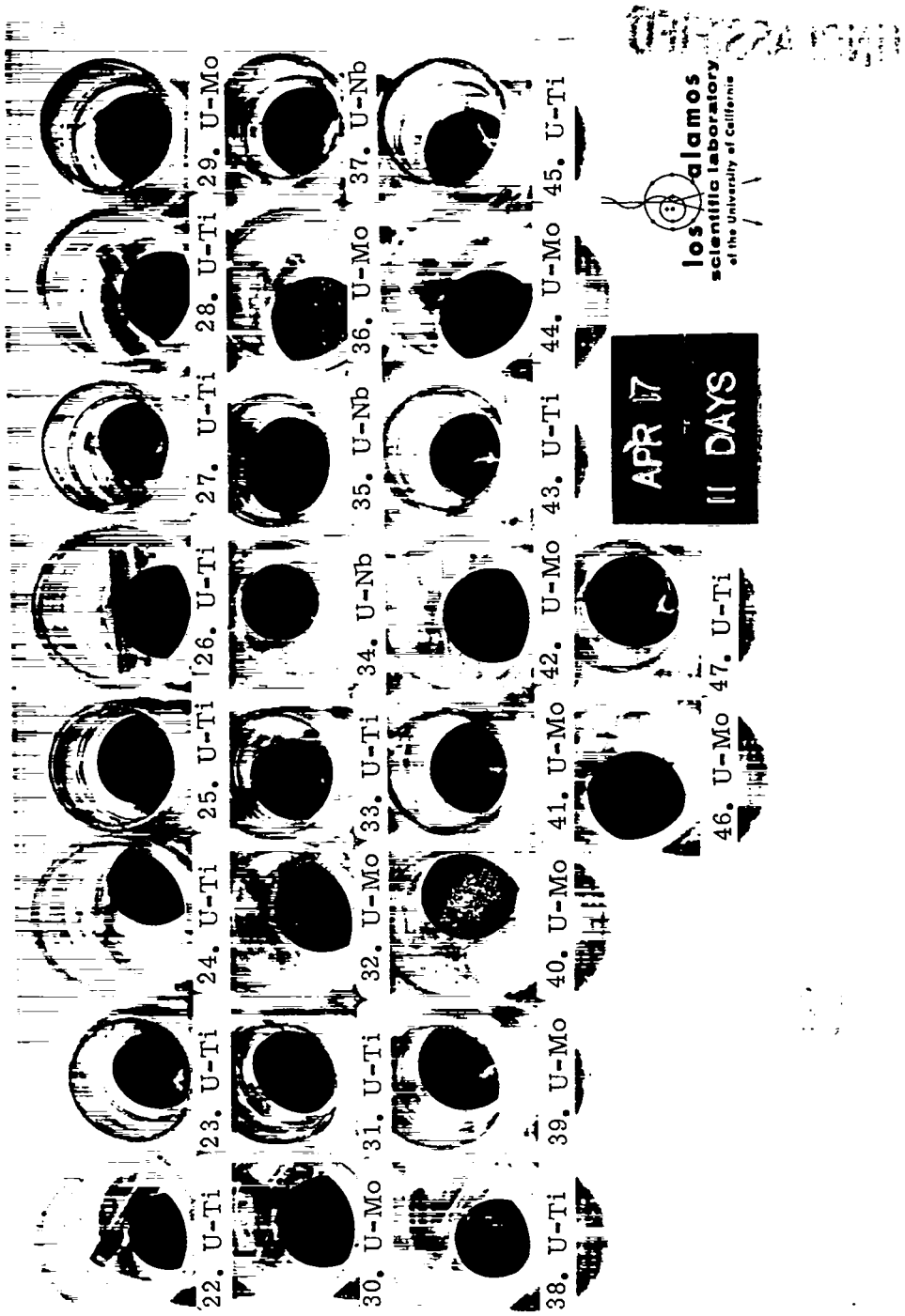

Fig. 23. Corrosion samples 22-47 after 11-day exposure to 165°F and 75% relative humidity.

UNCLASSIFIED

UNCLASSIFIED

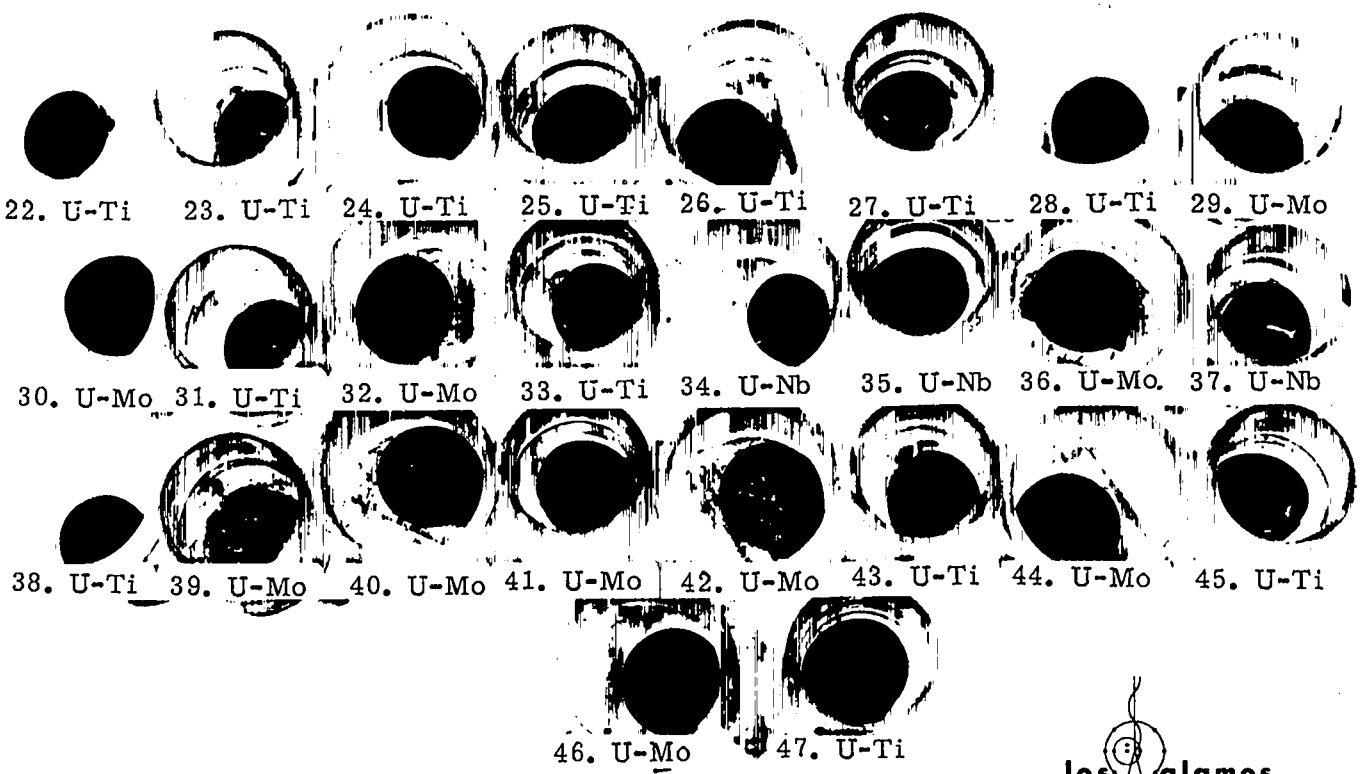

los alamos
scientific laboratory
of the University of California

Fig. 24. Corrosion samples 22-47 after 18-day exposure to 165°F and 75% relative humidity.

UNCLASSIFIED

UNCLASSIFIED

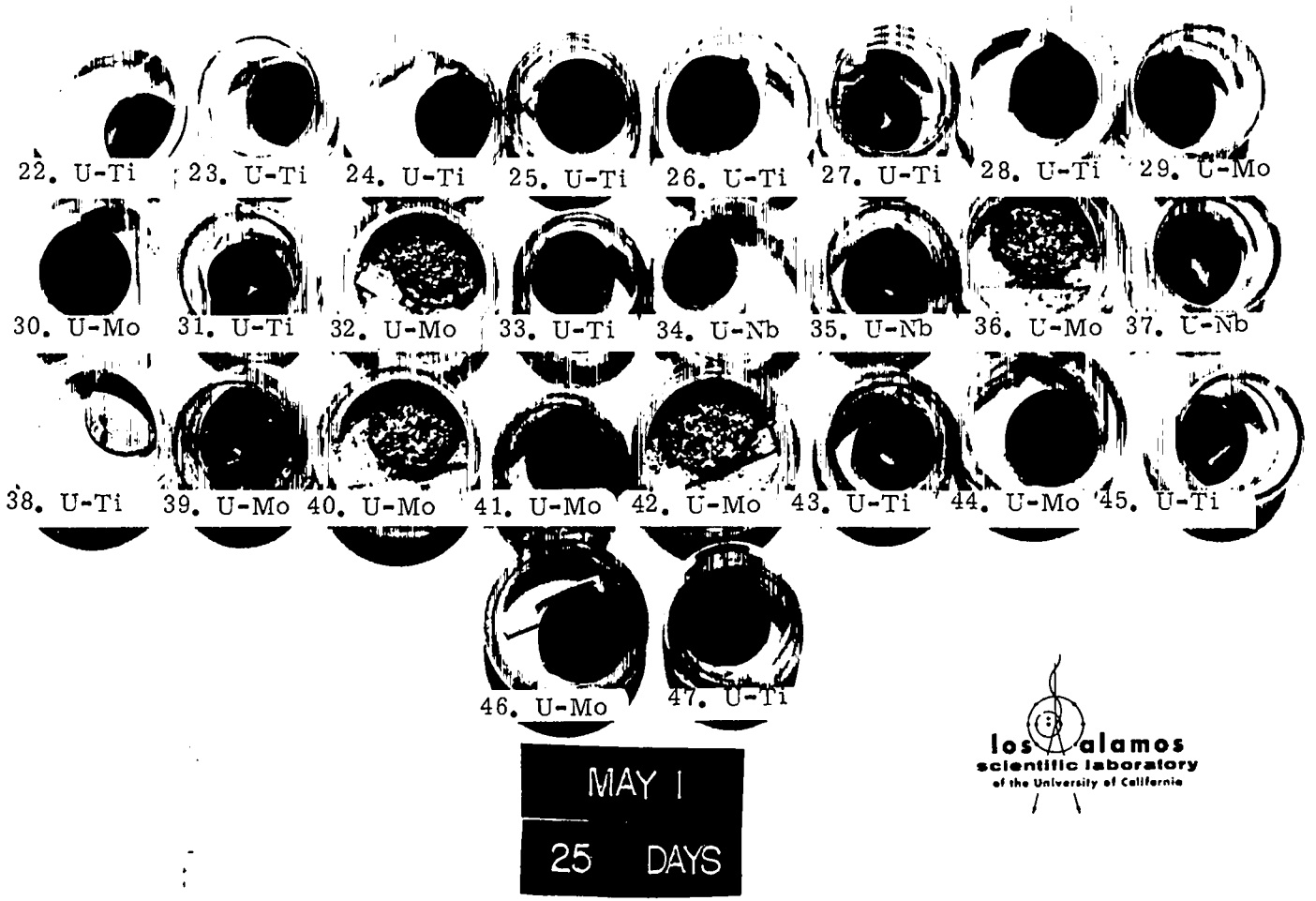

Fig. 25. Corrosion samples 22-47 after 25-day exposure to 165°F and 75% relative humidity.

APPROVED FOR PUBLIC RELEASE

UNCLASSIFIED

UNCLASSIFIED

UNCLASSIFIED

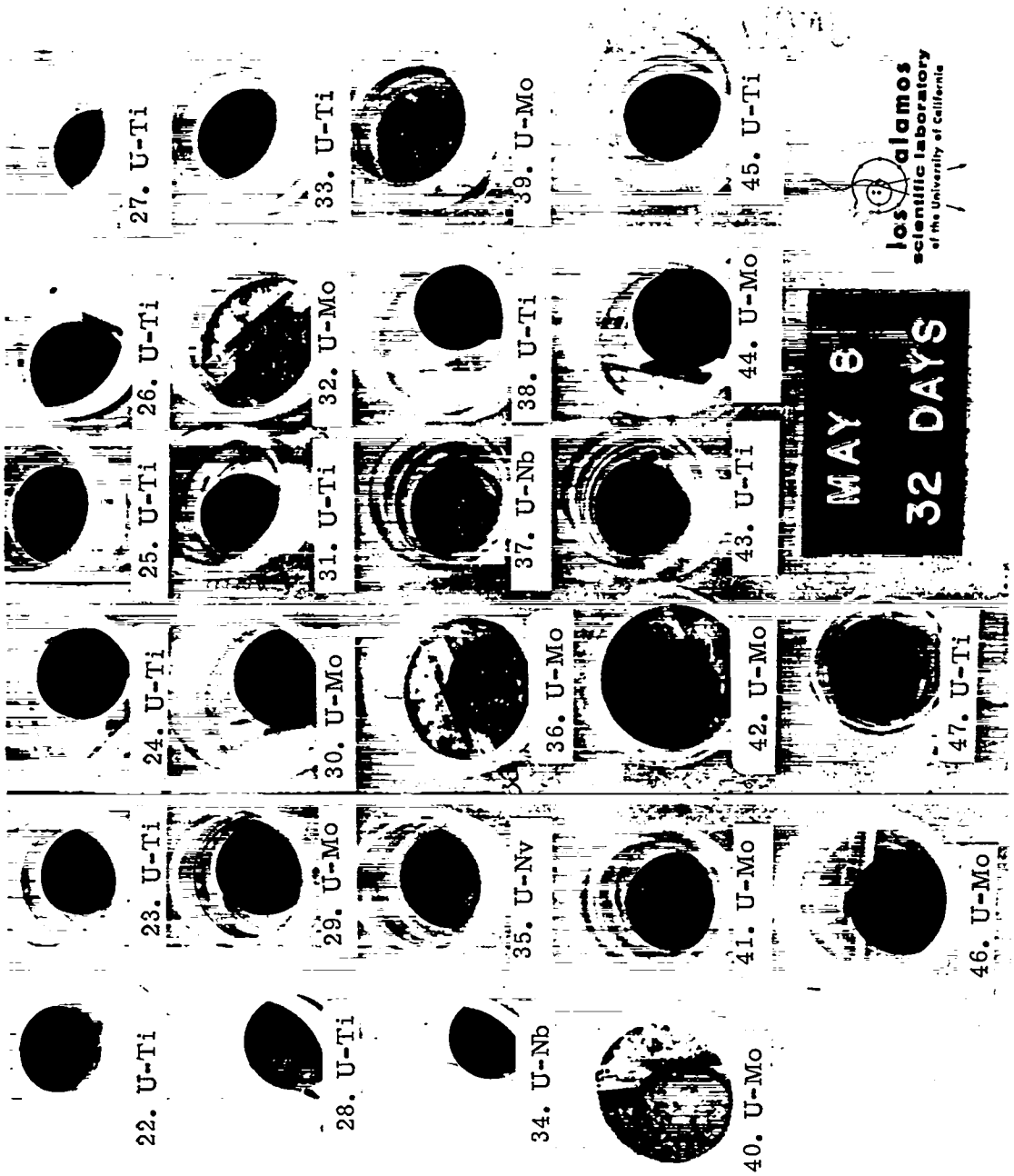

Fig. 26. Corrosion samples 22-47 after 32-day exposure to 165°F and 75% relative humidity.

UNCLASSIFIED

UNCLASSIFIED

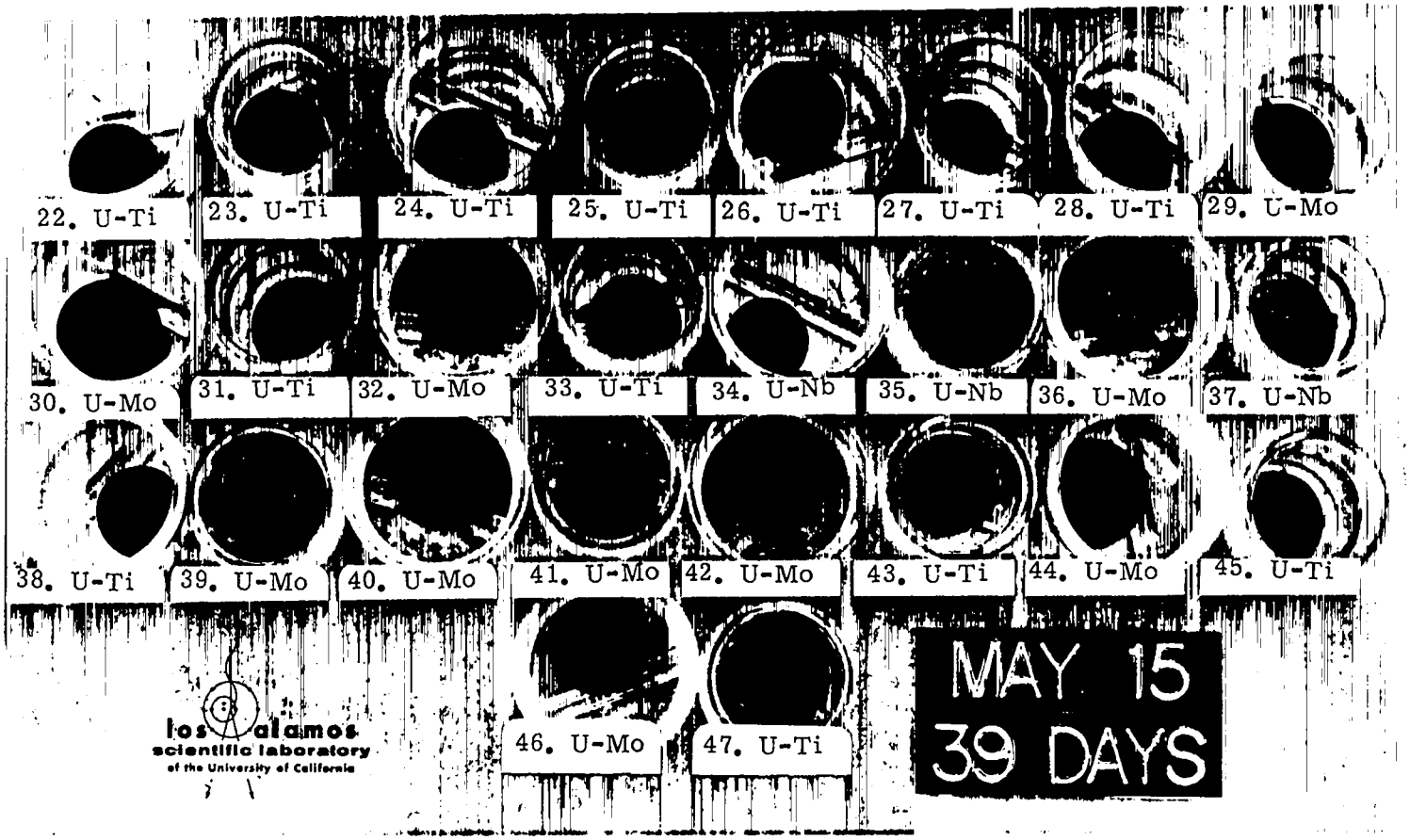

Fig. 27. Corrosion samples 22-47 after 39-day exposure to 165°F and 75% relative humidity.

UNCLASSIFIED

APPROVED FOR PUBLIC RELEASE

UNCLASSIFIED

UNCLASSIFIED

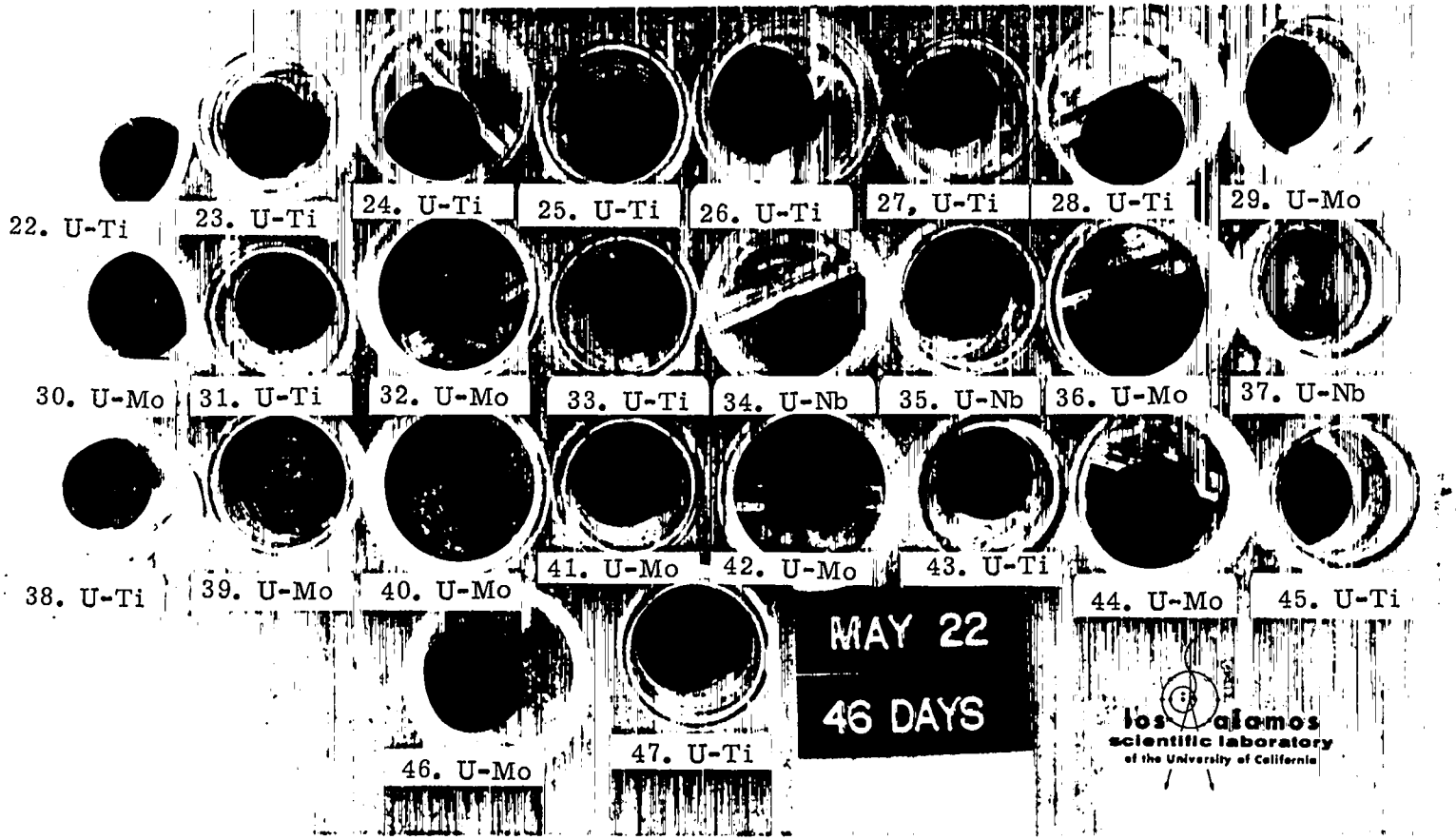

Fig. 28. Corrosion samples 22-47 after 46-day exposure to 165°F and 75% relative humidity.

UNCLASSIFIED

UNCLASSIFIED

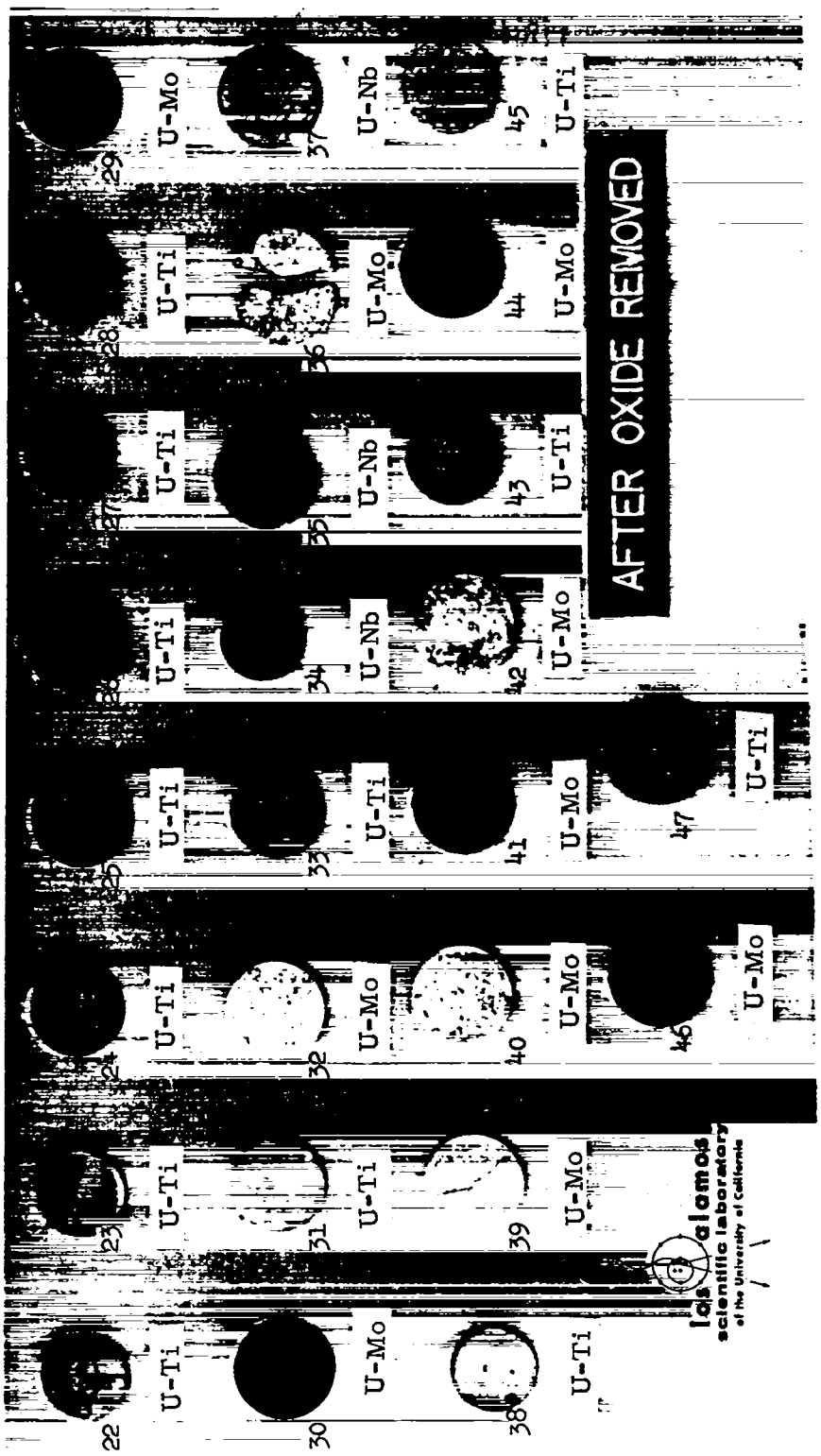

Fig. 29. Corrosion samples 22-47 after removal of oxide layer by pickling in nitric acid.

UNCLASSIFIED

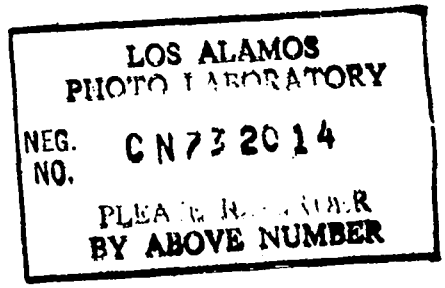

UNCLASSIFIED

[redacted]

TABLE VII

CORROSION-TEST RESULTS ARRANGED BY ALLOY COMPOSITION

Sample Number	Alloy Composition	Heat Treatment	Corrosion Rate ($mg/cm^2/day$)
7	U-2.04 wt% Mo	γ-quench + aged 300°C, 4 h	0.1523
36	U-1.94 wt% Mo	γ-quench + aged 300°C, 4 h	0.1860
32	U-1.94 wt% Mo	γ-quench + aged 300°C, 4 h	0.1453
39	U-1.94 wt% Mo	γ-quench + aged 300°C, 4 h	0.1536
40	U-2.03 wt% Mo	γ-quench + aged 300°C, 4 h	0.1101
42	U-2.03 wt% Mo	γ-quench + aged 300°C, 4 h	0.1048
30	U-2.04 wt% Mo	γ-quench + aged 450°C, 4 h	0.0608
29	U-2.04 wt% Mo	γ-quench + aged 550°C, 4 h	0.0307
21	U-2.04 wt% Mo	Isothermal quench at 500°C, 3 h	0.0792
46	U-1.94 wt% Mo	Isothermal quench at 500°C, 3 h	0.0421
41	U-2.03 wt% Mo	Isothermal quench at 500°C, 3 h	0.0637
44	U-2.03 wt% Mo	Isothermal quench at 500°C, 3 h	0.0710
14	U-4.65 wt% Nb	γ-quench + aged 300°C, 4 h	0.0016
37	U-4.68 wt% Nb	γ-quench + aged 300°C, 4 h	0.0021
35	U-4.68 wt% Nb	γ-quench + aged 450°C, 4 h	0.0034
11	U-4.65 wt% Nb	γ-quench + aged 500°C, 4 h	0.0206
34	U-4.68 wt% Nb	γ-quench + aged 550°C, 4 h	0.0177
8	U-1.20 wt% Nb -1.82 wt% Ti	γ-quench + aged 450°C, 4 h	0.0030
16	U-1.20 wt% Nb -1.82 wt% Ti	γ-quench + aged 500°C, 4 h	0.0033
13	U-1.20 wt% Nb -1.82 wt% Ti	Isothermal quench at 500°C, 3 h	0.0050
4	U (unalloyed)	Rolled sheet	0.1380
17	U (unalloyed)	As cast	0.1248
10	U-0.62 wt% Ti	γ-quench + aged 450°C, 4 h	0.0085

TABLE VII
(Continued)

Sample Number	Alloy Composition	Heat Treatment	Corrosion Rate ($mg/cm^2/day$)
28	U-0.62 wt% Ti	γ-quench + aged 450°C, 4 h	0.0077
20	U-0.62 wt% Ti	γ-quench + aged 550°C, 4 h	0.0140
26	U-0.62 wt% Ti	γ-quench + aged 550°C, 4 h	0.0131
15	U-0.62 wt% Ti	Isothermal quench at 500°C, 3 h	0.0142
33	U-0.73 wt% Ti	γ-quench + aged 300°C, 4 h	0.0050
45	U-0.71 wt% Ti	γ-quench + aged 450°C, 4 h	0.0051
47	U-0.73 wt% Ti	γ-quench + aged 450°C, 4 h	0.0033
27	U-0.76 wt% Ti	γ-quench + aged 450°C, 4 h	0.0086
9	U-0.77 wt% Ti	γ-quench + aged 450°C, 4 h	0.0204
38	U-0.73 wt% Ti	γ-quench + aged 450°C, 4 h	0.0105
43	U-0.71 wt% Ti	γ-quench + aged 550°C, 4 h	0.0175
31	U-0.76 wt% Ti	γ-quench + aged 550°C, 4 h	0.0134
18	U-0.76 wt% Ti	Isothermal quench at 500°C, 3 h	0.0137
19	U-0.84 wt% Ti	γ-quench + no age	0.0090
12	U-0.84 wt% Ti	γ-quench + aged 450°C, 4 h	0.0162
23	U-0.84 wt% Ti	γ-quench + aged 450°C, 4 h	0.0024
1	U-0.84 wt% Ti	γ-quench + aged 550°C, 4 h	0.0285
22	U-0.83 wt% Ti	γ-quench + aged 550°C, 4 h	0.0498
5	U-0.84 wt% Ti	Isothermal quench at 500°C, 3 h	0.0074
2	U-1.17 wt% Ti	γ-quench + aged 450°C, 4 h	0.0106
25	U-1.17 wt% Ti	γ-quench + aged 450°C, 4 h	0.0032
3	U-1.17 wt% Ti	γ-quench + aged 550°C, 4 h	0.0154
24	U-1.17 wt% Ti	γ-quench + aged 550°C, 4 h	0.0142
6	U-1.17 wt% Ti	Isothermal quench at 500°C, 3 h	0.0122

2. U-Nb-Ti Alloys. The U-Nb-Ti sample aged at 450°C had the second lowest corrosion rate, 0.003 $mg/cm^2/day$, of all candidate alloys. However, the fact that two out of three specimens developed cracks indicates that thorough stress-corrosion studies would be necessary before U-Nb-Ti could be recommended as a penetrator material.

3. U-Ti Alloys. Overaging of these alloys at 550°C was definitely harmful to their corrosion resistance, causing an average corrosion rate of 0.02 $mg/cm^2/day$, as compared to 0.0118 for the isothermally quenched alloys and 0.0077 for those aged at 450°C. Fortunately, the 450°C age also develops maximum penetration performance for this system.

4. U-Mo Alloys. The higher temperature heat treatments, 550°C age in vacuum and isothermal quench at 500°C, gave the best corrosion resistance, approaching that of the poorer U-Nb and U-Ti alloys. The specimens heat treated at 300°C had poor corrosion resistance, not appreciably better than that of unalloyed uranium.

To simplify comparison of the alloys, Fig. 30 shows the average corrosion rate for each candidate alloy in the heat-treatment condition necessary for optimum penetration performance. The rate for pure uranium is included for reference. On this basis, U-Ti and U-Nb are the most desirable candidates, since U-Nb-Ti is suspect because of stress-corrosion cracking.

TABLE VIII

CORROSION-TEST RESULTS ARRANGED BY SAMPLE NUMBER

Sample Number	Alloy Composition	Heat Treatment	Corrosion Rate (mg/cm^2/day)
1	U-0.84 wt% Ti	γ-quench + aged 550°C, 4 h	0.0285
2	U-1.17 wt% Ti	γ-quench + aged 450°C, 4 h	0.0106
3	U-1.17 wt% Ti	γ-quench + aged 550°C, 4 h	0.0154
4	U (unalloyed)	Rolled sheet	0.1248
5	U-0.84 wt% Ti	Isothermal quench at 500°C, 3 h	0.0074
6	U-1.17 wt% Ti	Isothermal quench at 500°C, 3 h	0.0122
7	U-2.04 wt% Mo	γ-quench + aged 300°C, 4 h	0.1523
8	U-1.20 wt% Nb -1.84 wt% Ti	γ-quench + aged 450°C, 4 h	0.0030
9	U-0.77 wt% Ti	γ-quench + aged 450°C, 4 h	0.0204
10	U-0.62 wt% Ti	γ-quench + aged 450°C, 4 h	0.0085
11	U-4.59 wt% Nb	γ-quench + aged 500°C, 4 h	0.0206
12	U-0.84 wt% Ti	γ-quench + aged 450°C, 4 h	0.0162
13	U-1.20 wt% Nb -1.84 wt% Ti	Isothermal quench at 500°C, 3 h	0.0050
14	U-4.59 wt% Nb	γ-quench + aged 300°C, 4 h	0.0016
15	U-0.62 wt% Ti	Isothermal quench at 500°C, 3 h	0.0142
16	U-1.20 wt% Nb -1.84 wt% Ti	γ-quench + aged 500°C, 4 h	0.0033
17	U (unalloyed)	As cast	0.1248
18	U-0.77 wt% Ti	Isothermal quench at 500°C, 3 h	0.0137
19	U-0.84 wt% Ti	γ-quench - no age	0.0090
20	U-0.62 wt% Ti	γ-quench + aged 500°C, 4 h	0.0140
21	U-2.03 wt% Mo	Isothermal quench at 500°C, 3 h	0.0792
22	U-0.83 wt% Ti	γ-quench + aged 550°C, 4 h	0.0498
23	U-0.84 wt% Ti	γ-quench + aged 450°C, 4 h	0.0024
24	U-1.17 wt% Ti	γ-quench+ aged 550°C, 4 h	0.0142

TABLE VIII
(Continued)

Sample Number	Alloy Composition	Heat Treatment	Corrosion Rate (mg/cm^2/day)
25	U-1.17 wt% Ti	γ-quench + aged 450°C, 4 h	0.0032
26	U-0.62 wt% Ti	γ-quench + aged 550°C, 4 h	0.0131
27	U-0.77 wt% Ti	γ-quench + aged 450°C, 4 h	0.0086
28	U-0.62 wt% Ti	γ-quench + aged 450°C, 4 h	0.0077
29	U-2.04 wt% Mo	γ-quench + aged 550°C, 4 h	0.0307
30	U-2.04 wt% Mo	γ-quench + aged 450°C, 4 h	0.0608
31	U-0.77 wt% Ti	γ-quench + aged 550°C, 4 h	0.0134
32	U-1.94 wt% Mo	γ-quench + aged 300°C, 4 h	0.1453
33	U-0.73 wt% Ti	γ-quench + aged 300°C, 4 h	0.0050
34	U-4.68 wt% Nb	γ-quench + aged 550°C, 4 h	0.0177
35	U-4.68 wt% Nb	γ-quench + aged 450°C, 4 h	0.0034
36	U-1.94 wt% Mo	γ-quench + aged 300°C, 4 h	0.1860
37	U-4.64 wt% Nb	γ-quench + aged 300°C, 4 h	0.0021
38	U-0.73 wt% Ti	γ-quench + aged 450°C, 4 h	0.0105
39	U-1.96 wt% Mo	γ-quench + aged 300°C, 4 h	0.1536
40	U-2.03 wt% Mo	γ-quench + aged 300°C, 4 h	0.1101
41	U-2.03 wt% Mo	Isothermal quench at 500°C, 3 h	0.0637
42	U-2.03 wt% Mo	γ-quench + aged 300°C, 4 h	0.1048
43	U-0.71 wt% Ti	γ-quench + aged 550°C, 4 h	0.0175
44	U-2.03 wt% Mo	Isothermal quench at 500°C, 3 h	0.0710
45	U-0.71 wt% Ti	γ-quench + aged 450°C, 4 h	0.0051
46	U-1.94 wt% Mo	Isothermal quench at 500°C, 3 h	0.0421
47	U-0.73 wt% Ti	γ-quench + aged 450°C, 4 h	0.0033

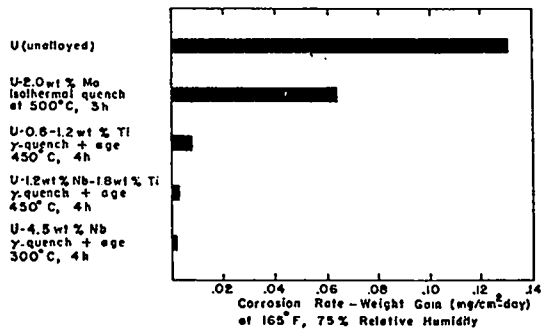

Fig. 30. Comparison of the corrosion rate of candidate uranium alloys.

IV. PENETRATION PERFORMANCE

A. Ballistic-Test Conditions

Although the goal of this project was to develop a penetrator alloy for use in 30-mm AP projectiles, we performed the bulk of the ballistic testing with .50-caliber projectiles. We believed that the relative performance of the alloys would be the same for both projectile sizes and that we could perform a more extensive test program within the time and money limitations of the contract if we used the scaled-down projectiles. In

fact, we fired about three times as many test shots as would have been possible with the 30-mm projectiles alone.

The ballistic testing consisted of establishing a protection ballistic limit (PBL) at 0, 30, and 60° obliquities (angle between projectile trajectory and the normal to the armor surface) using projectiles with penetrator cores fabricated from the candidate uranium alloys. The PBL as used in this report is defined as the average projectile velocity taken over the three highest velocities that failed to produce penetration of the target armor and the three lowest velocities that did. The maximum allowable velocity spread over the six shots must be ≤ 150 ft/sec. The armor is said to be penetrated when at least one hole is observed in a 0.020-in.-thick 2024-T3 aluminum witness plate located 6 in. behind the armor.

The armor-plate samples used for the PBL determinations were 1-ft square and varied in thickness from 0.50 to 2.0 in. They were cut from rolled, homogeneous, steel armor plate manufactured to MIL-S-12560B or 13812A, depending on thickness. These two specifications are the same for the purposes of these tests. The hardness (Brinell, 3000-kg load) of each 1-ft square armor target plate was determined from the average of four measurements on its front surface. The hardness so recorded was reproducible from plate to plate of the same thickness, and only the average hardness is reported for each PBL determination. The 30-mm penetration results probably were influenced somewhat by the small area of the target plates. However, this size was acceptable to the Air Force and should not affect the relative performance of the alloys.

The ballistic tests were conducted at the LASL projectile-testing facility shown schematically in Fig. 31. A massive backstop weighing more than 5000 lb when filled with sand was designed to hold the armor target plates. As additional insurance against motion, the backstop was

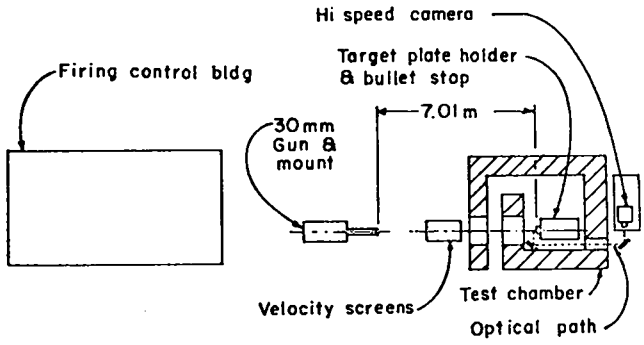

Fig. 31. The projectile-testing facility.

braced front and back against the 3 ft-thick steel-reinforced concrete walls of the firing chamber.

We determined the velocity of each projectile by measuring the time of flight between two electronic "break" screens located 3 ft apart. The first screen was located 12 ft from the muzzle to prevent its being broken prematurely by muzzle gases. The last screen was 15 ft from the target (Fig. 31). The time interval was displayed on an 8-MH_z Potter counter chronograph.

B. Performance of Scaled-Down (.50-Caliber) Penetrators

1. Projectile Design. The initial problem was to develop a .50-caliber projectile containing a uranium-alloy penetrator core that would be stable in flight 30 ft from the rifle muzzle. The design of the penetrator core used in this project was established by the Air Force Armament Laboratory and is illustrated in Fig. 32. This core is a scaled-down version of the 30-mm design and has the same length-to-diameter ratio. The flat nose on the core is reputed to improve performance when attacking at high angles of obliquity. Probably this design will not be the final one, but the results given here will apply to penetrators of this general design.

After more than a hundred shots and three modifications of the basic design we obtained a stable .50-caliber projectile. Figure 32 illustrates the .50-caliber projectile used for the PBL

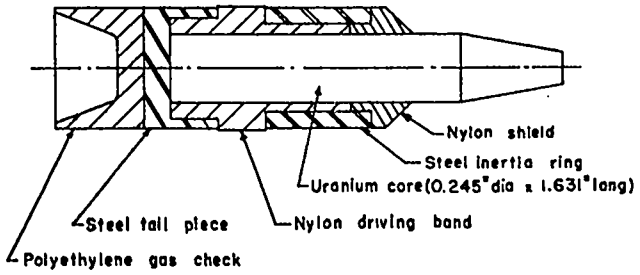

M= 32.7 grams

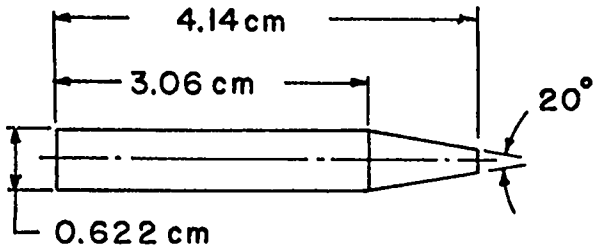

M = 20.4 grams

Fig. 32. The .50-caliber test projectile and uranium penetrator core.

determinations. This design proved stable at velocities exceeding 3500 ft/sec at the short ranges (~ 30 ft) used in these tests. Projectile stability was determined through framing-camera photographs (2.0 μsec/frame) of the projectile taken immediately before and during impact. The major modes of projectile failure were oblique impact because of flight instability, and disassembly of the projectile in flight.

2. Penetration Performance at 0° Obliquity.

Of the four candidate alloys, only U-0.6 to 1.2 wt% Ti, U-2 wt% Mo, and U-4.5 wt% Nb were tested in .50-caliber projectiles at 0° obliquity. The ternary alloy, U-2 wt% Nb - 1 wt% Ti, was reserved for 60° obliquity tests. Several heat treatments were tested for each alloy and a few shots were fired with soft, unalloyed uranium to establish a performance base line. These tests used 1-in.-thick MIL-S-12560B target armor.

Because we wished to include as many different alloy compositions and heat treatments as possible in these initial screening tests, we could fire only a few shots, usually 12 or less, using each material. Sometimes, an actual PBL was not determined in 12 shots, but the data were sufficient to permit comparison of the various alloys and heat treatments. In this section, the data for each material are summarized as a ballistic limit. However, the complete results for every shot are presented in Appendix A.

The most important feature of all the data is that the ballistic limit was nearly the same for all of the candidate materials. The best performing material, a U-Ti alloy, had a PBL of 2860 ft/sec. The material with the worst performance was the soft unalloyed uranium, as expected. We did not determine a PBL for this material, but it was less than 3050 ft/sec. This is only seven percent greater than the lowest PBL, even though the two materials ranged from 35 to 49.6 R_c in hardness. It thus became obvious from these initial screening tests at .50 caliber that we could not expect to develop a material with greatly increased penetration performance. The final choice of an optimum penetrator material, therefore, must rely heavily on other considerations, such as corrosion resistance and fabrication cost.

One of the variables studied in the .50-caliber, 0° obliquity tests was the effect of different titanium concentration on the performance of the U-Ti alloys. Table IX summarizes these data. The difference in PBL's for materials with 0.62 to 1.17 wt% titanium concentration was well within the experimental error. In addition, for a reasonably large range of alloy hardness (44.4 to 56.4 R_c) the PBL remains nearly constant. From these data, we conclude that, at 0° obliquity, a wide range of hardness and alloy composition do not appreciably affect penetration performance of the U-Ti alloy system. This indicates that production tolerances for a U-Ti penetrator material could be rather large, which should greatly reduce fabrication costs.

TABLE IX

EFFECT OF VARYING TITANIUM CONTENT ON PENETRATION PERFORMANCE OF .50-CALIBER PROJECTILES WITH U-Ti ALLOY CORES AT 0° OBLIQUITY (Armor thickness and hardness - 1.0 in., 331 BHN)

Alloy	Heat Treatment	Density (g/cm^3)	Hardness (R_c)	PBL (ft/sec)
U(unalloyed)	As cast	18.70	35.0	< 3050
U-0.62 wt% Ti	γ-quench + aged 450°C, 4 h, in vac.	18.65	49.6	2860
U-0.77 wt% Ti	γ-quench + aged 550°C, 4 h, in vac.	18.57	44.4	2880
U-1.17 wt% Ti	γ-quench + aged 450°C, 4 h, in vac.	18.31	56.4	2890

Possibly the most interesting variable in the ballistic study was the comparison of the various alloys with each other. Table X lists the material with the lowest PBL from each alloy group tested at normal incidence. These data show clearly that the U-Ti and U-Mo alloys are superior to the U-Nb alloys. The U-Nb-Ti ternary alloy was not included in the 0° obliquity tests because of difficulty in casting it with the desired composition. Since only a limited quantity of this material was available, we reserved it for the 60° obliquity tests in hopes that we could make a greater distinction in alloy performance.

3. Penetration Performance at 60° Obliquity. In the proposed application of these penetrators, high angles of obliquity are the rule, rather than the exception. Hence, we spent much effort on this testing. Further, we switched some alloy-comparison tests planned at 0° obliquity, to 60° obliquity in the hope that larger differences would appear. Table XI lists the results for the vacuum-aged alloys. The U-Nb alloy was not included in the 60° obliquity tests because its performance at 0° obliquity was measureably poorer than that of either the U-Ti or the U-Mo. The ballistic performance of the other three alloys is about the same. However, the U-Nb-Ti ternary is relatively expensive to produce and also had a marked tendency toward stress-corrosion cracking (Sec. III).

Vacuum aging of the penetrator alloys was first thought to be necessary to minimize the hydrogen impurity concentration that can significantly degrade the low-strain-rate ductility of uranium alloys. However, vacuum aging requires special furnaces that might not be available at prospective production facilities, thus increasing the cost of the mass-produced material. Since our preliminary tests of the alloys' dynamic properties did not reveal any significant difference between vacuum and lead- or salt-bath aging, we decided to determine the effect of lead-bath aging on penetration performance of the alloys. This was done by firing

TABLE X

EFFECT OF DIFFERENT ALLOY SYSTEMS ON PENETRATION PERFORMANCE OF .50 CALIBER PROJECTILES AT 0° OBLIQUITY (Armor thickness and hardness - 1.0 in., 331 BHN)

Alloy	Heat Treatment	Density (g/cm^3)	Hardness (R_c)	PBL (ft/sec)
U-0.62 wt% Ti	γ-quench + aged 450°C, 4 h, in vac.	18.64	49.6	2860
U-1.94 wt% Mo	γ-quench + aged 300°C, 4 h, in vac.	18.53	49.5	2900
U-4.68 wt% Nb	γ-quench + aged 300°C, 4 h, in vac.	17.68	45.7	3000

TABLE XI

EFFECT OF DIFFERENT ALLOY SYSTEMS ON PENETRATION PERFORMANCE OF .50 CALIBER PROJECTILES AT 60° OBLIQUITY (Armor thickness and hardness - 0.5 in., 366 BHN)

Alloy	Heat Treatment	Density (g/cm^3)	Hardness (R_c)	PBL (ft/sec)
U-0.71 wt% Ti	γ-quench + aged 450°C, 4 h, in vac.	18.63	51.4	3190
U-1.96 wt% Mo	γ-quench + aged 300°C, 4 h, in vac.	18.48	45.6	3220
U-2.53 wt% Nb + 1.27 wt% Ti	γ-quench + aged 450°C, 4 h, in vac.	17.95	46.5	3240

a series of shots at 60° obliquity using two lead-aged U-Ti alloys and one lead-aged U-Mo alloy. Table XII lists these results along with results for equivalent vacuum-aged alloys. These data show that the lead-aged alloys make as good a penetrator as the vacuum-aged alloys, to within experimental error. Hence, the lead-aged alloys are a logical choice as penetrator materials on the basis of their reduced cost and equivalent ballistic properties.

Another variable we examined was the effect on PBL of increasing the penetrator ductility through overaging. Although overaging decreases hardness, we felt that the increased ductility might prove an advantage at high angles of obliquity. The materials chosen for this test were U-0.71 wt% Ti alloys, one aged four hours at 450° C (Appendix A, Table A-IX) and the other aged four hours at 550° C (Table A-X). The 450° C aged U-Ti alloy had a hardness of 51.4 R_c and a PBL of 3190 ft/sec at 60° obliquity, whereas the overaged alloy, with a hardness of 44.5 R_c, had a PBL of 3300 ft/sec at 60° obliquity. This large a difference in PBL is significant, and we eliminated the overaged materials as candidate penetrator materials.

TABLE XII

EFFECT OF LEAD-BATH AND VACUUM AGING ON PENETRATION PERFORMANCE OF .50-CALIBER PROJECTILES AT 60° OBLIQUITY
(Armor thickness and hardness - 0.5 in., 364 BHN)

Alloy	Heat Treatment	Density (g/cm3)	Hardness (Rc)	PBL (ft/sec)
U-0.77 wt% Ti	γ-quench + aged 450°C, 4 h, in lead bath	18.60	52.2	3260
U-0.77 wt% Ti	Isothermal quench 500°C, 3 h, in lead bath	18.61	46.5	3260
U-0.71 wt% Ti	γ-quench + aged 450°C, 4 h, in vac.	18.63	51.4	3190
U-2.03 wt% Mo	Isothermal quench (850°C-1h) 500°C, 3 h, in lead bath	18.58	51.1	3100
U-1.94 wt% Mo	γ-quench + aged 300°C, 4 h, in vac.	18.48	45.6	3220

In summary, the .50-caliber testing showed that the U-Ti, U-Mo, and U-Nb-Ti alloys behave much the same. We chose the two alloys to be tested in 30-mm projectiles on the basis of relative cost, ease of fabrication, and lack of tendency toward stress-corrosion cracking. On this basis, we chose the gamma-quenched, lead-aged, U-0.75 wt% Ti and the isothermal-quenched, lead-aged, U-2 wt% Mo alloys.

C. Penetration Performance of 30-mm Projectiles

The 30-mm tests consisted of determining PBL's for penetrators fabricated from the two selected alloys (U-0.75 wt% Ti and U-2.0 wt% Mo) at 0, 30, and 60° obliquity. Figure 33 shows both the penetrator core and the assembled 30-mm projectile used for these tests. The diameters are such that the end cap, driving band, and inertia ring all contact the rifling. Projectiles of this design were stable at velocities exceeding 3300 ft/sec., at a range of 23 ft. Figure 34 shows the 30-mm projectile and core compared with the corresponding .50-caliber parts.

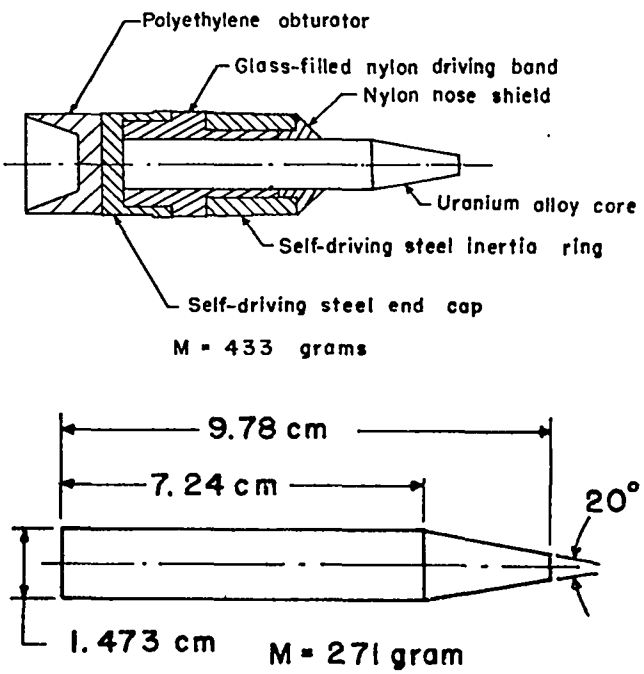

Fig. 33. The 30-mm test projectile and uranium penetrator core.

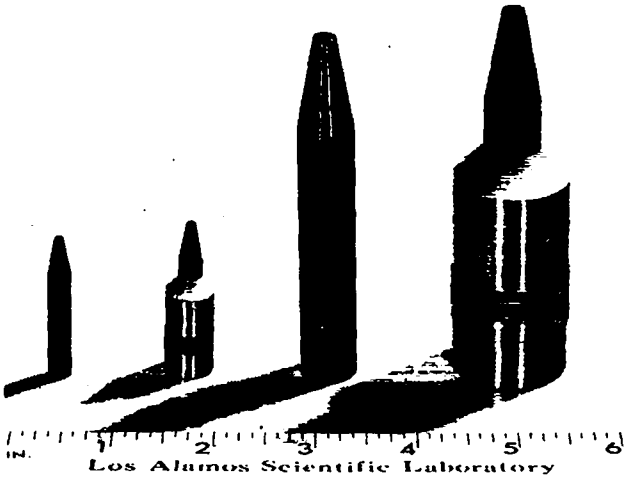

Fig. 34. The 30-mm and .50-caliber test projectiles and cores.

The 30-mm gun barrel and breech used in these tests were built by Mathewson Tool Company, according to GW Amron Corporation drawings. Figure 35 shows the gun in the modified Frankfort mount. The 30-mm aluminum cases and primers were obtained through Eglin AFB. The powder used was CIL 1379C, also provided by Eglin AFB.

The data from the 30-mm penetration tests are summarized in Table XIII and presented in detail in Appendix A. These data confirm the results of the .50-caliber tests, in that the penetration performance is the same within the experimental error for these two alloys. Final choice of a penetrator material must, then, be based on other factors, and we recommend the U-0.75 wt% Ti alloy because it is much more resistant to corrosion and is probably more economical to produce.

TABLE XIII

30-MM BALLISTIC TEST RESULTS

Alloy	Heat Treatment	Density (g/cm^3)	Hardness (Rc)	PBL (ft/sec)
Armor: 2-in.-thick MIL-S-13812A, BHN 280				
Obliquity Angle - 0°				
U-0.75 to 0.83 wt% Ti	γ-quench + aged 450°C, 4 h, lead bath	18.59	52.2	2260
U-2.12 wt% Mo	Isothermal quench aged 500°C, 3 h, lead bath	18.60	50	2330
Obliquity Angle - 30°				
U-0.62 to 0.70 wt% Ti	γ-quench + aged 450°C, 4 h, lead bath	18.62	52.7	2460
U-1.84 wt% Mo	Isothermal quench aged 500°C, 3 h, lead bath	18.66	48.5	2550
Armor: 1.25-in.-thick MIL-S-12560B, BHN 304				
Obliquity Angle - 60°				
U-0.70 to 0.83 wt% Ti	γ-quench + aged 450°C, 4 h, lead bath	18.61	53	3030
U-1.84 wt% Mo	Isothermal quench aged 500°C, 3 h, lead bath	18.68	48	3070

Fig. 35. The 30-mm gun used for penetration-performance tests.

V. PHENOMENOLOGY OF URANIUM PENETRATOR-ARMOR INTERACTION

Although the mechanics of armor penetration by kinetic-energy projectiles has been studied for many years, it has recently received renewed effort. This largely results from the development of two-dimensional hydrodynamic computer codes that make it possible to attempt numerical solutions to the complex equations of motion governing the impact response of penetrators and armor.[32-34] The intent is to develop numerical or analytical models that correctly describe the observed response, in hopes of using them to predict

penetration performance on the basis of material properties and initial projectile geometry. These models could, in turn, greatly reduce the experimental work required in developing an optimum penetrator material or design.

So far, there has been little work concerning the system of interest in this project, penetration of relatively thick metallic armor (thickness several times greater than projectile diameter) by high-density penetrator cores. A thorough theoretical study of uranium penetrators was beyond the scope of this project, but we did some work to develop an understanding of the qualitative behavior of uranium penetrators, in hopes that this will guide the way toward furture investigations and optimization of penetrator design.

This effort consisted of high-speed photography of .50-caliber projectile core impacts, flash radiography of 30-mm test projectiles penetrating armor, and post-impact metallography of penetrators and armor. Each is discussed separately below.

A. High-Speed Photography of .50-Caliber Projectile Core Impacts.

Fairly early in the project, we devised a method for using a high-speed framing camera to observe the impact process on a microsecond time scale. Our intent was to compare the resistance to tip deformation of the various candidate alloys directly. The camera was a Beckman-Whitley, Model-189, synchronous-framing camera, capable of more than one million frames per second. However, since only 25 exposures can be obtained per shot, we typically used a framing rate of 330,000 frames/sec to obtain longer coverage of the penetration process.

For these experiments, we could not use a gun to launch the .50-caliber projectile cores, because the time of impact must be synchronized with the rotating mirror of the camera to within a few microseconds. The firing of a gun cannot be timed that precisely, so we had to reverse the impact and use high explosives to drive sections of the test armor against stationary penetrator cores. Detonation of explosives can be timed easily to a microsecond, and, for 0° obliquity impacts, the penetration process is affected only by the relative velocity of core and target. This technique has the added advantage of allowing several cores made from different alloys to be tested at the same time. Excerpts from the framing-camera records on two of these experiments are shown in Figs. 36 and 37.

In Fig. 36 the steel plate is a section of MIL-S-12560B armor identical to those used in the penetration-performance tests. Its velocity is approximately 2800 ft/sec, chosen to be near the ballistic limit for the uranium cores. The cores are identical to those used in the .50-caliber ballistic-limit tests (Fig. 37), except that one was made from 1095 steel, hardened to approximately 65 R_c, instead of uranium.

The behavior of the steel core graphically points up the advantage of using high-density materials for penetrators. The steel is much harder than any of the uranium cores, yet it exhibits much more back-spray, or spall, with a resultant decrease in the kinetic energy being delivered to the target. This is not surprising, since, for these flat-nosed projectiles and at these velocities, pressures of approximately 200 kbar are generated at the penetrator-armor interface. Since the dynamic compressive strengths or Hugoniot elastic limits of both uranium and steel are much lower than this (Table XIV) only a small amount of the stress tending to shear off an element of penetrator material at the interface can be transferred to the penetrator as a whole. At these impact velocities, then, localized inertial forces are much more important in controlling the radial flow of penetrator material than is the material's shear strength. The highest density material will thus undergo the least deformation. In other words, the penetrator-material's strength becomes less important as impact velocity increases. These remarks apply

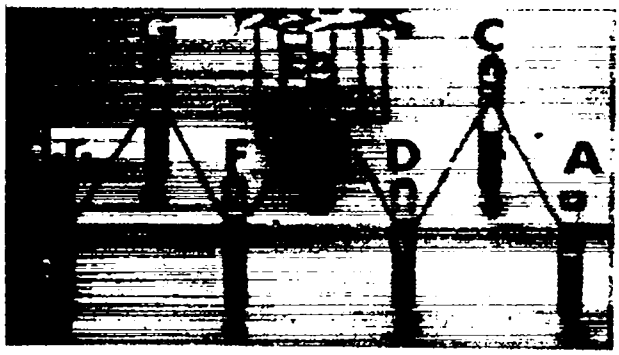

0 μsec

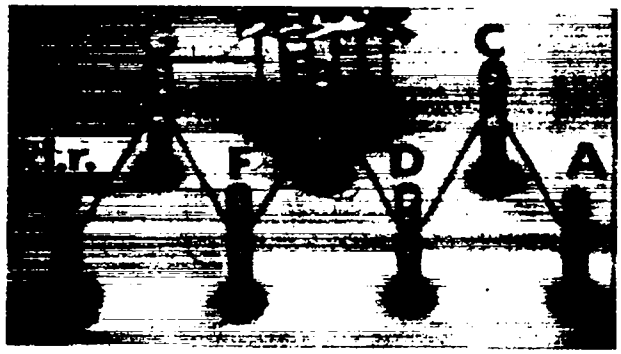

24 μsec

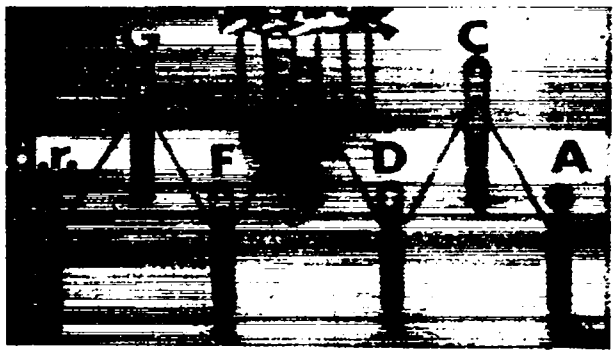

6 μsec

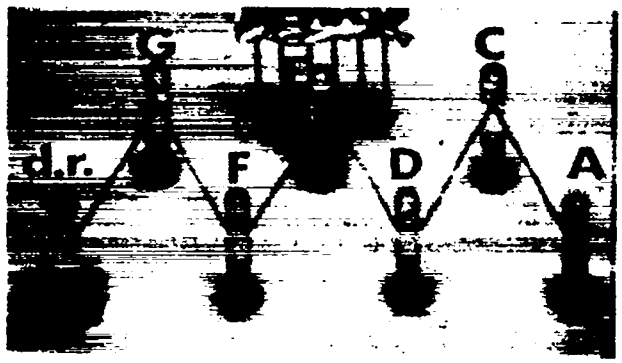

30 μsec

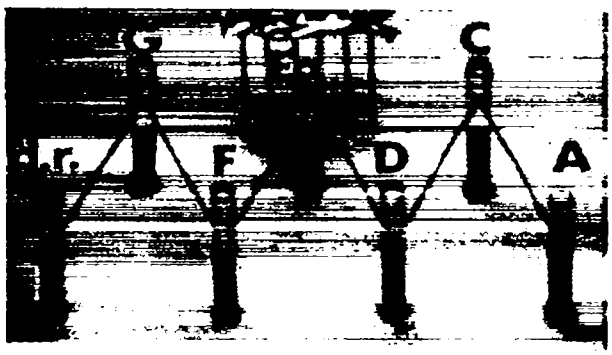

12 μsec

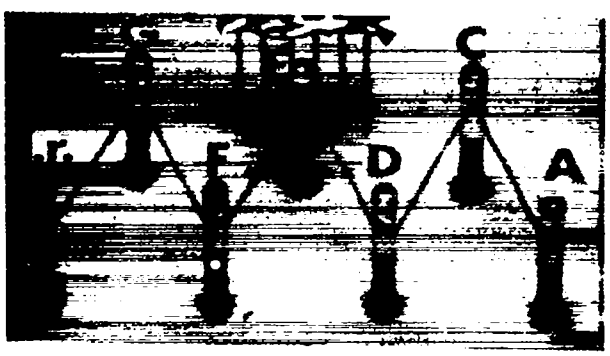

18 μsec

Fig. 36. Framing-camera photographs of explosively driven section of 1-in.-thick steel armor (MIL-S-12560B) striking .50-caliber projectile cores. The approximate time after initial impact is shown for each frame. The core material is as follows:

A. Cast, unalloyed uranium, hardness 35 R_C
C. U-2 wt% Mo, isothermal quench, 3 h, in lead, hardness 51 R_C
D. U-0.75 wt% Ti, γ-quench + age, 450°C, 4 h, in lead, hardness 52 R_C
E. U-0.75 wt% Ti, γ-quench + age, 550°C, 4 h, in vac., hardness 44 R_C
F. U-4.65 wt% Nb, γ-quench + age, 300°C, 4 h, in vac., hardness 46 R_C
G. U-2.5 wt% Nb-1.25 wt% Ti, γ-quench + aged, 450°C, 4 h, in vac., hardness 46 R_C
d.r. 1095 steel, hardness ~ 65 R_C

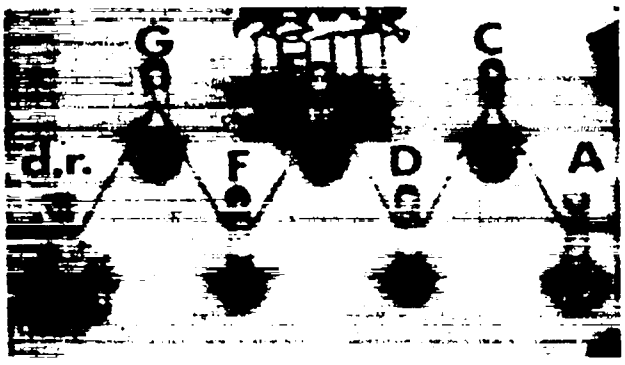

36 μsec

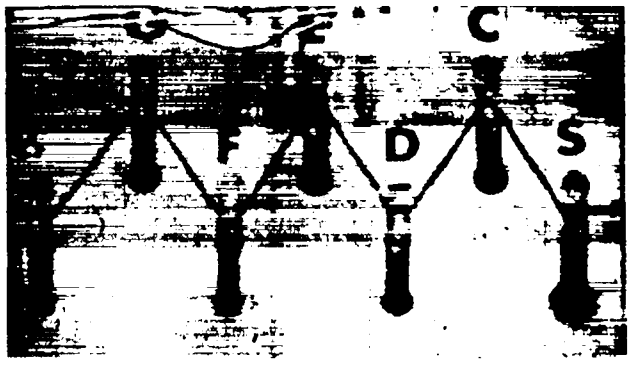

12 μsec

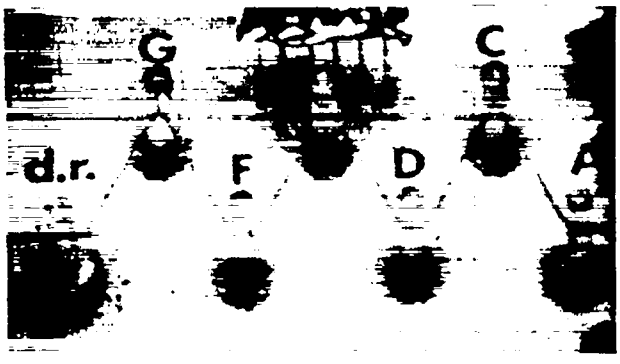

42 μsec

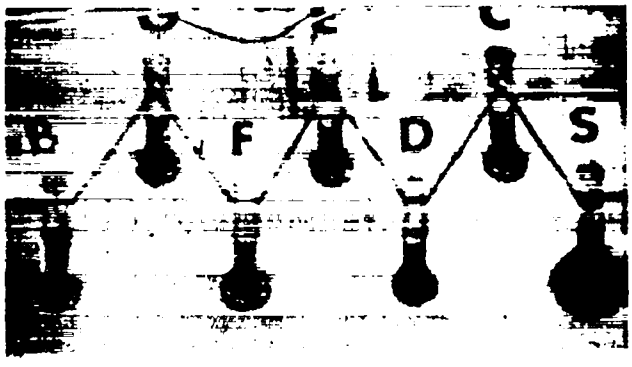

18 μsec

Fig. 36. Continued.

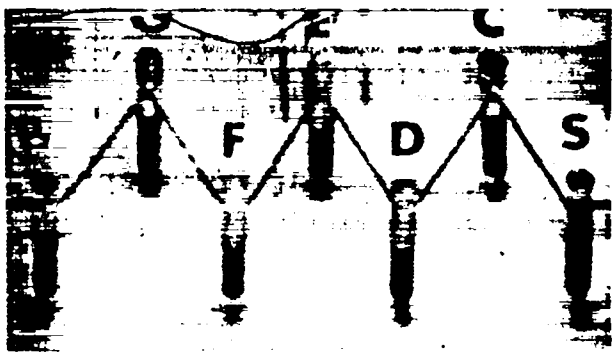

0 μsec

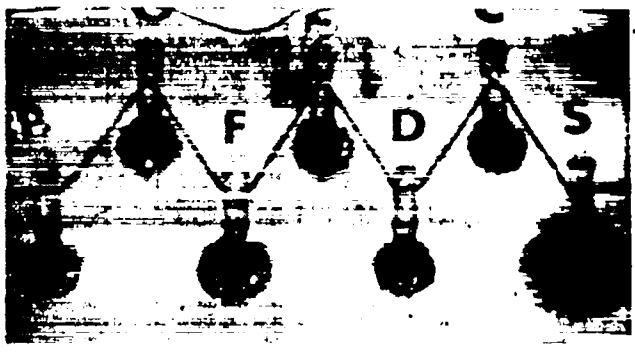

24 μsec

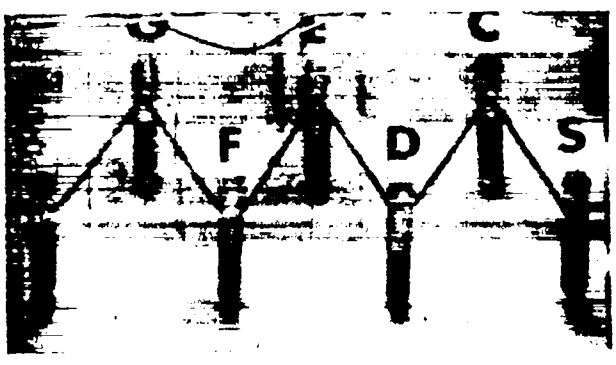

6 μsec

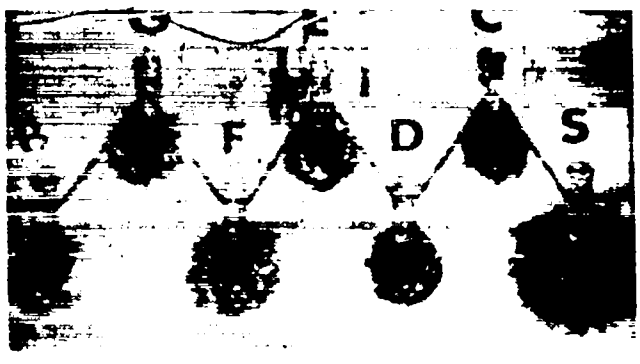

30 μsec

[redacted]

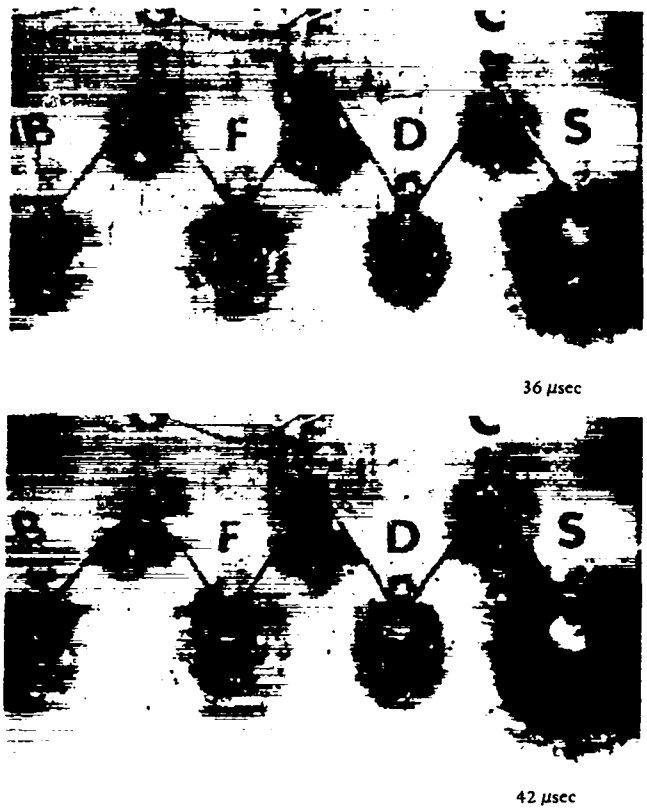

Fig. 37. Framing-camera photographs of explosively driven 1-in.-thick section of 4340 steel (hardness, 50 R_c) striking .50-caliber projectile cores. Core materials are as follows:

- B. U-2 wt% Mo, γ-quench + age, 300°C, 4 h, in vac., hardness 50 R_c
- C. U-2 wt% Mo, isothermal quench, 3 h, in lead, hardness 51 R_c
- D. U-0.75 wt% Ti, γ-quench + age, 450°C, 4 h, in lead, hardness 52 R_c
- E. U-0.75 wt% Ti, γ-quench + age, 550°C, 4 h, in vac., hardness 46 R_c
- F. U-4.65 wt% Nb, γ-quench + age, 300°C, 4 h, in vac., hardness 46 R_c
- G. U-2.5 wt% Nb-1.25 wt% Ti, γ-quench + age, 450°C, 4 h, in vac., hardness 46 R_c
- S. 1095 steel, hardness ~ 65 R_c

TABLE XIV

SOME PROPERTIES OF ARMOR-PIERCING PENETRATOR MATERIALS

Material	Density (g/cm³)	Bulk Sound Velocity (km/sec)	Bar Sound Velocity (km/sec)	Hugoniot Elastic Limit (kbar)
U-0.84 wt% Ti	18.49	2.44	3.21	20 - 24
Tungsten	19.27	4.01	4.62	32
Tungsten carbide	15.00	4.91	6.50	40
High-strength steel	7.86	4.59	5.16	20 - 25

only to flat-nosed penetrators that penetrate by punching out a plug of the armor. It is, in fact, possible for a sharp-pointed steel projectile to penetrate standard armor at low obliquity with little or no tip deformation. The Air Force chose the flat-nosed projectile design because of its greater effectiveness when attacking at high angles of obliquity.

There is one other notable difference in the behavior exhibited by the steel and uranium cores in Fig. 36 which is worth discussing because it may contribute to the high penetration performance of uranium alloys in general. About 30 μsec after impact, the Plexiglas rod on which the steel core is mounted is being crushed by the stress waves travelling up the penetrator shaft, although the rods supporting the uranium cores are not deformed even after 42 μsec. The time required for those stress waves generated at the penetrator-armor interface to travel to the rear of the penetrator is governed by bar sound velocity, C_{BAR}, in the material and, as can be seen in Table XIV, this is lower for uranium than for steel or other high-density materials like tungsten and tungsten carbide. The bulk sound velocity, C_o, that affects the velocity of large-amplitude shock waves in the material is also much lower for uranium. This implies that gross deformation or "mushrooming" of the penetrator shaft will not extend very far

[redacted]

back from the penetrator-armor interaction zone, and enables the penetrator's kinetic energy to be delivered to the smallest possible volume of the armor. This can be seen in the radiographs to be discussed in Sec. B.

In Fig. 36 there is little or no difference in the amount of back-spray of the various uranium alloys. This is even true for the over aged U-0.75 wt% Ti alloy which is appreciably softer than the others. It is not surprising, then, that the ballistic results discussed in Sec. IV show little variation of ballistic limit with hardness above about 45 R_c. The much softer unalloyed uranium (core "A" in Fig. 36), on the other hand, does exhibit somewhat more back-spray than the alloys.

In Fig. 37, the armor plate has been replaced with a 1-in.-thick section of 4340 steel hardened to 49-50 R_c. This was done to investigate the possibility that even though most of the candidate alloys were about equally effective against the relatively soft homogeneous armor, one or more of them might shatter or exhibit other undesirable characteristics when attacking armor about as hard as the penetrators themselves. In fact, there do seem to be some differences in the amount of back-spray from the various alloys when the harder steel is used, and the difference in behavior of the steel and uranium core is even more striking. However, none of the candidate alloys showed evidence of shattering, and their relative penetration performance is probably still about the same. The U-0.75 wt% Ti core exhibits as little back-spray as any of the alloys, thus adding confidence to our recommending it as the preferred penetrator material.

In addition to framing-camera photographs, we took conventional high-speed motion pictures of several of the .50-caliber penetration tests to determine whether there was any visible difference in the pyrophoric effects obtained with the various candidate alloys. On the basis of this admittedly crude experiment, all of the candidate alloys seemed to produce the same amount of burning fragments at equal impact velocities. We made no further attempt to differentiate the alloys on the basis of pyrophoricity.

B. Radiographic Study of the Penetration Process.

To gain a better understanding of the behavior of uranium penetrators, we took a series of radiographs of the full-scale 30-mm projectiles penetrating steel armor at 0 and 60° angles of obliquity. To be able to resolve the uranium cores inside the armor plate, we had to move the 30-mm gun and backstop assembly (Sec. IV) to the high-intensity, 28-Mev, PHERMEX flash x-ray facility. We also had to reduce the width of the target armor sections from 12 in. to 6 in. and to provide 2-in.-thick steel masking plates on either side of the penetration zone so that the core image would have enough contrast both inside and outside of the target plate. The x-ray beam was triggered by using the projectile impact to short a copper foil mounted on the target surface. However, it was possible to vary the time delay between shorting pulse and x-ray beam firing, thus allowing the radiographs to be taken at various depths of penetration. Armor thicknesses were the same as those used for the ballistic-limit tests, 2 in. for 0° obliquity and 1-1/4 in. for 60° obliquity. The impact velocities were generally chosen to be about 100 ft/sec above the respective ballistic limits.

Figure 38 is a sequence of radiographs of nominal U-0.75 wt% cores penetrating at 0° obliquity, and Fig. 39 is a similar sequence for U-2 wt% Mo cores. As would be expected from the nearly equal ballistic limits, there is no detectable difference in the behavior of the two materials. The most interesting feature of these radiographs is that, throughout the penetration process, projectile deformation is confined to a fairly narrow zone adjacent to the uranium-steel interface. This deformation consists of rapid radial

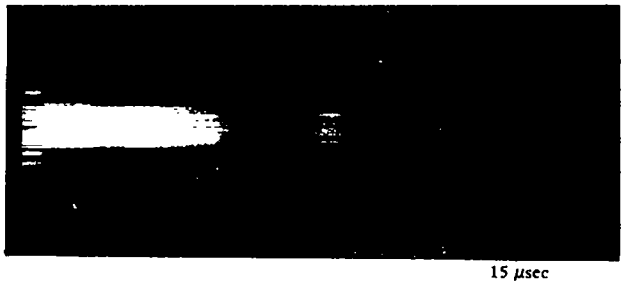

15 μsec

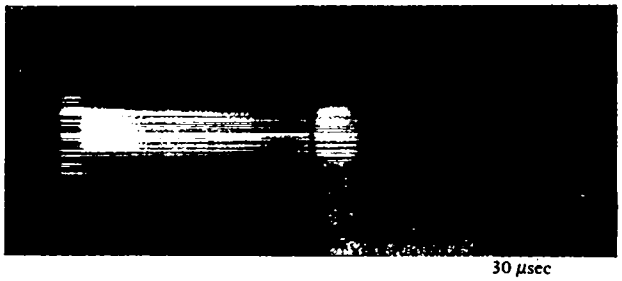

30 μsec

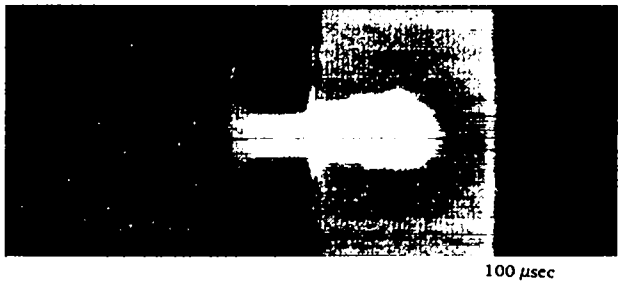

100 μsec

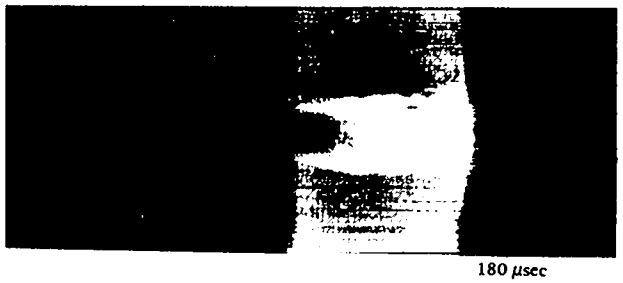

180 μsec

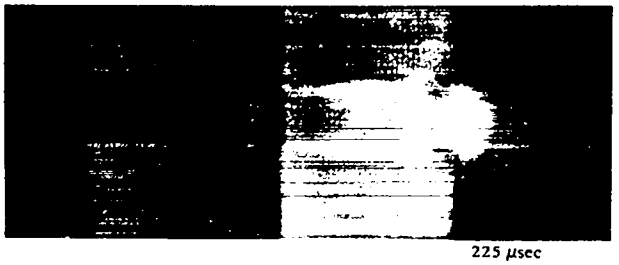

225 μsec

Fig. 38. Radiographs of a 30-mm projectile with a U-0.75 wt% Ti core penetrating 2-in.-thick steel armor at 0° obliquity. Average impact velocity was 2400 ft/sec. The approximate time after initial impact is shown for each radiograph.

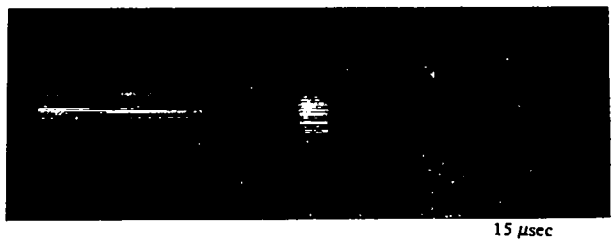

15 μsec

30 μsec

100 μsec

180 μsec

Fig. 39. Radiographs of a 30-mm projectile with a U-2 wt% Mo core penetrating 2-in.-thick armor plate at 0° obliquity. Average impact velocity was 2400 ft/sec. The approximate time after initial impact is shown for each radiograph.

displacement of the core material which begins at the moment of impact and continues until either a plug is sheared out of the armor or the kinetic energy of the projectile is dissipated. The displaced material is sheared away from the penetrator shaft and deposited on the sides of the hole. The rest of the penetrator shaft continues to travel through this liner of displaced uranium completely

undeformed. As discussed in the previous section, the shock velocity for any stress level in uranium is low because of the low bulk sound velocity. Appreciable deformation at any point along the penetrator shaft will not occur until the shock wave has reverberated several times between that point and the uranium-steel interface, but by then the material has traveled down to the immediate interaction zone and the deformation is always confined to that region. This is a greatly oversimplified explanation of the process, but a thorough treatment becomes a complicated problem in two-dimensional hydrodynamics.

Figure 40 shows a sectioned piece of penetrated armor and two of the residual penetrator shafts and armor plugs recovered from these shots.

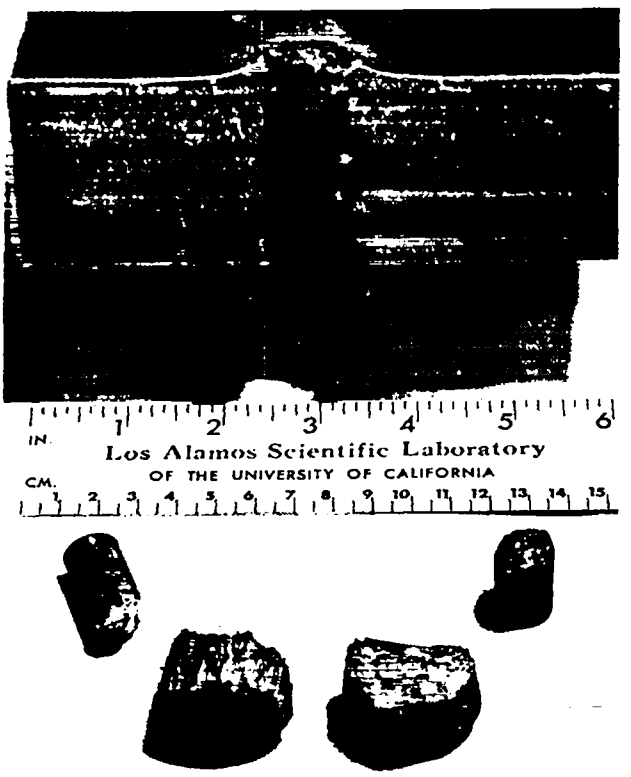

Fig. 40. Section of penetrated armor and recovered armor plugs and penetrator core fragments. Average impact velocity for these shots was 2400 ft/sec at 0° obliquity.

Much of the uranium that was sheared off the projectile shaft remains inside the armor, and a large part of the material that actually penetrated is contained in the residual penetrator shaft. The diameter of the penetrator fragments shown is equal to the original core diameter to within 0.05 mm, and their masses are 77.5 and 82.7 g as compared with the original core mass of 271 g. The two recovered armor plugs shown in Fig. 40 weighed 87.5 and 87.9 g, were typical for this impact velocity of 2400 ft/sec. We did not try to recover the fragments from every shot, but inspection of the penetrated armor showed that it always failed by having a single plug punched out, with possibly a few much smaller fragments being ejected from the plug's periphery. This was true over the range of impact velocities, 2200-3300 ft/sec, used in the ballistic-limit tests.

Figures 41 and 42 are radiographic studies of 30-mm projectiles penetrating at 60° obliquity, the core materials being U-2 wt% Mo and a nominal U-0.75 wt% Ti, respectively. Again, there is no detectable difference in the behavior of the two materials. The penetration process at 60° obliquity is much the same as that at 0° obliquity. Again, the uranium flows laterally from a narrow zone at the uranium-steel interface, but the flow is, of course, no longer axisymmetric. The displaced uranium is not confined in these high-angle impacts, and some of the projectile's kinetic energy is expended in the lateral flow of uranium and steel. The penetrator shaft seems to remain undistorted until it reaches the interaction zone, and this is substantiated by the appearance of the residual cores shown in Fig. 43. Compared to the 0° obliquity penetrations, a larger part of the original core mass is sheared away, but this is mainly because the effective armor thickness is greater. The low sound speed in uranium, which minimizes the amount of stress transferred to the tail of the penetrator, probably helps to keep it from being deflected at these high impact angles.

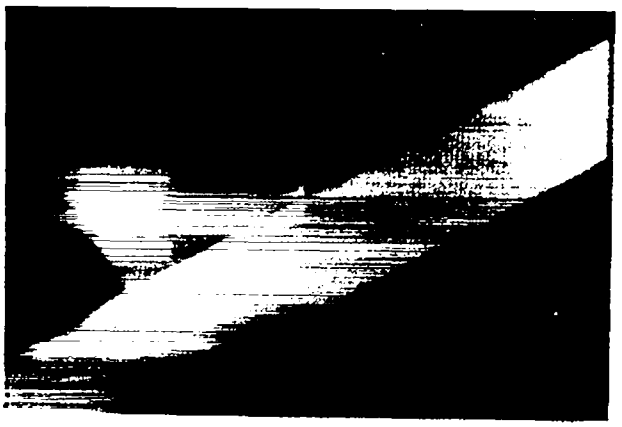

15 μsec

140 μsec

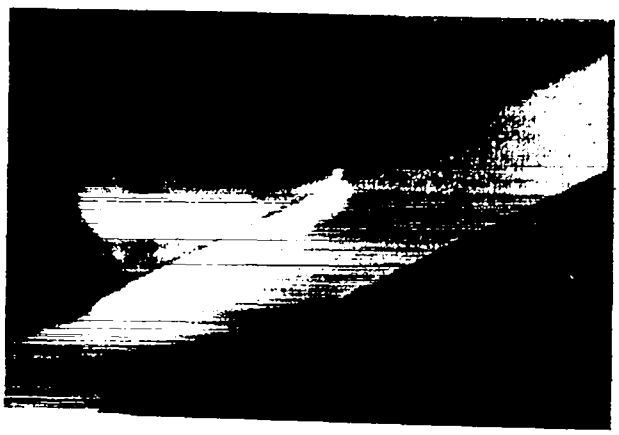

40 μsec

200 μsec

Fig. 41. Radiographs of a 30-mm projectile with a U-2 wt% Mo core penetrating 1-1/4-in.-thick steel armor at 60° obliquity. The average impact velocity was 3250 ft/sec.

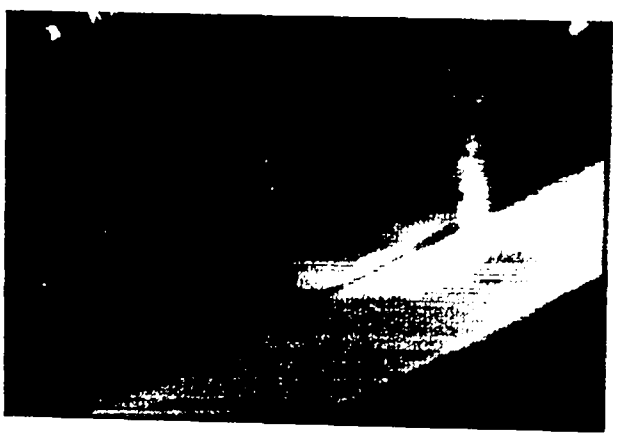

80 μsec

Again, the armor seems to fail in the simple plugging mode, and two of the recovered plugs are also shown in Fig. 43. There is a much wider variation in the masses of the recovered cores, 58.9 and 48.9 g, and plugs, 70.2 and 53.3 g, shown in Fig. 43, than in those recovered from 0° obliquity shots.

A few 0° obliquity radiographs, Fig. 44, were also obtained for impact velocities about 150 ft/sec below the ballistic limit. The behavior of the penetrators is apparently not affected by the lower velocity, and part of the penetrator shaft is stopped without appreciable deformation. This can be seen in Fig. 45 which shows sections of

Fig. 42. Radiographs of a 30-mm projectile with a U-0.75 wt% Ti core penetrating 1-1/4-in.-thick armor at 60° obliquity. The average impact velocity was 3250 ft/sec.

partially penetrated armor for 0, 30, and 60° impacts. The boundary between the region of plastic flow and the undeformed shaft can be seen in the 30 and 60° obliquity sections.

C. Post-Impact Metallography of Penetrator-Armor Section.

To determine how the large stresses generated at the penetrator-armor interface might affect the properties of the steel and uranium, we conducted a metallographic examination on the armor-penetrator section shown in Fig. 46. This was a nominal U-0.75 wt% Ti core tested at 0° obliquity and 2100 ft/sec. First, we measured the hardness at various points on the penetrator and adjacent steel. The steel hardness had increased from an

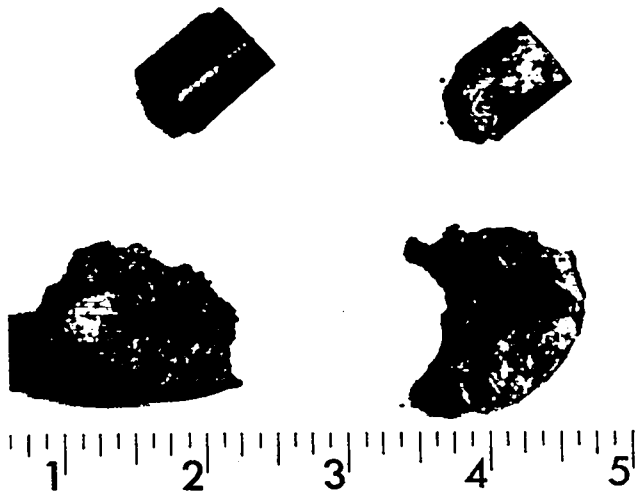

Fig. 43. Recovered armor plugs and penetrator fragments from 30-mm projectiles penetrating 1-1/4-in.-thick armor at 60° obliquity. Average impact velocity was 3250 ft/sec.

initial value of 275 DPH to 360 DPH in the highly wrought zone along the penetrator-armor interface. In contrast, the uranium hardness was almost unchanged, being 540 DPH along the centerline and 500 DPH in the sheared-off material deposited along the sides of the hole.

Figure 47 shows a region surrounding the uranium-steel interface near the front corner of the penetrator core. Note that the original diameter of the back section of the core is still well defined and, in fact, is continuous to the leading edge as is indicated by the shear line in the micrograph.

Figures 48 and 49 are photomicrographs of the steel parent metal and wrought zone, and the highly wrought steel structure along the steel-uranium interface is shown in Fig. 50. Several extended cracks were noted in the steel as a result of the impact. Figure 51 shows parts of one crack near the leading edge of the penetrator. Some uranium alloy has been injected into the crack.

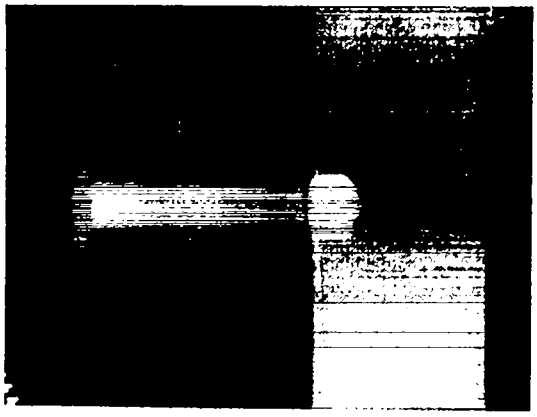

35 μsec

115 μsec

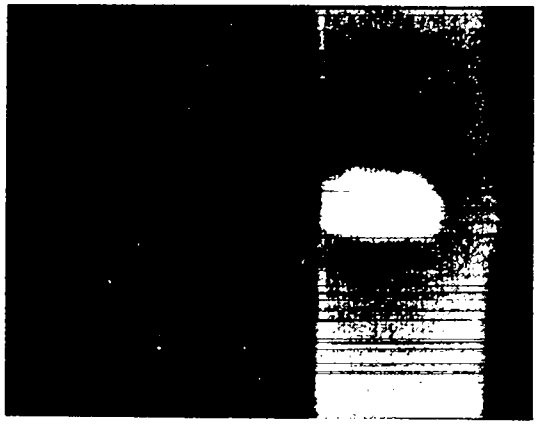

STATIC

Fig. 44. Radiographs of partial penetration of 2-in.-thick armor by 30-mm projectiles with U-2 wt% Mo cores. Average impact velocity was 2140 ft/sec. The last photo is a static shot of the core embedded in the armor.

Fig. 45. Sectioned pieces of steel armor showing partial penetration by 30-mm projectile cores at 0, 30, and 60° obliquity.

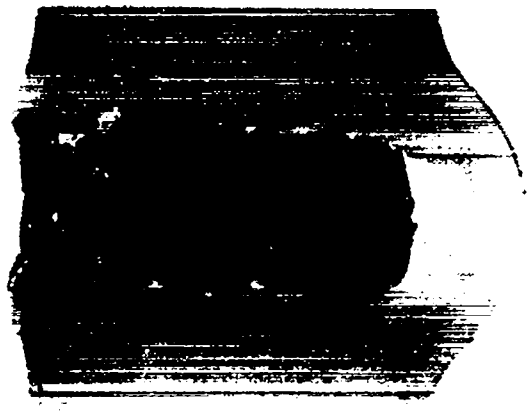

Fig. 46. Partially penetrated armor section used for post-impact metallography.

Fig. 47. Magnification of region around uranium-steel interface.

Fig. 48. Underformed steel microstructure.

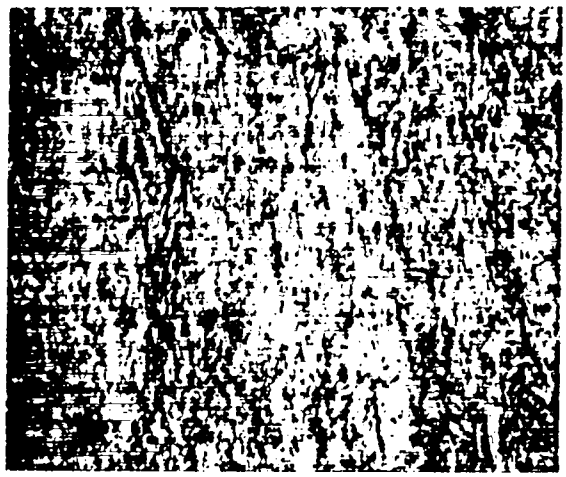

Fig. 49. Wrought steel microstructure.

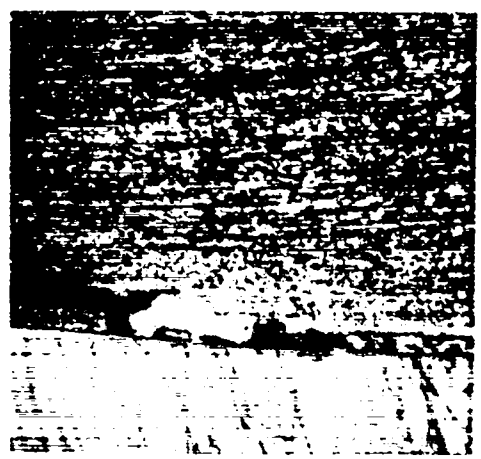

Fig. 50. Highly wrought steel microstructure along uranium-steel interface.

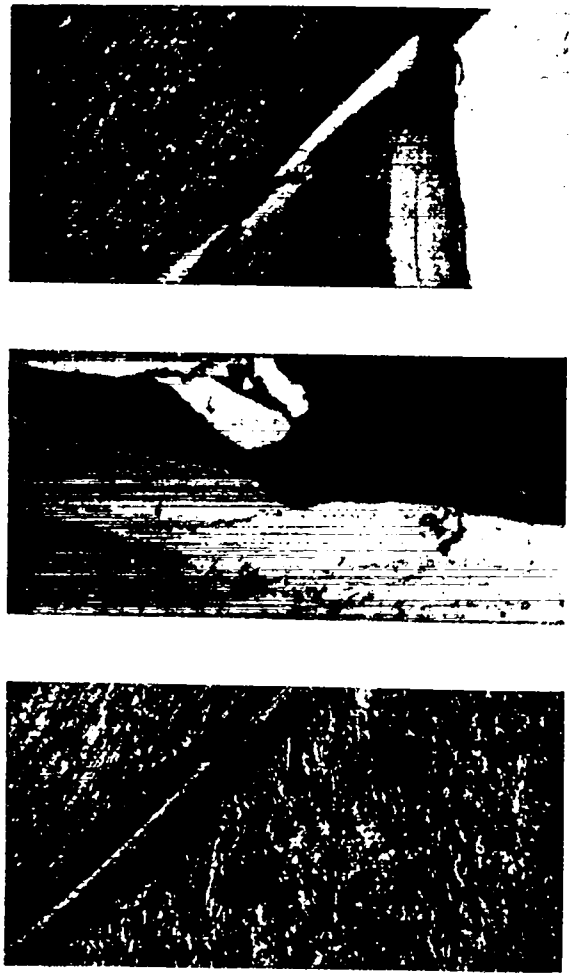

Fig. 51. Cracks in armor resulting from impact.

The microstructure of the penetrator along the uranium-steel interface is shown in Fig. 52. Some melting and possible alloying with the steel was evident along the interface, but most of the sheared material, Fig. 53, has the same gamma-quenched and aged microstructure as that found near the center of the undeformed core, Fig. 54. The microstructure along the shear line was transformed as shown in Fig. 55.

Before performing this metallographic study, we thought that most of the uranium in the interaction zone was being melted. We speculated that the uranium might, in fact, be forming a low-melting-point eutectic with the steel. This is not the case, since the photomicrographs showed no

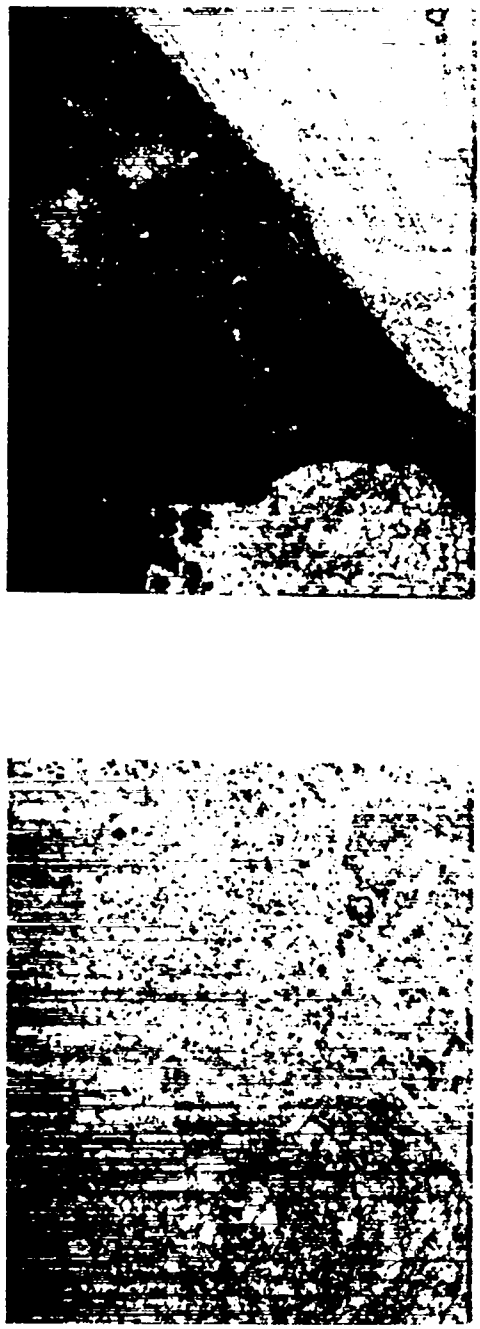

Fig. 52. Penetrator microstructure along uranium-steel interface.

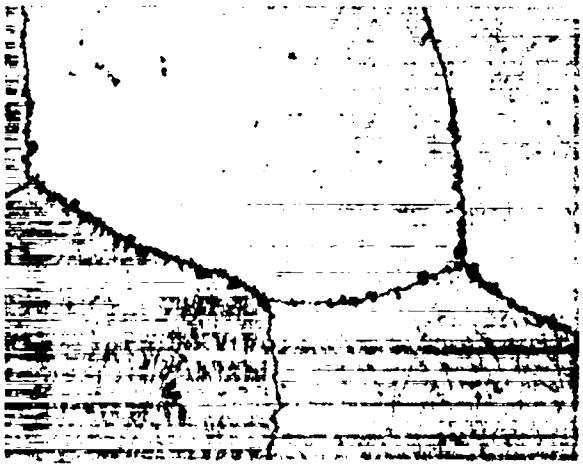

Fig. 53. Microstructure of uranium in sheared-off zone or sheath.

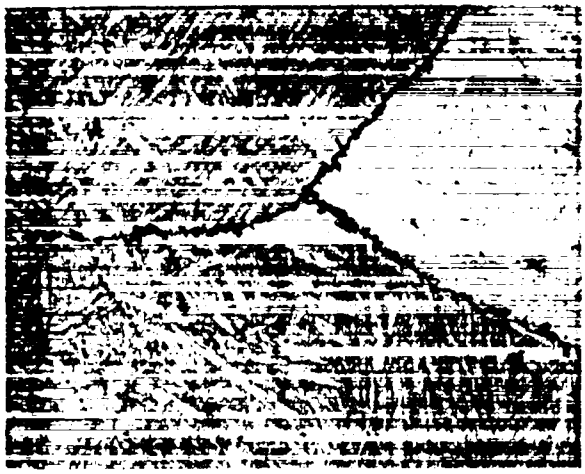

Fig. 54. Microstructure of underformed uranium core.

evidence of eutectic formation and indicated that only a very small region along the uranium-steel interface had melted.

We also performed a metallographic study on a completely penetrated armor section, with similar results. Most of the uranium deposited in the penetration hole still showed the original microstructure, and only slight melting had occurred. Apparently the only significant change in material properties during penetration is work-hardening of the armor. Any melting or transformation of the uranium alloy is highly localized,

Fig. 55. Microstructure of uranium along shear line between penetrator shaft and sheath.

the bulk of the core material being in the same condition before and after impact.

VI. CONCLUSION

Four basic uranium alloy systems, with variations of composition and heat treatment producing a total of 16 different materials, were evaluated in this project. They were selected from a large number of previously studied alloys because they provided nearly the full range of mechanical properties available with uranium and also promised to be relatively economical for mass production of penetrators.

The principal goal of this project was to determine the alloy that had maximum penetration effectiveness. However, ballistic-limit tests using scaled-down .50-caliber projectiles indicated that the performance of three of the alloys was essentially the same, even at 60° obliquity. Only the U-4.5 wt% Nb alloy could be eliminated from consideration on the basis of penetration performance. High-speed photography and radiography revealed that, for uranium alloy penetrators in general, the large impact stresses producing plastic flow of the core extend only over a relatively narrow zone at the penetrator-armor interface. In this zone, the stress is much larger than the dynamic compressive

strength of any of the alloys, so variations in strength have little effect on performance.

The nominal U-0.75 wt% Ti and U-2 wt% Mo alloys were finally selected as the two best materials, the U-2 wt% Nb-1 wt% Ti ternary being eliminated because it was more difficult to cast with the desired composition and because it was thought to be more susceptible to stress-corrosion cracking. Full-scale 30-mm penetration tests again showed the U-Ti and U-Mo to be about equal in performance. However, the U-Ti is about eight times as resistant to corrosion as the U-Mo, and, in addition, the tests showed its performance to be insensitive to precise composition. It also offers lower material cost and can be easily heat-treated by water-quenching with subsequent aging in a lead bath. We therefore recommend the U-0.75 wt% Ti alloy as providing performance comparable to that of any alloy, along with reasonable corrosion resistance and minimum manufacturing cost.

ACKNOWLEDGMENTS

It is a pleasure to acknowledge the assistance furnished by many members of the Los Alamos Scientific Laboratory especially of Groups CMB-1, CMB-6, M-1, M-2, M-6, and WX-2 without whose help this project could not have been done.

In Group CMB-6 for material preparation, corrosion testing, metallographic studies and mechanical testing we wish to accord special thanks to G. E. Jaynes, R. E. Siegmiller, B. W. Powell, G. S. Hanks, T. I. Jones, E. P. Ehart, and C. A. Javorsky. In addition, we thank J. M. Taub and W. W. Martin for their guidance of these activities and their many helpful suggestions.

We gratefully acknowledge the assistance of P. E. Rexroth, Group CMB-11, for collecting much of the ballistic data and L. E. Edwards, Group WX-3, and D. L. Upham, Group WX-2, for design of the projectiles and test equipment.

We extend special thanks to R. G. McQueen, Group M-6, J. W. Taylor, Group M-2, L. C. Smith, Group WX-2, and M. L. Brooks, WX-DO, for their technical guidance and critical review of this work.

APPENDIX A

BALLISTIC-LIMIT DATA

This appendix contains all of the data collected during testing of both .50-caliber and 30-mm projectiles with uranium alloy penetrator cores. The data are listed in tables and also plotted; for example, the data listed in Table A-I is plotted in Fig. A-1. If a protection ballistic limit (PBL) was established, it is recorded both in the table heading and on the plot. For all tables, a "P" in the result column means that the witness plate was penetrated, and "N" indicates that it was not penetrated.

All penetration tests were performed against one-foot-square pieces of military-specification, rolled, homogeneous armor. The 1/2-, 1-, and 1-1/4 in.-thick armor was manufactured to MIL-S-12560B, except that the 1/2- and 1-in.-thick pieces were machined from nominal 3/4- and 1-1/4-in.-thick armor plate, respectively. The 2-in.-thick pieces were manufactured to MIL-S-13812A, the two specifications being the same as far as these tests are concerned. The average hardness of the armor used in each test series is recorded in the tables.

The .50-caliber test results, grouped according to alloy, are presented first, and the full-scale, 30-mm results are at the end of the listing.

TABLE A-I

PERFORMANCE DATA
FOR .50-CALIBER PROJECTILES

Penetrator alloy : U-0.62 wt% Ti
Heat treatment : γ-quench + age 450°C, 4 h, vac.
Penetrator density and hardness : 18.64 g/cm^3, 49.6 R_c
Target thickness and hardness : 1.0 in., 338 BHN
Obliquity : 0°
PBL : 2860 ft/sec

Shot No.	Core Wt (grains)	Projectile Wt (grains)	Impact Velocity (ft/sec)	Result
1	316.5	498.4	3021	P
2	316.4	499.5	2503	N
3	316.7	498.0	2679	N
4	316.7	499.0	2727	N
5	316.5	499.5	2830	N
6	316.9	499.5	2749	N
7	316.7	499.5	2908	P
8	316.8	499.4	2808	N
9	314.4	495.8	2903	P
10	316.7	499.4	2881	P
11	315.3	497.5	2886	P
12	313.2	495.9	2820	N

TABLE A-II

PERFORMANCE DATA
FOR .50-CALIBER PROJECTILES

Penetrator alloy : U-0.62 wt% Ti
Heat treatment : γ-quench + age 550°C, 4 h, vac.
Penetrator density and hardness : 18.63 g/cm^3, 42.3 R_c
Target thickness and hardness : 1.0 in., 329 BHN
Obliquity : 0°
PBL : No PBL established

Shot No.	Core Wt (grains)	Projectile Wt (grains)	Impact Velocity (ft/sec)	Result
1	315.6	498.8	3038	P
2	316.7	500.0	2861	N
3	316.9	498.5	2782	N
4	316.3	499.5	3024	P
5	316.8	499.5	2851	N
6	316.2	498.6	2846	N
7	316.7	500.0	2923	N
8	316.5	499.5	2946	N

[redacted]

TABLE A-III

PERFORMANCE DATA
FOR .50-CALIBER PROJECTILES

Penetrator alloy : U-0.73 wt% Ti
Heat treatment : γ-quench + age 450°C, 4 h, vac.
Penetrator density and hardness : 18.56 g/cm^3, 50.8 R_c
Target thickness and hardness : 1.0 in., 324 BHN
Obliquity : 0°
PBL : No PBL established

Shot No.	Core Wt (grains)	Projectile Wt (grains)	Impact Velocity (ft/sec)	Result
1	315.3	499.0	2765	N
2	315.3	499.2	2959	P
3	315.4	498.0	2981	P
4	315.4	499.0	2860	P
5	315.5	497.5	2773	N
6	315.5	497.4	2917	P
7	315.5	497.4	2768	N
8	315.5	498.3	2932	P
9	315.6	499.0	3027	P
10	315.2	499.1	2695	N
11	315.6	499.1	2933	P
12	315.6	498.5	3061	P

TABLE A-IV

PERFORMANCE DATA
FOR .50-CALIBER PROJECTILES

Penetrator alloy : U-0.77 wt% Ti
Heat treatment : γ-quench + age 450°C, 4 h, vac.
Penetrator density and hardness : 18.57 g/cm^3, 56.5 R_c
Target thickness and hardness : 1.0 in., 324 BHN
Obliquity : 0°
PBL : No PBL established

Shot No.	Core Wt (grains)	Projectile Wt (grains)	Impact Velocity (ft/sec)	Result
1	315.4	505.1	3033	P
2	315.6	504.7	2985	P
3	315.2	502.9	2665	N
4	315.6	507.0	2771	N
5	315.6	506.0	2581	N

TABLE A-V

PERFORMANCE DATA
FOR .50-CALIBER PROJECTILES

Penetrator alloy : U-0.77 wt% Ti
Heat treatment : γ-quench + age 550°C, 4 h, vac.
Penetrator density and hardness : 18.57 g/cm^3, 44.4 R_c
Target thickness and hardness : 1.0 in., 326 BHN
Obliquity : 0°
PBL : 2880 ft/sec

Shot No.	Core Wt (grains)	Projectile Wt (grains)	Impact Velocity (ft/sec)	Result
1	315.2	507.0	2874	P
2	315.2	506.3	2862	N
3	315.8	509.5	2902	P
4	315.6	506.5	2742	N
5	315.6	506.2	2809	N
6	315.1	505.5	2875	N
7	315.5	505.3	2984	P
8	315.5	505.6	2833	N
9	315.6	506.8	2957	P

TABLE A-VI

PERFORMANCE DATA
FOR .50-CALIBER PROJECTILES

Penetrator alloy : U-1.17 wt% Ti
Heat treatment : γ-quench + age 450°C, 4 h, vac.
Penetrator density and hardness : 18.31 g/cm^3, 56.5 R_c
Target thickness and hardness : 1.0 in., 330 BHN
Obliquity : 0°
PBL : 2890 ft/sec

Shot No.	Core Wt (grains)	Projectile Wt (grains)	Impact Velocity (ft/sec)	Result
1	311.6	494.5	3009	P
2	311.5	495.5	2853	N
3	311.5	494.7	2956	P
4	311.4	494.1	2885	P
5	310.6	493.7	2928	P
6	311.4	494.0	3054	P
7	309.6	493.2	2834	N
8	310.1	492.8	2861	N
9	311.5	495.0	2957	P

TABLE A-VII

PERFORMANCE DATA
FOR .50-CALIBER PROJECTILES

Penetrator alloy : U-1.17 wt% Ti
Heat treatment : γ-quench + age 550°C, 4 h, vac.
Penetrator density and hardness : 18.38 g/cm^3, 45.0 R_c
Target thickness and hardness : 1.0 in., 323 BHN
Obliquity : 0°
PBL : No PBL established

Shot No.	Core Wt (grains)	Projectile Wt (grains)	Impact Velocity (ft/sec)	Result
1	312.0	495.5	2742	N
2	312.2	494.5	3087	P
3	312.1	495.1	3023	P
4	312.1	494.5	3046	P
5	312.4	494.5	2868	N
6	312.3	494.1	3046	P
7	312.0	495.0	2865	N
8	310.0	493.9	3040	P
9	312.1	494.5	2886	N

TABLE A-VIII

PERFORMANCE DATA
FOR .50-CALIBER PROJECTILES

Penetrator alloy : U-0.73 wt% Ti
Heat treatment : γ-quench + age 450°C, 4 h, in lead
Penetrator density and hardness : 18.58 g/cm^3, 49.2 R_c
Target thickness and hardness : 1.0 in., 331 BHN
Obliquity : 0°
PBL : No PBL established

Shot No.	Core Wt (grains)	Projectile Wt (grains)	Impact Velocity (ft/sec)	Result
1	315.8	507.6	2400	N
2	315.9	507.5	2709	N
3	315.5	507.5	2862	N
4	315.9	508.0	2841	N
5	315.8	507.7	2678	N
6	315.7	507.7	2684	N
7	315.8	508.0	2693	N
8	315.4	508.1	2766	N
9	315.6	507.3	2883	P

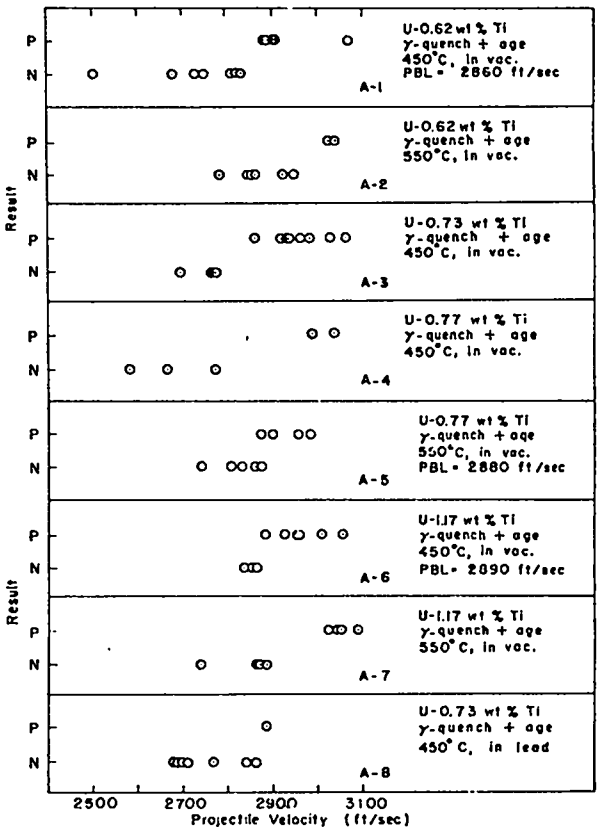

Figs. A-1-8. Ballistic-test results for .50-caliber projectiles with U-Ti cores striking 1-in.-thick armor at 0° obliquity.

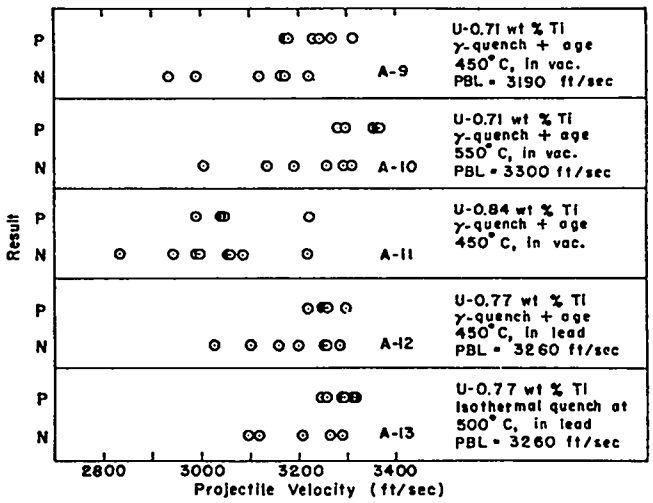

Figs. A-9-13. Ballistic-test results for .50-caliber projectiles with U-Ti cores striking 1/2-in.-thick armor at 60° obliquity.

TABLE A-IX

PERFORMANCE DATA
FOR .50-CALIBER PROJECTILES

Penetrator alloy : U-0.71 wt% Ti
Heat treatment : γ-quench + age 450°C, 4 h, vac.
Penetrator density and hardness : 18.63 g/cm^3, 51.4 R_c
Target thickness and hardness : 0.5 in., 366 BHN
Obliquity : 60°
PBL : 3190 ft/sec

Shot No.	Core Wt (grains)	Projectile Wt (grains)	Impact Velocity (ft/sec)	Result
1	316.5	508.0	2935	N
2	316.5	507.8	2991	N
3	316.4	508.8	3120	N
4	316.5	507.6	3247	P
5	316.5	507.4	3272	P
6	316.6	508.8	3316	P
7	316.6	508.3	3223	N
8	316.6	507.8	3234	P
9	316.3	507.8	3174	N
10	316.3	508.1	3176	P
11	316.5	509.0	3164	N
12	316.4	508.0	3183	P

TABLE A-X

PERFORMANCE DATA
FOR .50-CALIBER PROJECTILES

Penetrator alloy : U-0.71 wt% Ti
Heat treatment : γ-quench + age 550°C, 4 h, vac.
Penetrator density and hardness : 18.59 g/cm^3, 44.5 R_c
Target thickness and hardness : 0.5 in., 366 BHN
Obliquity : 60°
PBL : 3300 ft/sec

Shot No.	Core Wt (grains)	Projectile Wt (grains)	Impact Velocity (ft/sec)	Result
1	316.1	508.1	3009	N
2	316.0	505.9	3137	N
3	315.8	508.0	3195	N
4	315.9	507.9	3313	N
5	315.9	507.5	3303	P
6	316.0	507.3	3296	N
7	315.9	507.4	3357	P
8	315.9	507.5	3363	P
9	316.0	507.0	3367	P
10	315.9	508.3	3262	N
11	315.8	507.5	3285	P

TABLE A-XI

PERFORMANCE DATA
FOR .50-CALIBER PROJECTILES

Penetrator alloy : U-0.84 wt% Ti
Heat treatment : γ-quench + age 450°C, 4 h, vac.
Penetrator density and hardness : 18.51 g/cm^3, 55.4 R_c
Target thickness and hardness : 0.5 in., 363 BHN
Obliquity : 60°
PBL : No PBL established

Shot No.	Core Wt (grains)	Projectile Wt (grains)	Impact Velocity (ft/sec)	Result
1	310.5	501.7	3044	P
2	314.6	506.5	2833	N
3	310.8	503.3	2944	N
4	314.5	506.1	2993	P
5	313.3	505.1	2988	N
6	314.9	506.8	2999	N
7	314.6	505.4	3055	N
8	314.3	505.4	3048	P
9	314.3	506.4	3087	N
10	314.4	506.1	3062	N
11	314.8	506.8	3219	N
12	314.6	506.9	3228	P

TABLE XII

PERFORMANCE DATA
FOR .50-CALIBER PROJECTILES

Penetrator alloy : U-0.77 wt% Ti
Heat treatment : γ-quench + age 450°C, 4 h, in lead
Penetrator density and hardness : 18.60 g/cm^3, 52.2 R_c
Target thickness and hardness : 0.5 in., 363 BHN
Obliquity : 60°
PBL : 3260 ft/sec

Shot No.	Core Wt (grains)	Projectile Wt (grains)	Impact Velocity (ft/sec)	Result
1	316.5	508.7	3028	N
2	316.1	507.0	3102	N
3	316.0	508.3	3224	P
4	315.9	507.8	3253	P
5	316.1	508.2	3300	P
6	316.0	506.6	3158	N
7	316.0	507.8	3200	N
8	315.9	507.1	3254	N
9	315.9	507.5	3257	N
10	315.7	507.4	3259	P
11	315.9	507.9	3212	P
12	316.2	508.2	3285	N

[redacted]

TABLE XIII

PERFORMANCE DATA
FOR .50-CALIBER PROJECTILES

UNCLASSIFIED

Penetrator alloy : U-0.77 wt% Mo
Heat treatment : Isothermal quench at 500°C, 3 h, in lead
Penetrator density and hardness : 18.61 g/cm^3, 46.5 R_c
Target thickness and hardness : 0.5 in., 364 BHN
Obliquity : 60°
PBL : 3260 ft/sec

Shot No.	Core Wt (grains)	Projectile Wt (grains)	Impact Velocity (ft/sec)	Result
1	316.2	507.3	3097	N
2	316.3	507.5	3120	N
3	316.3	508.4	3208	N
4	316.2	508.4	3264	N
5	316.1	508.3	3295	P
6	316.1	508.4	3312	P
7	316.2	507.9	3258	P
8	316.0	507.5	3245	P
9	315.9	508.1	3293	N
10	316.2	507.2	3288	P
11	316.3	508.1	3316	P

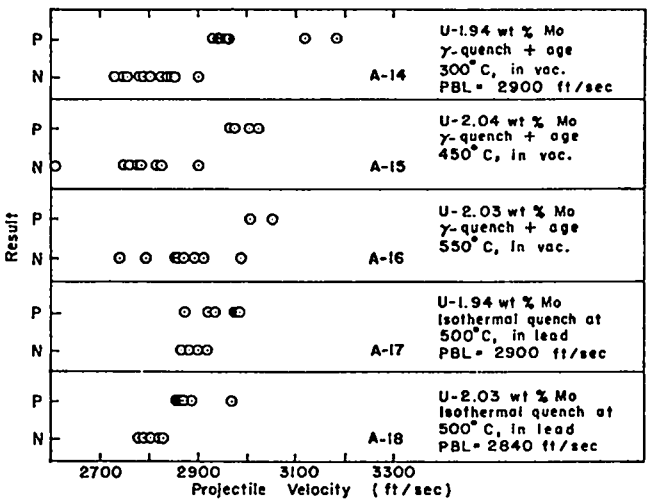

Figs. A-14-18. Ballistic-test results for .50-caliber projectiles with U-2 wt% Mo cores striking 1-in.-thick armor at 0° obliquity.

TABLE XIV

PERFORMANCE DATA
FOR .50-CALIBER PROJECTILES

Penetrator alloy : U-1.94 wt% Mo
Heat treatment : γ-quench + age 300°C, 4 h, vac.
Penetrator density and hardness : 18.53 g/cm^3, 49.5 R_c
Target thickness and hardness : 1.0 in., 328 BHN
Obliquity : 0°
PBL : 2900 ft/sec

Shot No.	Core Wt (grains)	Projectile Wt (grains)	Impact Velocity (ft/sec)	Result
1	314.5	497.6	2757	N
2	314.5	497.5	2731	N
3	314.6	498.3	3185	P
4	314.7	496.5	2790	N
5	314.5	497.8	2945	P
6	314.9	497.5	3120	P
7	314.6	496.7	2748	N
8	314.9	497.5	2801	N
9	315.3	507.9	2957	P
10	314.9	507.5	2949	P
11	314.9	507.2	2928	P
12	315.3	507.5	2825	N
13	315.1	508.1	2838	N
14	315.1	507.3	2842	N
15	314.9	498.5	2854	N
16	315.0	498.7	2901	N
17	314.8	498.5	2784	N

UNCLASSIFIED

[redacted]

TABLE XV

PERFORMANCE DATA
FOR .50-CALIBER PROJECTILES

Penetrator alloy : U-2.04 wt% Mo
Heat treatment : γ-quench + age 450°C, 4 h, vac.
Penetrator density and hardness : 18.61 g/cm^3, 45.4 R_c
Target thickness and hardness : 1.0 in., 331 BHN
Obliquity : 0°
PBL : No PBL established

Shot No.	Core Wt (grains)	Projectile Wt (grains)	Impact Velocity (ft/sec)	Result
1	316.0	498.1	3025	P
2	316.1	498.7	2825	N
3	316.4	499.9	2975	P
4	316.3	499.6	2775	N
5	316.3	499.9	3004	P
6	316.1	499.5	2608	N
7	316.7	498.8	2814	N
8	315.7	498.3	2900	N
9	316.5	499.6	2784	N
10	316.6	499.4	2747	N
11	315.9	499.5	2759	N
12	316.4	500.4	2964	P

TABLE XVI

PERFORMANCE DATA
FOR .50-CALIBER PROJECTILES

Penetrator alloy : U-2.03 wt% Mo
Heat treatment : γ-quench + age 550°C, 4 h, vac.
Penetrator density and hardness : 18.62 g/cm^3, 35.4 R_c
Target thickness and hardness : 1.0 in., 327 BHN
Obliquity : 0°
PBL : No PBL established

Shot No.	Core Wt (grains)	Projectile Wt (grains)	Impact Velocity (ft/sec)	Result
1	316.7	499.5	3052	P
2	316.3	500.0	2739	N
3	316.4	500.0	2793	N
4	316.6	498.5	2870	N
5	316.2	499.7	2857	N
6	316.4	500.0	2891	N
7	316.4	499.5	2855	N
8	316.1	499.5	2910	N
9	316.3	498.7	2986	N
10	316.1	500.0	3005	P

TABLE XVII

PERFORMANCE DATA
FOR .50-CALIBER PROJECTILES

Penetrator alloy : U-1.94 wt% Mo
Heat treatment : Isothermal quench at 500°C, 3 h, in lead
Penetrator density and hardness : 18.60 g/cm^3, 50.4 R_c
Target thickness and hardness : 1.0 in., 335 BHN
Obliquity : 0°
PBL : 2900 ft/sec

Shot No.	Core Wt (grains)	Projectile Wt (grains)	Impact Velocity (ft/sec)	Result
1	316.0	505.6	2975	P
2	316.0	506.8	2985	P
3	316.0	508.3	2982	P
4	316.1	507.2	2935	P
5	316.1	507.5	2901	N
6	316.2	506.8	2919	P
7	316.2	507.9	2882	N
8	315.9	508.0	2920	N
9	315.9	507.4	2871	P
10	316.1	507.8	2867	N

TABLE XVIII

PERFORMANCE DATA
FOR .50-CALIBER PROJECTILES

Penetrator alloy : U-2.03 wt% Mo
Heat treatment : Isothermal quench at 500°C, 3 h, in lead
Penetrator density and hardness : 18.61 g/cm^3, 52.3 R_c
Target thickness and hardness : 1.0 in., 337 BHN
Obliquity : 0°
PBL : 2840 ft/sec

Shot No.	Core Wt (grains)	Projectile Wt (grains)	Impact Velocity (ft/sec)	Result
1	316.4	507.1	2790	N
2	316.4	507.8	2969	P
3	316.4	507.4	2860	P
4	316.4	507.4	2869	P
5	316.1	508.0	2856	P
6	316.2	508.1	2803	N
7	316.0	507.3	2820	N
8	316.0	507.6	2778	N
9	315.8	507.9	2886	P
10	315.8	508.0	2828	N

TABLE A-XIX

PERFORMANCE DATA
FOR .50-CALIBER PROJECTILES

Penetrator alloy : U-1.96 wt% Mo
Heat treatment : γ-quench + age 300°C, 4 h, vac.
Penetrator density and hardness : 18.48 g/cm^3, 45.6 R_c
Target thickness and hardness : 0.5 in., 366 BHN
Obliquity : 60°
PBL : 3220 ft/sec

Shot No.	Core Wt (grains)	Projectile Wt (grains)	Impact Velocity (ft/sec)	Result
1	314.2	505.6	2845	N
2	312.6	504.5	2975	N
3	313.9	505.0	3071	N
4	311.4	502.8	3152	N
5	314.4	505.8	3223	P
6	311.6	503.8	3248	P
7	314.1	505.4	3236	N
8	311.4	503.6	3341	P
9	314.1	505.8	3375	P
10	311.9	504.3	3221	N
11	313.5	506.4	3241	P

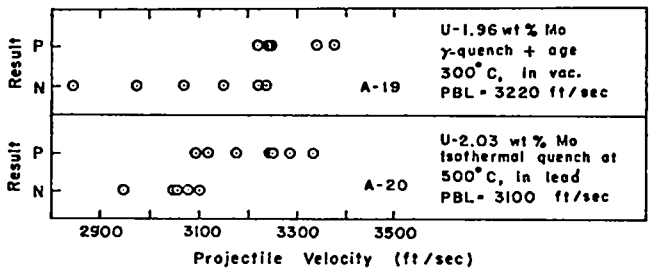

Figs. A-19-20. Ballistic-test results for .50-caliber projectiles with U-2 wt% Mo cores striking 1/2-in.-thick armor at 60° obliquity.

TABLE A-XX

PERFORMANCE DATA
FOR .50-CALIBER PROJECTILES

Penetrator alloy : U-2.03 wt% Mo
Heat treatment : Isothermal quench at 500°C, 3 h, in lead
Penetrator density and hardness : 18.58 g/cm^3, 51.1 R_c
Target thickness and hardness : 0.5 in., 365 BHN
Obliquity : 60°
PBL : 3100 ft/sec

Shot No.	Core Wt (grains)	Projectile Wt (grains)	Impact Velocity (ft/sec)	Result
1	315.8	507.0	2945	N
2	315.7	508.4	3079	N
3	315.8	508.2	3244	P
4	315.9	508.0	3250	P
5	315.8	507.6	3284	P
6	315.8	508.1	3332	P
7	315.5	507.6	3094	P
8	315.5	506.3	3176	P
9	315.7	508.1	3055	N
10	315.8	507.9	3102	N
11	315.6	507.8	3047	N
12	315.7	506.4	3117	P

TABLE A-XXI

PERFORMANCE DATA
FOR .50-CALIBER PROJECTILES

Penetrator alloy : U-4.64 wt% Nb
Heat treatment : γ-quench + age 300°C, 4 h, vac.
Penetrator density and hardness : 17.68 g/cm^3, 45.7 R_c
Target thickness and hardness : 1.0 in., 330 BHN
Obliquity : 0°
PBL : 3000 ft/sec

Shot No.	Core Wt (grains)	Projectile Wt (grains)	Impact Velocity (ft/sec)	Result
1	300.7	492.6	2886	N
2	299.0	491.0	2927	N
3	300.9	492.9	2948	N
4	301.1	493.0	3001	P
5	299.1	491.0	3012	N
6	300.9	491.7	3047	P
7	300.6	492.3	3057	P

[redacted] UNCLASSIFIED

TABLE A-XXII

PERFORMANCE DATA
FOR .50-CALIBER PROJECTILES

Penetrator alloy : U-4.68 wt% Nb
Heat treatment : γ-quench + age 550°C, 4 h, vac.
Penetrator density and hardness : 17.78 g/cm^3, 40.4 R_c
Target thickness and hardness : 1.0 in., 329 BHN
Obliquity : 0°
PBL : 2970 ft/sec

Shot No.	Core Wt (grains)	Projectile Wt (grains)	Impact Velocity (ft/sec)	Result
1	302.1	493.8	3027	P
2	302.2	495.0	2874	N
3	302.1	495.3	2895	P
4	302.0	495.0	2942	N
5	302.0	495.2	2960	N
6	302.2	495.0	2996	N
7	302.2	494.5	3029	P
8	302.2	494.0	3030	P
9	302.1	494.6	3024	P

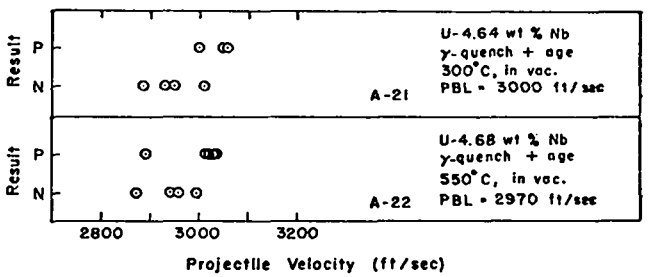

Figs. A-21-22. Ballistic-test results for .50-caliber projectiles with U-4.65 wt% Nb cores striking 1-in.-thick armor at 0° obliquity.

TABLE A-XXIII

PERFORMANCE DATA
FOR .50-CALIBER PROJECTILES

Penetrator alloy : U-2.53 wt% Nb-1.27 wt% Ti
Heat treatment : γ-quench + age 450°C, 4 h, vac.
Penetrator density and hardness : 17.95 g/cm^3, 46.5 R_c
Target thickness and hardness : 0.5 in., 366 BHN
Obliquity : 60°
PBL : 3240 ft/sec

Shot No.	Core Wt (grains)	Projectile Wt (grains)	Impact Velocity (ft/sec)	Result
1	304.8	497.4	2808	N
2	304.9	497.0	2908	N
3	305.1	497.2	3065	N
4	304.9	497.3	3170	N
5	305.0	496.7	3277	P
6	304.8	495.7	3315	N
7	305.3	497.2	3319	P
8	305.3	497.3	3363	P
9	305.0	498.0	3347	P
10	304.9	496.7	3265	P
11	305.0	497.0	3257	P
12	305.2	497.7	3178	N

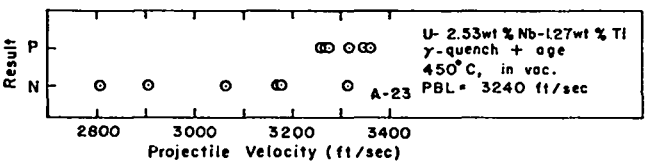

Fig. A-23. Ballistic-test results for .50-caliber projectiles with U-2.53 wt% Nb-1.27 wt% Ti cores striking 1/2-in.-thick armor at 60° obliquity.

UNCLASSIFIED

[redacted]

[redacted]

TABLE A-XXIV

PERFORMANCE DATA
FOR .50-CALIBER PROJECTILES

Penetrator alloy : Unalloyed uranium
Heat treatment : None
Penetrator density and hardness : 18.93 g/cm^3, 35 R_c
Target thickness and hardness : 1.0 in., 327 BHN
Obliquity : 0°
PBL : No PBL established

Shot No.	Core Wt (grains)	Projectile Wt (grains)	Impact Velocity (ft/sec)	Result
1	322.9	515.0	3046	P
2	323.2	515.4	3009	N
3	323.1	512.4	2766	N
4	322.9	513.3	3128	P
5	323.0	513.3	3067	P
6	323.1	513.9	2999	N

TABLE XXV

PERFORMANCE DATA
FOR 30-MM PROJECTILES

Penetrator alloy : U-(0.75-0.83) wt% Ti
Heat treatment : γ-quench + age 450°C, 4 h, in lead
Penetrator density and hardness : 18.59 g/cm^3, 52.2 R_c
Target thickness and hardness : 2.0 in., 280 BHN
Obliquity : 0°
PBL : 2260 ft/sec

Shot No.	Core Wt (grams)	Projectile Wt (grams)	Impact Velocity (ft/sec)	Result
1	271.1	432.9	2355	P
2	271.1	432.5	2258	P
3	271.3	432.8	2169	N
4	270.5	432.6	2231	N
5	270.9	432.1	2268	N
6	271.3	432.5	2239	P
7	270.6	432.8	2209	N
8	271.2	432.9	2343	P
9	270.5	432.9	2143	N

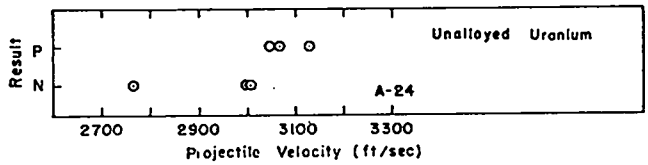

Fig. A-24 Ballistic-test results for .50-caliber projectiles with unalloyed uranium cores striking 1-in.-thick armor at 0° obliquity.

TABLE A-XXVI

PERFORMANCE DATA
FOR 30-MM PROJECTILES

Penetrator alloy : U-2.12 wt% Mo
Heat treatment : Isothermal quench at 500°C, 3 h, in lead
Penetrator density and hardness : 18.60 g/cm^3, 50 R_c
Target thickness and hardness : 2.0 in., 280 BHN
Obliquity : 0°
PBL : 2330 ft/sec

Shot No.	Core Wt (grams)	Projectile Wt (grams)	Impact Velocity (ft/sec)	Result
1	271.0	433.2	2383	P
2	271.3	432.7	2389	P
3	270.8	432.3	2034	N
4	271.4	433.0	2096	N
5	270.8	432.8	2305	N
6	270.3	432.0	2297	N
7	270.6	432.5	2354	N
8	271.3	432.6	2307	P
9	270.7	432.1	2393	P
10	271.0	432.4	2330	P

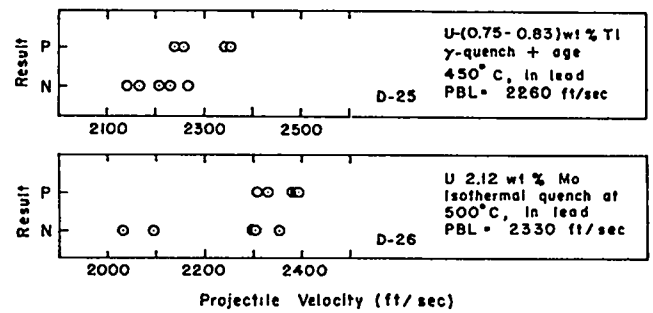

Figs. A-25-26. Ballistic-test results for 30-mm projectiles with uranium alloy cores striking 2-in.-thick armor at 0° obliquity.

[redacted]

 0000 0000 1143 1401

TABLE A-XXVII

PERFORMANCE DATA
FOR 30-MM PROJECTILES

Penetrator alloy : U-(0.62-0.70) wt% Ti
Heat treatment : γ-quench + age 450°C, 4 h,
Penetrator density in lead
and hardness : 18.62 g/cm^3, 52.7 R_C
Target thickness
and hardness : 2.0 in., 283 BHN
Obliquity : 30°
PBL : 2460 ft/sec

Shot No.	Core Wt (grams)	Projectile Wt (grams)	Impact Velocity (ft/sec)	Result
1	271.2	433.1	2455	P
2	272.2	433.9	2455	N
3	272.1	433.6	2536	N
4	267.5	429.4	2533	P
5	272.2	433.8	2598	P
6	272.2	434.0	2387	N
7	276.8	432.1	2483	P
8	272.2	432.5	2463	P
9	271.3	432.4	2394	N

TABLE XXVIII

PERFORMANCE DATA
FOR 30-MM PROJECTILES

Penetrator alloy : U-1.84 wt% Mo
Heat treatment : Isothermal quench at 500°C,
Penetrator density 3 h, in lead
and hardness : 18.68 g/cm^3, 48.5 R_C
Target thickness
and hardness : 2.0 in., 278 BHN
Obliquity : 30°
PBL : 2550 ft/sec

Shot No.	Core Wt (grams)	Projectile Wt (grams)	Impact Velocity (ft/sec)	Result
1	271.9	433.8	3087	P
2	271.9	434.0	2542	P
3	272.2	434.0	2400	N
4	271.9	434.0	2406	N
5	272.1	433.4	2562	N
6	272.4	433.7	2486	N
7	272.5	433.9	2618	P
8	272.2	433.2	2548	P
9	271.9	433.6	2540	N

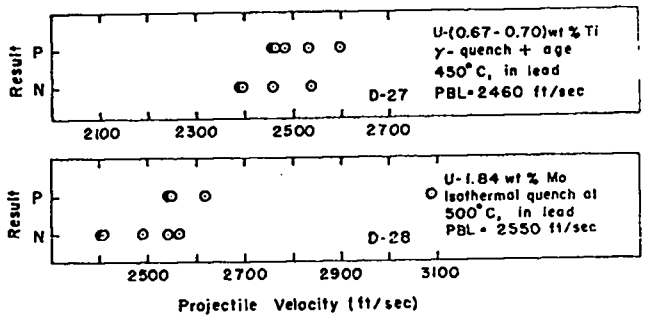

Figs. A-27-28. Ballistic-test results for 30-mm projectiles with uranium alloy cores striking 2-in.-thick armor at 30° obliquity.

TABLE XXIX

PERFORMANCE DATA
FOR 30-MM PROJECTILES

Penetrator alloy : U-(0.70-0.83) wt% Ti
Heat treatment : γ-quench + age 450°C, 4 h,
Penetrator density in lead
and hardness : 18.61 g/cm^3, 53 R_C
Target thickness
and hardness : 1.25 in., 304 BHN
Obliquity : 60°
PBL : 3033 ft/sec

Shot No.	Core Wt (grams)	Projectile Wt (grams)	Impact Velocity (ft/sec)	Result
1	270.9	432.4	3038	N
2	271.2	432.5	3121	P
3	271.2	432.8	3043	P
4	271.1	432.4	2969	N
5	271.2	432.7	2968	N
6	271.3	432.8	2935	N
7	271.3	432.6	2936	N
8	271.4	433.4	3077	P
9	271.6	433.3	3004	N
10	270.5	433.0	3118	P
11	270.9	432.9	3066	P
12	271.0	431.9	3099	P

UNCLASSIFIED

[redacted]

TABLE A-XXX

PERFORMANCE DATA
FOR 30-MM PROJECTILES

Penetrator alloy : U-1.84 wt% Mo
Heat treatment : Isothermal quench at 500°C, 3 h, in lead
Penetrator density and hardness : 18.68 g/cm^3, 48 R_C
Target thickness and hardness : 1.25 in., 304 BHN
Obliquity : 60°
PBL : 3074 ft/sec

Shot No.	Core Wt (grams)	Projectile Wt (grams)	Impact Velocity (ft/sec)	Result
1	272.2	433.6	3052	P
2	272.2	433.1	3134	N
3	272.2	433.8	3006	N
4	272.1	433.3	3093	N
5	272.2	433.7	3074	P
6	272.0	433.6	3088	P
7	271.6	433.0	3165	P
8	272.1	433.6	3279	P
9	272.2	434.3	3218	P
10	272.2	433.6	2918	N
11	272.0	433.7	3250	P
12	272.0	433.2	3236	P

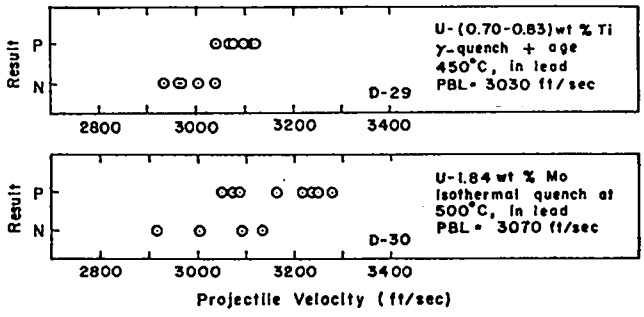

Figs. A-29-30. Ballistic-test results for 30-mm projectiles with uranium alloy cores striking 1-1/4-in.-thick armor at 60° obliquity.

APPENDIX B

CASTING AND FABRICATION OF URANIUM ALLOYS

I. CASTING

The vacuum melting and casting are done in furnaces designed and built at LASL. Figure B-1 is a schematic of the general furnace design.

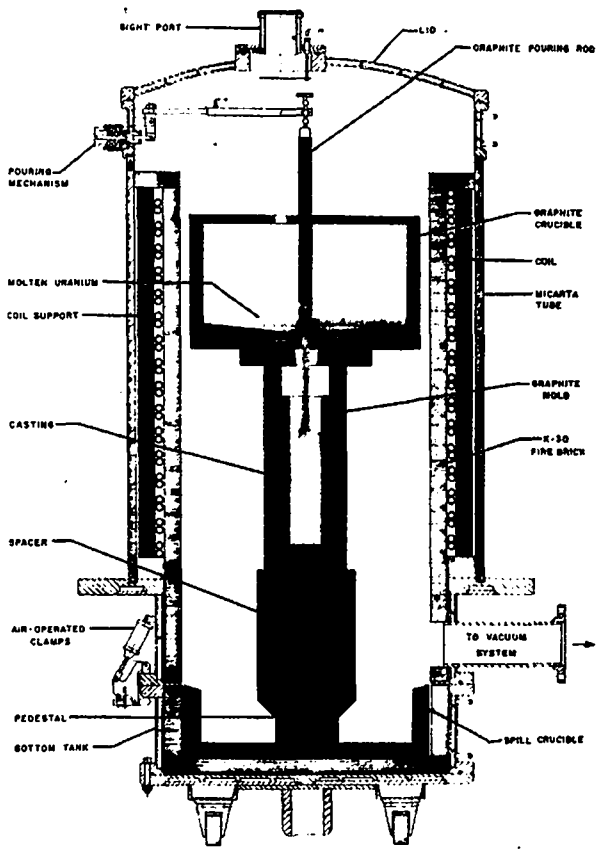

Fig. B-1. A uranium-alloy casting furnace.

The furnace can be divided essentially into four components: the top section, a steel tank that includes the furnace lid and side-pour mechanism; the center section, the Micarta tube containing the induction coil; the lower steel tank section whose upper flange rests on the furnace platform and supports the Micarta tube and top section; and the base plate which is the closure for the furnace bottom. Connections to the vacuum system are made through the lower tank section. A photograph of the furnace area, Fig. B-2, shows the operating platform from which the furnaces are suspended and where all furnace operations take place. The vacuum pumps and motor-generator power equipment are located in the basement area. The melting capacity of the furnaces shown on the platform in Fig. B-2 ranges from a few pounds in the small furnaces to over 4000 lb of uranium in the largest one.

We use the bottom-pour casting method in which the charge of metal is inductively heated in a crucible installed directly over the rod ingot mold. Before heating, the furnace is evacuated to a pressure of less than 50 μ of mercury. After the charge has been melted and outgassed and the desired casting temperature is reached, a graphite stopper rod is remotely lifted, allowing the charge to pour into the mold. Alloying takes place between the super-heat temperature (1350-1450°C) and the final pour temperature (1335-1350°C). The graphite mold is placed on a copper pedestal to ensure a temperature gradient between the bottom and top of the casting to provide proper directional solidification. Thermocouples placed in the mold 6.35 mm from each end record the mold temperature. The melt temperature is read through a sight glass in the top of the furnace using an optical pyrometer.

Certain alloying elements, such as titanium and niobium, are strong carbide formers and react with the carbon in the uranium, as well as with exposed carbon of the crucible. Most of the carbides formed have low densities and liquate in the melt or in the casting during solidification. Such behavior causes pronounced segregation of the alloying element. It is therefore necessary to apply a coating to the crucible or mold to inhibit

Fig. B-2. Uranium -casting facility at LASL.

metal-graphite reactions, thereby preventing carbon pickup in the uranium melt, and reducing the amount of alloying element lost through carbide reaction. For these castings, we used a combination molybdenum-zirconium oxide coating. The molybdenum in the form of 3.18-mm-diam wire is flame-sprayed onto the bare graphite surface of the crucible or mold to a thickness of ~0.13 mm, followed by an ~0.20-mm-thick coating of ZrO_2 in powder form. This process is repeated to give a double coat free of pinholes.

The starting material for casting the penetrator stock was high-purity uranium combined with master-alloy buttons. The high-purity uranium was obtained from the Y-12 plant of Union Carbide Nuclear Corporation. A typical impurity analysis of this material is given in Table B-I. The master-alloy buttons were prepared by arc melting or by co-precipitation in a bomb-reduction process. Nominal compositions of the master alloys were U-10 wt% Mo, U-4.5 wt% Ti, and U-6 wt% Nb, with typical impurity analyses being given in Tables B-II-B-IV.

The cast ingot is homogenized under vacuum (50-100 μ of Hg) at 950 to 1000°C for four hours after which two extrusion billets are machined from each casting. The initial hardness of each billet is measured, and samples are removed for chemical analysis. An as-cast ingot and a machined extrusion billet are shown in Fig. B-3. The effectiveness of the mold wash is reflected in the relatively clean surface finish of the casting. Figure B-4 is a schematic of a typical ingot indicating the relative position of the two extrusion billets and the regions from which the chemical-analysis samples were taken. Table B-V is a listing of all of the heats cast for this project, along with casting temperatures, hardnesses, and chemical analyses for most of the ingots.

II. EXTRUSION AND HEAT TREATMENT

To obtain rod stock of a diameter suitable for manufacturing the test projectile cores, we impact extruded all of the cast alloys before heat treating them. Extrusion also refines the grain structure and produces a material relative free of any internal defects that might affect performance.

TABLE B-I

TYPICAL CHEMICAL ANALYSIS OF UNALLOYED URANIUM

Impurity Elements	Concentration (ppm)
Cd	<0.1
B	<0.1
Be	<0.1
Li	<0.2
Ge	<1
Na	<1
Co	<1
V	<1
Pd	<1
Bi	<1
Ga	<1
Sb	<2
Cr	<2
Ba	<2
Mg	<2
Ca	<10
Mo	<10
Nb	<10
Sn	<10
Sr	<20
P	<100
W	<100
Ti	5
Mn	7
Cu	9
Ac	10
Ni	15
Al	20
Pb	21
Fe	30
C	80
Si	155

TABLE B-II

TYPICAL CHEMICAL ANALYSIS OF A U-10 WT% Mo MASTER-ALLOY BUTTON

Impurity Elements	Concentration (ppm)
Li	<0.5
Be	<3
B	<3
Na	<5
Al	<5
Mn	<5
Sn	<5
Pb	<5
Cd	<10
Cr	<25
V	<100
P	<200
Cu	4
Mg	10
Cr	25
Si	25
Ca	50
Fe	50
C	80

Extrusion is done in two steps, the first reducing the original billet diameter (Fig. B-3) from a nominal 10.2 cm to 5.1 cm. This corresponds to a 4 to 1 extrusion ratio (reduction in area) which is about the minimum required to produce a uniformly "worked" structure. All of the plane-wave impact and ultrasonic elastic-modulus tests were performed on samples taken from the 5.1-cm-diam stock, but for manufacture of the test AP cores, a second extrusion was required to reduce the stock to approximately 1.5 cm in diameter.

Extrusion was done using a Model 1800 Horizontal Dynapak machine manufactured by the General Dynamics Corporation. This is a high-energy-rate forming machine, shown schematically in Fig. B-5. The material is driven through the extrusion die by striking it with a heavy ram that is first accelerated to a velocity of up to 13.7 m/sec by the gas in chamber "A." The ram is initially retained in the cocked position by pressurizing chamber "B" to about 200 psi. As long as the seal at the back of the piston is unbroken, the area of the piston exposed to chamber "A" is small enough that the net force on the piston is directed backwards. To fire the machine, air pressure is directed into the annular region around the seal. This starts the motion of the ram, breaks the seal, and permits the full area of the piston to be exposed to the driving pressure. An important feature of the Dynapak machine is that the press frame and die assembly are not rigidly mounted, but are free to move back toward the accelerating ram in accordance with the law of conservation of momentum. The kinetic energy of both the ram and the press frame are then used to extrude the material through the die. Figure B-6

TABLE B-III

TYPICAL ANALYSIS OF A U-4.5 WT% Ti MASTER-ALLOY BUTTON

Impurity Elements	Concentration (ppm)
Li	<0.1
B	<0.2
Be	<0.5
Na	<1
Ag	<1
Cd	<1
Pb	<1
Bi	<1
Cr	<5
Sb	<5
Ba	<10
Sr	<40
Al	<50
P	<50
V	<50
Zn	<50
Cu	3
Mn	5
Sn	12
Si	15
Ca	15
Ni	25
Mo	50
C	50
Fe	70
Mg	200

TABLE B-IV

TYPICAL ANALYSIS OF A U-6 WT% Nb MASTER-ALLOY BUTTON

Impurity Elements	Concentration (ppm)
Li	<0.1
Be	<0.5
Bi	<1
Na	<1
Ag	<1
Cd	<1
B	<0.2
Sb	<5
Cr	<10
Zn	<25
Ba	<40
Al	<50
P	<50
V	<500
Mn	2
Sn	3
Cu	5
Pb	5
Ni	10
Si	40
Mg	40
Fe	80
C	110
Mo	300
Ca	500

shows the Dynapak installation, with the machine itself on the right and the operator console and heating controls on the left. The operator is isolated from the machine by two layers of bullet-proof glass to protect him against possible catastrophic tool failure.

The following simple formula can be used to approximate the pressure P required to drive the extrusion:

$$P = K \ln \frac{A_o}{A_1},$$

where A_o and A_1 are the initial and extruded cross-sectional areas of the material, and K is the so-called extrusion constant characteristic of the material and the temperature at which the extrusion is performed. All of the uranium alloys were extruded at 900°C which transforms them

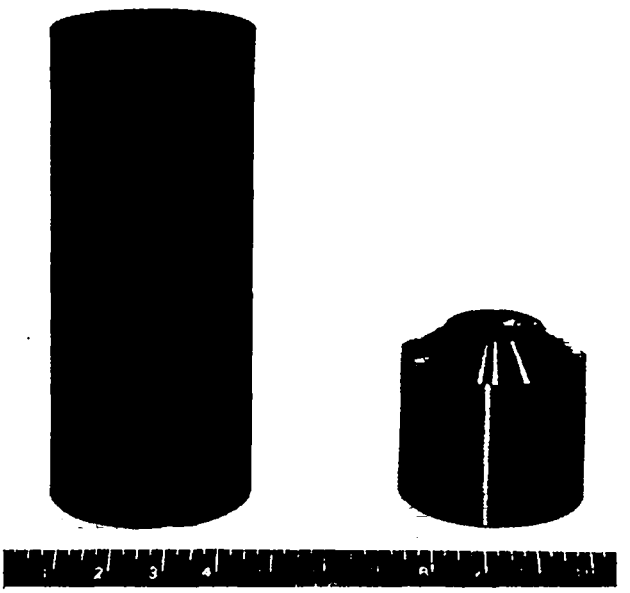

Fig. B-3. Typical uranium-Alloy casting and extrusion billet.

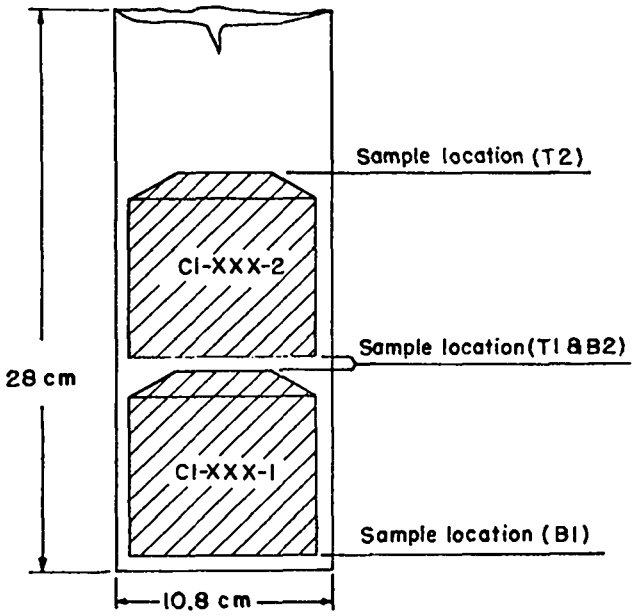

Fig. B-4. Schematic of a uranium-alloy casting indicating regions samples for chemical analysis and initial position of the extrusion billets.

into the softer bcc gamma phase. At this temperature, the extrusion constant, K, is about 20,000 psi.

The billet is initially heated by suspending it in a water-cooled induction coil. This is illustrated in Fig. B-7 which shows a billet positioned in the Dynapak ready for firing. The induction heating coil is wound from 9.5-mm-diam copper tubing and is destroyed on every shot. Billet temperature is determined using an optical pyrometer or thermocouple. A 5.1-cm-diam extrusion die and 10.2-cm-diam punch are shown in Fig. B-8. The die is made of H-11 tool steel, heat-treated to a hardness of 54 R_c, and the punch is made from an S-2 tool steel, triple tempered to 50-52 R_c. The lead-in surface of the die has a flame-sprayed coating of zirconium oxide for lubrication. Figure B-9 shows a 5.1-cm-diam extruded bar and a starting billet. The billet is coated with silver to prevent oxidation of the uranium during heating.

The alloys are heat treated before being machined into penetrator cores. All alloys were first solutionized for about one hour in the gamma phase at 850°C. This is done by heating the stock in a copper can inserted in a small muffle furnace. Dry argon gas is continuously flowed through the can to prevent rapid oxidation of the uranium. After solutionizing, the material is either quenched directly into water, or for the isothermal-quench treatment, transferred directly to a molten-lead pot at the desired aging temperature. The water-quenched material is reheated to the desired aging temperature (300-550°C) in either a vacuum furnace or a pot containing molten lead or salt.

Before final machining of the penetrator cores, the heat-treated stock is inspected for internal flaws that might affect penetrator performance. Both x-ray and ultrasonic examinations are performed on each piece of stock, and any regions with internal cracks or voids are discarded.

TABLE B-V

CHEMICAL ANALYSIS, HARDNESS AND CASTING TEMPERATURE OF URANIUM ALLOY CASTINGS

Nominal Composition (wt%)	Casting Item Number	Hardness Brinell 3000 kg Load	Hardness R_C	Chemical Analysis (wt%) at Indicated Location (B1)	(T1-B2)	(T2)	Carbon (ppm)	Mold Temp Top (°C)	Mold Temp Bottom (°C)	Super Heat Temp (°C)	Pour Temp (°C)
U-0.5% Ti	C1-498-1	285-277-285	25	0.63 Ti	0.62 Ti		40	915	815	1450	1350
	C1-498-2	285-285-285	26		0.62 Ti	0.62 Ti	40	915	815	1450	1350
U-0.75% Ti	C1-494-1	321-311-302	31	0.76 Ti	0.77 Ti		50	915	815	1450	1350
	C1-494-2	280-295-300	30		0.77 Ti	0.75 Ti	50	915	815	1450	1350
U-0.84% Ti	C1-493-1	341-311-302	34	0.86 Ti	0.83 Ti		70	915	815	1450	1350
	C1-493-2	352-331-321	36		0.83 Ti	0.83 Ti	70	915	815	1450	1350
U-1% Ti	C1-499-1	341-341-331	38	1.18 Ti	1.17 Ti		70	875	650	1450	1350
	C1-499-2	341-341-341	38		1.17 Ti	1.17 Ti	60	875	650	1450	1350
U-2% Mo	C1-496-1	277-269-269	28	2.04 Mo	2.03 Mo		120	825	700	1350	1335
	C1-496-2	285-277-285	30		2.03 Mo	2.04 Mo	140	825	700	1350	1335
U-2% Nb -1% Ti	C1-500-2	352-352-352	38	1.27 Nb 1.78 Ti	1.06 Nb 1.77 Ti		90	875	700	1450	1350
U-4.5% Nb	C1-497-1	363-375-363	39	4.59 Nb	4.71 Nb		180	915	815	1450	1350
U-0.75% Ti	C1-502-1	331-331-331	36	0.72 Ti	0.73 Ti		40	900	650	1450	1350
	C1-502-2	331-331-331	36		0.73 Ti	0.73 Ti	65	900	650	1450	1350
U-4.5% Nb	C1-503-1	363-363-363	39	4.57 Nb	4.72 Nb		190	900	700	1450	1450
	C1-503-2	363-363-363	39		4.72 Nb	4.76 Nb	200	900	700	1450	1450
U-0.75% Ti	C1-504-1	293-302-302	32	0.70 Ti	0.71 Ti		50	900	700	1450	1375
	C1-504-2	293-285-285	32		0.71 Ti	0.71 Ti	70	900	700	1450	1375
U-2% Mo	C1-506-1	269-269-269	28	1.90 Mo	1.95 Mo		180	800	600	1335	1335
	C1-506-2	269-262-269	28		1.95 Mo	1.98 Mo	170	800	600	1335	1335
U-2% Mo	C1-507-1	277-269-277	28	2.01 Mo	2.05 Mo		180	800	600	1335	1335
	C1-507-2	277-269-277	28		2.05 Mo	2.03 Mo	160	800	600	1335	1335
U-2% Nb -1% Ti	C1-508-1	388-388-388	41	2.52 Nb		2.54 Nb		925	775	1450	1450
	C1-508-2	388-388-388	41	1.27 Ti		1.28 Ti		925	775	1450	1450
U-4.5% Nb	C1-509-1	383-375-383	41	4.75 Nb	4.8 Nb			950	850	1450	1450
	C1-509-2	375-375-375	40		4.8 Nb	4.56 Nb		950	850	1450	1450
U-0.75% Ti	C1-510-1	293-293-293	31	0.78 Ti			50	900	675	1450	1375
	C1-510-2	293-293-293	31			0.73 Ti	50	900	675	1450	1375
U-0.75% Ti	C1-511-1	293-293-293	31	0.78 Ti			50	900	675	1450	1375
	C1-511-2	293-293-293	31			0.77 Ti	70	900	675	1450	1375
U-0.75% Ti	C1-512-1	293-293-285	31	0.84 Ti			40	900	675	1450	1375
	C1-512-2	293-293-293	31			0.82 Ti	20	900	675	1450	1375
U-0.75% Ti	C1-513-1	277-277-269	29	0.69 Ti	0.70 Ti			900	675	1450	1375
U-2% Mo	C1-514-1	262-255-255	25	2.05 Mo	2.02 Mo			850	650	1335	1335
	C1-514-2	255-255-255	25		2.02 Mo	2.04 Mo		850	650	1335	1335
U-2% Mo	C1-515-1	269-269-269	28	2.09 Mo	2.12 Mo			825	650	1335	1335
	C1-515-2	269-269-269	28		2.12 Mo	2.14 Mo		825	650	1335	1335
U-2% Mo	C1-516-1	262-262-262	26	1.81 Mo	1.85 Mo			825	650	1335	1335
	C1-516-2	269-269-262	27		1.85 Mo	1.86 Mo		825	650	1335	1335
U-2% Mo	C1-517-1	269-269-269	28	1.85 Mo	1.80 Mo			825	650	1335	1335
	C1-517-2	262-262-262	26		1.80 Mo	1.86 Mo		825	650	1335	1335
U-4.5% Nb	C1-518-1	375-375-375	40	5.11 Nb	5.2 Nb			950	750	1450	1450
	C1-518-2	375-375-375	40		5.2 Nb	5.17 Nb		950	750	1450	1450

TABLE B-V
(Continued)

Nominal Composition (wt%)	Casting Item Number	Hardness Brinell 3000 kg Load	Hardness R_C	Chemical Analysis (wt%) at Indicated Location (B1)	(T1-B2)	(T2)	Carbon (ppm)	Mold Temp Top (°C)	Mold Temp Bottom (°C)	Super Heat Temp (°C)	Pour Temp (°C)
U-4.5% Nb	C1-520-1	375-375-375	40					900	700	1450	1450
	C1-520-2	375-375-375	40					900	700	1450	1450
U-0.75% Ti	C1-519-1	285-277-277	30	0.70 Ti	0.70 Ti			900	700	1450	1375
	C1-519-2	293-277-293	30		0.70 Ti	0.69 Ti		900	700	1450	1375
U-2% Mo	C1-523-1	270-270-270	28	2.05 Mo	2.04 Mo		170	800	700	1335	1335
	C1-523-2	270-270-270	28		2.04 Mo	2.03 Mo	170	800	700	1335	1335
U-0.75% Ti	C1-526-1	269-277-277	29	0.61 Ti				900	700	1450	1375
	C1-526-2	269-269-269	28			0.62 Ti		900	700	1450	1375
U-0.75% Ti	C1-527-1	269-269-277	28	0.67 Ti				900	700	1450	1375
	C1-527-2	277-277-277	29			0.63 Ti		900	700	1450	1375
U-2% Mo	C1-528-1	269-269-269	28					800	700	1335	1335
	C1-528-2	269-269-269	28					800	700	1335	1335
U-0.75% Ti	C1-529-1							900	700	1450	1375
	C1-529-2							900	700	1450	1375

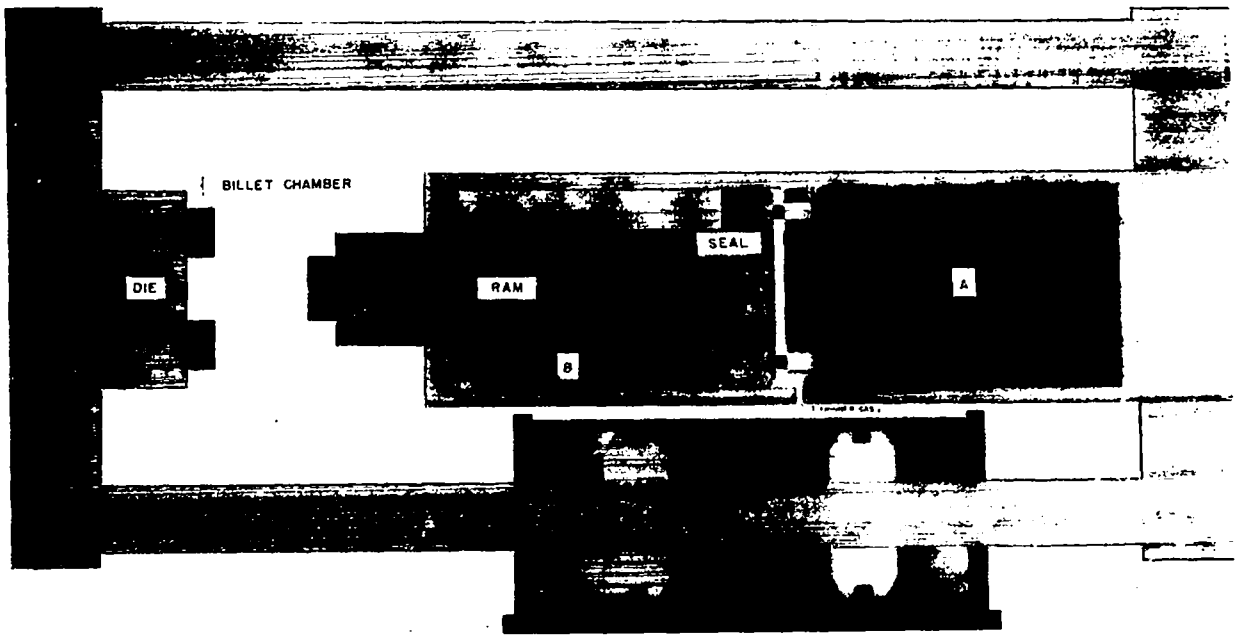

Fig. B-5. Schematic of the Dynapak extrusion machine.

Fig. B-6. Extrusion facility for uranium alloy stock.

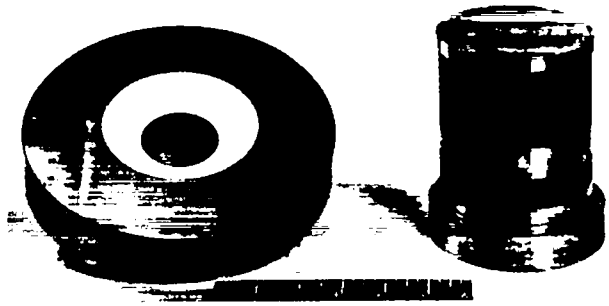

Fig. B-8. Typical punch and die used in extruding 5.08-cm-diam uranium-alloy stock.

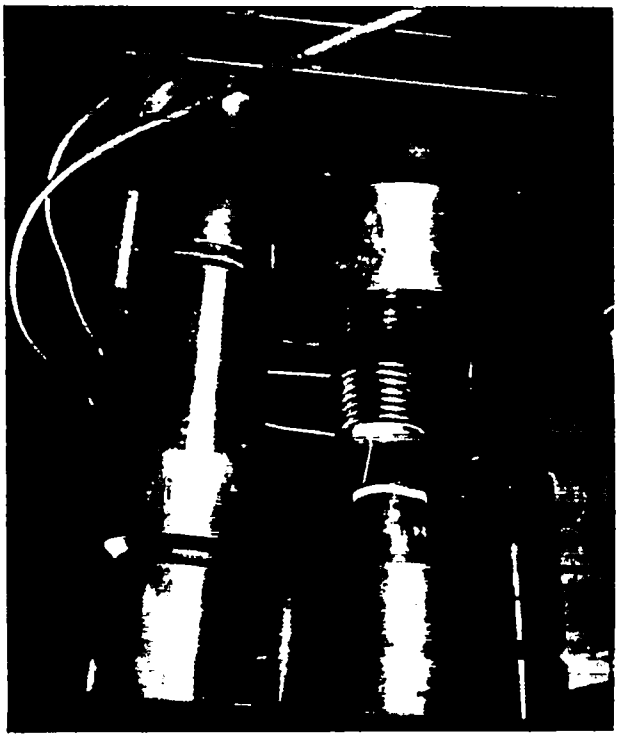

Fig. B-7. A uranium-alloy billet in the Dynapak extrusion machine ready for impact.

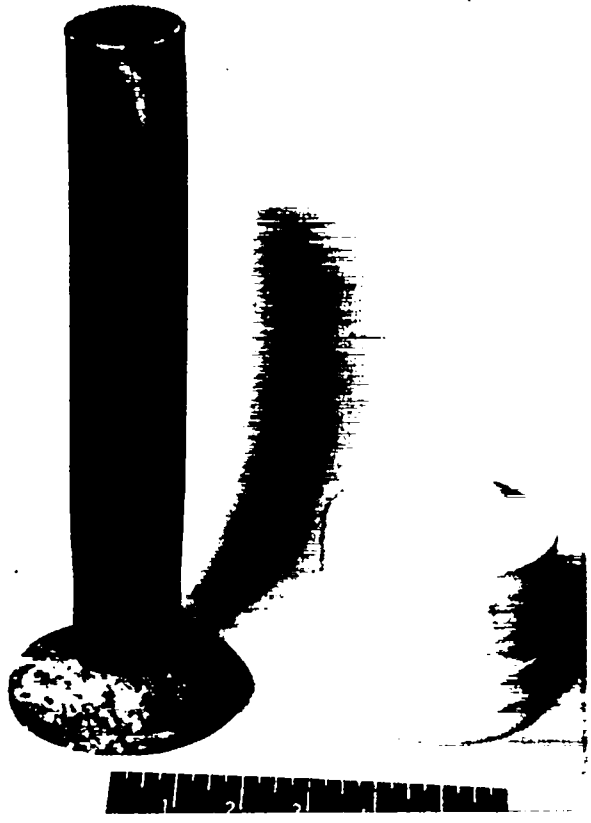

Fig. B-9. Silver-coated uranium-alloy extrusion billet and 5.08-cm-diam extruded bar.

APPENDIX C

PLANE-WAVE IMPACT TESTS AND SOUND-VELOCITY MEASUREMENTS

Since many materials have strongly rate-dependent mechanical properties, the standard parameters, such as modulus, quasistatic compressive and tensile strengths, and hardness, that characterize structural materials may be misleading when one is choosing materials for applications involving very high strain rates. Development of a material for use in AP penetrator cores is a case in point. For this reason, we substituted impact testing for the standard tensile-and compressive-strength measurements for most of the candidate alloys.

This test consisted of driving a plane stress wave into a 4.13-cm-diam by 0.95-cm-thick disk of the uranium alloy. The wave is generated by striking the sample with a 0.48-cm-thick copper disk launched from a 5.08-cm-diam smooth-bore gun. The experiment is illustrated schematically in Fig. C-1. The projectile is accelerated by compressed helium gas up to the impact velocity of 0.27 mm/μsec. A set of contact pins is used to determine both projectile velocity and tilt over the last 1.3 cm of travel. Tilt is usually no greater than 0.1°, and the velocity is reproducible to within a few percent.

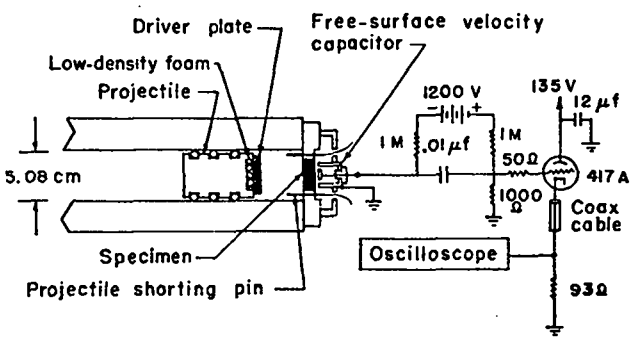

Fig. C-1. The gun, transducer and read-out circuit used in plane-wave impact tests.

When the stress wave reaches the free surface of the target, its amplitude can be determined by measuring the resulting free-surface velocity. This is done with a capacitive transducer developed by M. H. Rice[35] which consists of a shielded plate initially positioned about 1.5 mm from the surface. This plate is charged to 1200 V, and it forms a simple parallel-plate capacitor with the grounded surface of the sample. When the surface moves, the capacitance increases, and, since the charging voltage is held constant, the charge must also increase. This causes a current to flow and a voltage to be developed across the 1000-ohm load resistor in the read-out circuit (Fig. C-1). Neglecting transient effects, the output signal is given by the simple formula:

$$V(t) = E_o R_L \frac{dC}{dx} U_{fs}(t), \text{ where}$$

E_o = charging voltage

R_L = load resistance (1000 Ω)

$\frac{dC}{dx}$ = derivative of capacitance with respect to the surface displacement, x

U_{fs} = free-surface velocity.

The free-surface velocity and output signal have been written as explicit functions of time, t, to emphasize the fact that there will often be structure in the stress wave that produces a time-varying free-surface velocity. It is, in fact, necessary to resolve this structure to determine the dynamic compressive and tensile strengths for the sample. The capacitor signal is connected directly to a cathode-follower circuit used to drive a coaxial cable. This transmits the signal to the instrumentation bunker where it is recorded on several fast-rise oscillographs. Before the shot, the transducer capacitance is measured as a

function of displacement, x, using a General Radio capacitance bridge. These values are then used to translate the voltage vs time signal into a free-surface-velocity vs time curve.

Figure C-2 is a series of schematic diagrams of the compression and rarefaction waves propagating in the driver and target at various times after impact. The compression wave in the target has two components. The initial target compression is one-dimensional elastic, and it generates an elastic stress wave propagating at the material's longitudinal sound velocity. The amplitude of this wave is limited by the fact that one-dimensional strain develops large shear stresses along acute angles to the impact plane which finally cause the material to yield and flow plastically to a state of hydrostatic compression. The rest of the impact stress is thus propagated as a plastic wave whose velocity is governed by the bulk compressibility of the material. The amplitude of the elastic precursor is the Hugoniot elastic limit (HEL) for the material and is a measure of its high-strain-rate (10^4 to 10^5-cm/sec) compressive strength. The compression wave in the annealed copper driver is shown as a single plastic front because its elastic limit is too low to produce a significant precursor.

When the compression waves reach the free surface of the driver and target, they are reflected as rarefactions. The driver thickness is chosen so that the rarefactions meet in the target. This produces tension which, if it is larger than the dynamic tensile strength, spalls a layer of the target. A tension wave is generated which, in turn, decreases the free-surface velocity by an amount proportional to the spall strength. This is illustrated in the last two diagrams of Fig. C-2.

The stress associated with a wave whose shape is constant in time is given by one of the Rankine-Hugoniot relations[36] as

$$\sigma = \rho u_s u_p$$

where

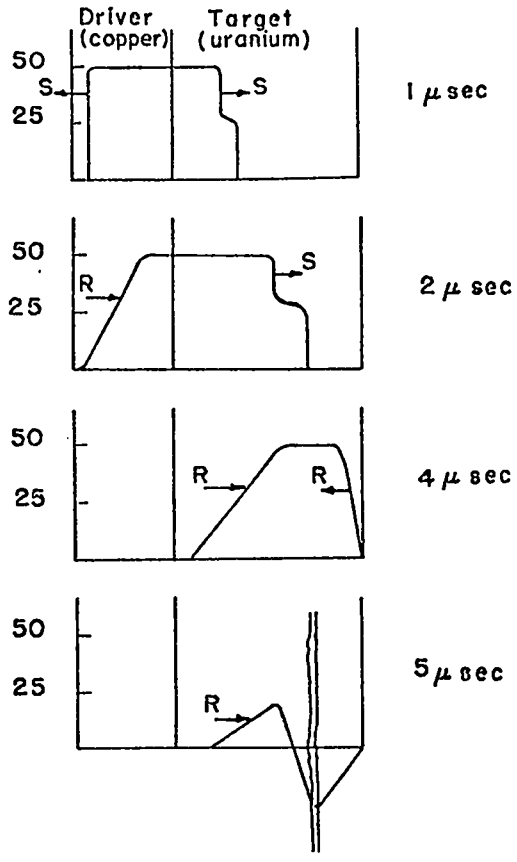

Fig. C-2. Stress vs position of the waves generated in target and driver by the impact tests. Stress is measured in kilobars along the vertical axis, and the horizontal axis indicates position in the sample. The approximate time after impact is indicated, and compression and rarefaction waves are labeled S and R respectively.

ρ = initial density

u_s = wave-propagation velocity

u_p = particle or material velocity produced by the wave.

For these materials, the free-surface velocity U_{fs} is well approximated by

$$U_{fs} = 2\, u_p.$$

Using this relation and taking the propagation velocity of the elastic precursor and the tensile wave to be the longitudinal sound speed C_ℓ,

one can use the measured free-surface velocity to calculate both the HEL and the spall strength:

$$\sigma_{HEL} = 1/2\ \rho\ C_\ell U_{fs\ (HEL)}$$

$$\sigma_{SPALL} = 1/2\ \rho\ C_\ell \Delta U_{fs\ (SPALL)}$$

where $U_{fs\ (HEL)}$ is the free-surface velocity produced by the elastic wave, and $\Delta U_{fs\ (SPALL)}$ is the decrease in free-surface velocity produced by the tension wave.

A representative set of free-surface velocity vs time curves for some of the candidate uranium alloys is shown in Figs. C-3 through C-14.

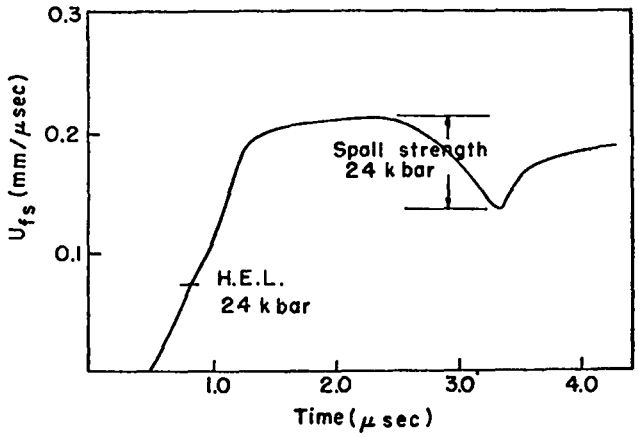

Fig. C-3. Free-surface velocity vs time profile for a U-0.83 wt% Ti sample.

γ-quench + aged 450°C, 4 h, in vac.

The complete results from all of the impact tests are included in Table C-I. As the figures show, the HEL is calculated from the value of U_{fs} at the "knee" of the elastic wave. However, for many of the samples, especially those that had been over aged, the two-wave structure is not well defined. Also, the wave front may not be completely stabilized after traversing the 0.95 cm-thick sample, so the results are uncertain by at least 10%. Even so, all the samples were tested under the same conditions, and the relative performance of the alloys is reasonably reliable.

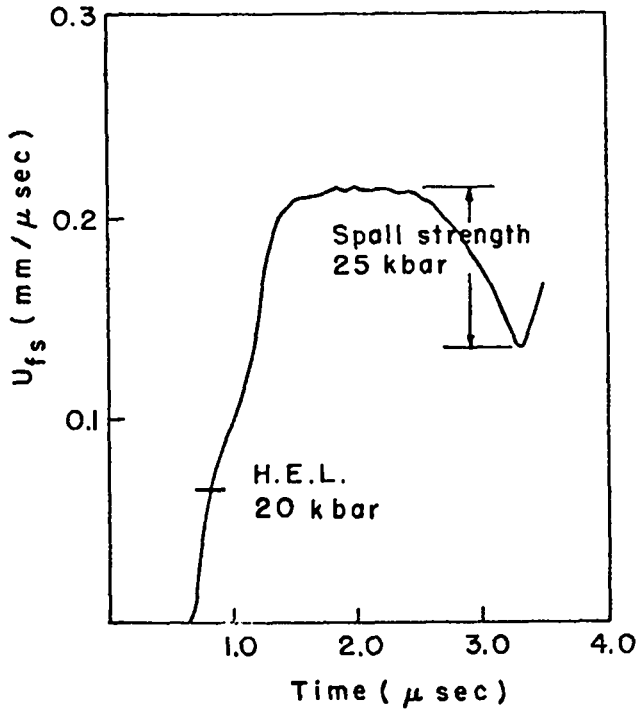

Fig. C-4. Free-surface velocity vs time profile for a U-0.84 wt% Ti sample.

γ-quench + aged 450°C, 4 h, in lead.

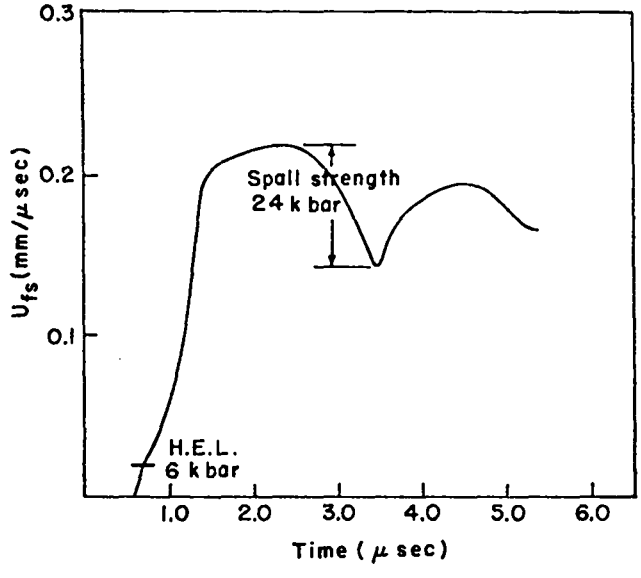

Fig. C-5. Free-surface velocity vs time profile for a U-0.77 wt% Ti sample.

γ-quench + aged 550°C, 4 h, in vac.

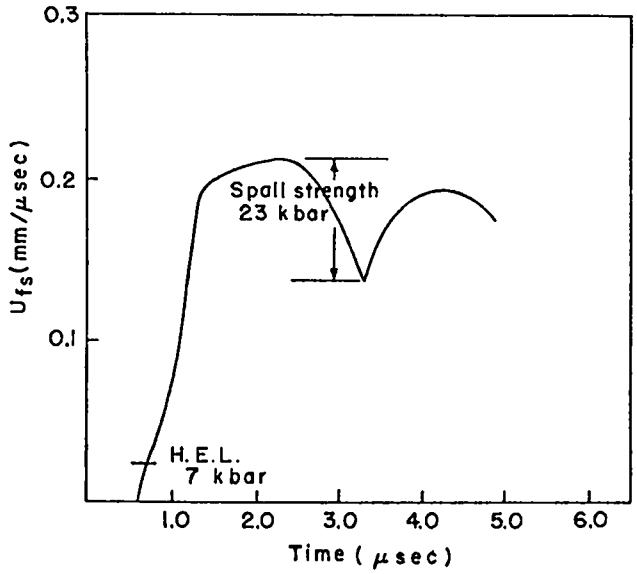

Fig. C-6. Free-surface velocity vs time profile for a U-0.77 wt% Ti sample.

Isothermal quench, 550°C, 3 h, in lead.

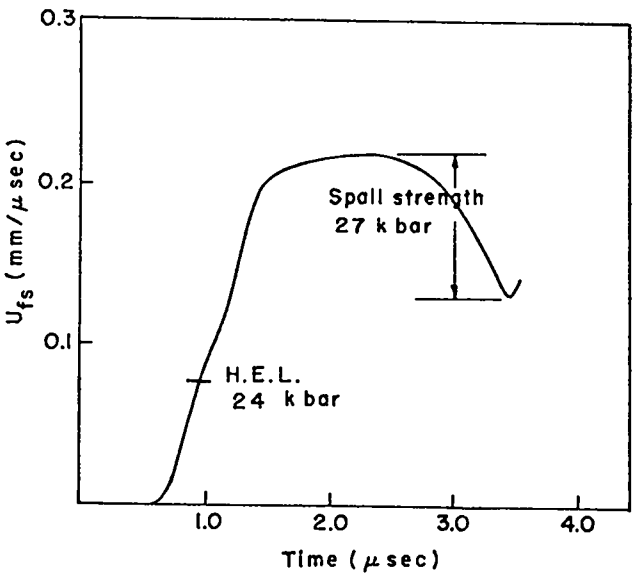

Fig. C-7. Free-surface velocity vs time profile for a U-0.62 wt% Ti sample.

γ-quench + aged 450°C, 4 h, in vac.

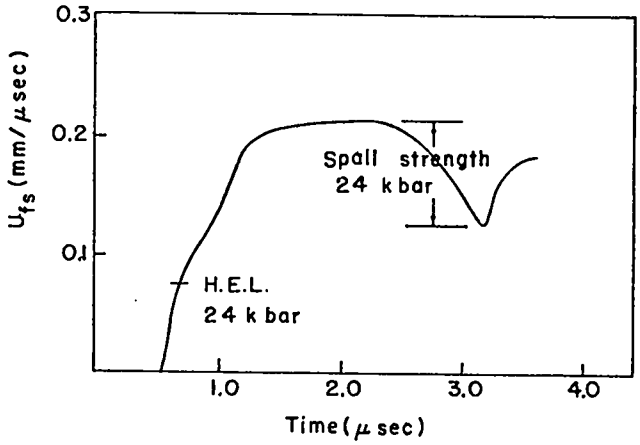

Fig. C-8. Free-surface velocity vs time profile for a U-1.18 wt% Ti sample.

γ-quench + aged 450°C, 4 h, in vac.

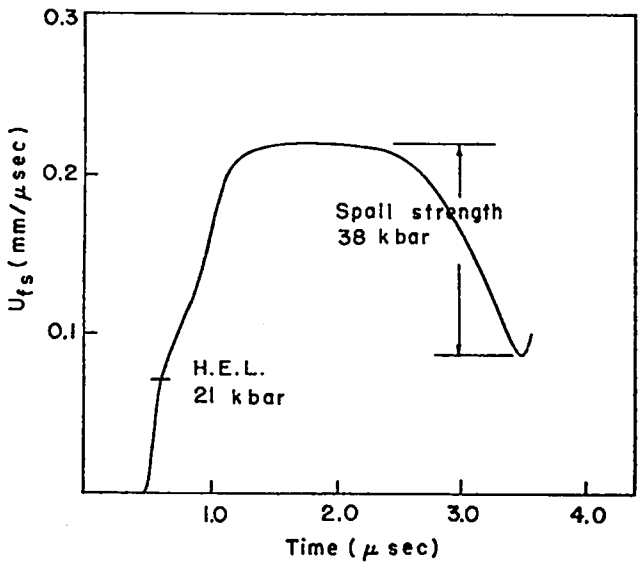

Fig. C-9. Free-surface velocity vs time profile for a U-2.04 wt% Mo sample.

γ-quench + aged 300°C, 4 h, in vac.

UNCLASSIFIED

[redacted]

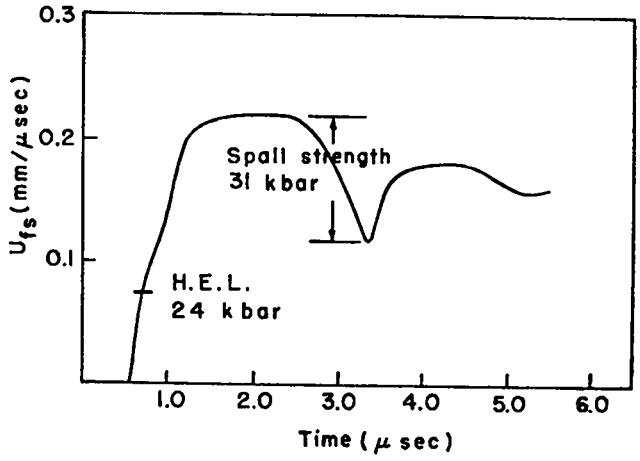

Fig. C-10. Free-surface velocity vs time profile for a U-2.04 wt% Mo sample.

γ-quench + aged 500°C, 4 h, in vac.

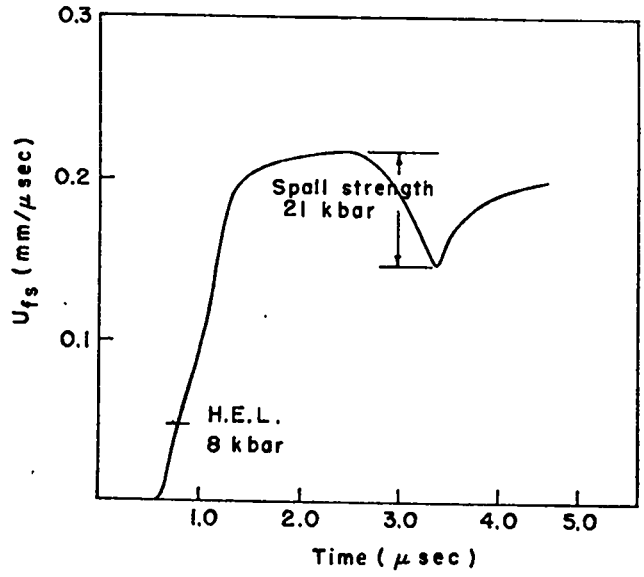

Fig. C-12. Free-surface velocity vs time profile for a U-4.65 wt% Nb sample.

γ-quench + aged 500°C, 4 h, in vac.

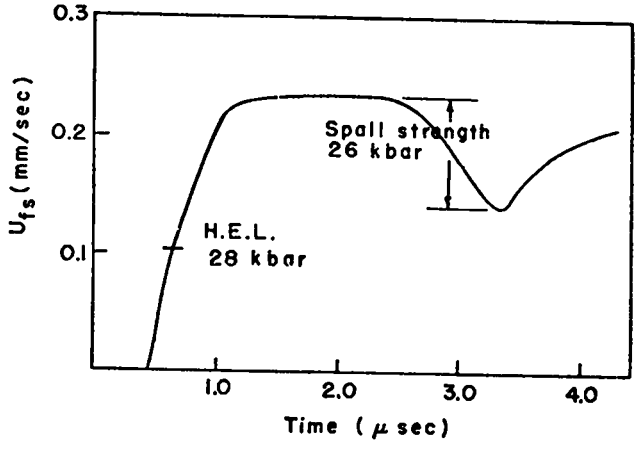

Fig. C-11. Free-surface velocity vs time profile for a U-4.65 wt% Nb sample.

γ-quench + aged 300°C, 4 h, in vac.

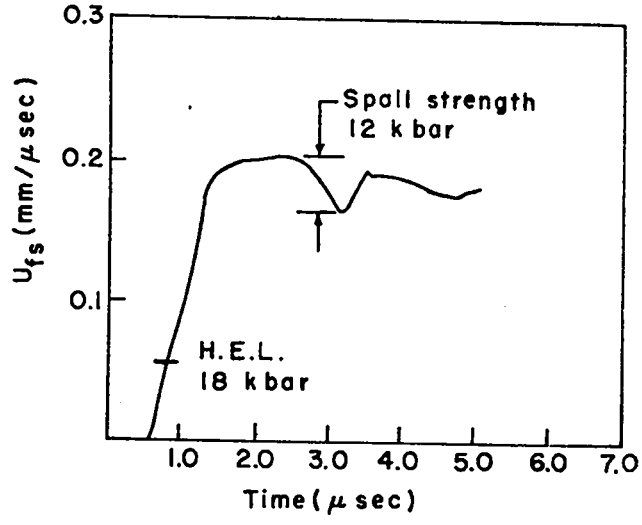

Fig. C-13. Free-surface velocity vs time profile for a U-2.53 wt% Nb-1.28 wt% Ti sample.

γ-quench + aged 450°C, 4 h, in vac.

[redacted]

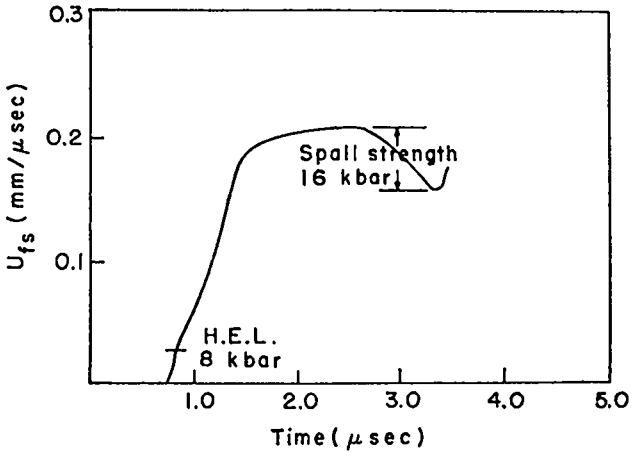

Fig. C-14. Free-surface velocity vs time profile for a U-2.53 wt% Nb-1.28 wt% Ti sample.

γ-quench + aged 550°C, 4 h, in vac.

The longitudinal sound velocity, C_ℓ, used in calculating the HEL and spall strength was measured ultrasonically using a pulse-superposition technique.[37] The samples were identical to those used in the impact tests, in that they were taken from the same piece of alloy stock and all were heat-treated together. The shear-wave velocity was also measured, and the results, along with calculated values of Young's modulus and the shear modulus, are shown in Table C-I.

TABLE C-I

PLANE-WAVE IMPACT AND ULTRASONIC DATA FOR URANIUM ALLOYS

Heat Treatment	Hardness (R_C)	Density (g/cm^3)	Longitudinal Sound Vel. (mm/μsec)	Shear Velocity (mm/μsec)	Shear Modulus (10^6 psi)	Young's Modulus (10^6 psi)	Hugoniot Elastic Limit (kbar)	Spall Strength (kbar)
				U-0.84 wt% Ti				
γ-quench + age, 550°C, 4 h, in salt	39.9	18.52	3.45	2.11	12.0	28.7	5	22
				U-1.17 wt% Ti				
γ-quench + age, 450°C, 4 h, in vac.	53.6	18.36	3.43	2.08	11.5	27.9	24	24
γ-quench + age, 550°C, 4 h, in vac.	42.5	18.36	3.47	2.13	12.1	28.9	7	24
Isothermal quench, 500°C, 3 h, in Pb	49.8	18.34	3.43	2.08	11.5	27.8	8	23

TABLE C-1

(Continued)

Heat Treatment	Hardness (R_C)	Density (g/cm^3)	Longitudinal Sound Vel. (mm/μsec)	Shear Velocity (mm/μsec)	Shear Modulus (10^6 psi)	Young's Modulus (10^6 psi)	Hugoniot Elastic Limit (kbar)	Spall Strength (kbar)
			U-2.04 wt% Mo					
γ-quench + age, 300°C, 4 h, in vac.	45.8	18.51	3.19	1.74	8.1	20.9	21	38
Isothermal quench, 500°C, 3 h, in Pb	53.0	18.59	3.33	1.93	10.0	25.0	24	37
γ-quench + age, 450°C, 4 h, in Pb	45.8	18.60	3.20	1.96	10.4	24.9	11	21
γ-quench + age, 550°C, 4 h, in salt	32.0	18.57	3.29	1.94	10.1	25.0	6	23
			U-4.65 wt% Nb					
γ-quench + age, 300°C, 4 h, in vac.	47.6	17.68	3.13	1.69	7.3	19.0	28	26
γ-quench + age, 500°C, 4 h, in vac.	45.6	17.86	3.42	1.98	10.1	25.3	8	21
			U-1.18 wt% Nb-1.81 wt% Ti					
γ-quench + age, 450°C, 4 h, in vac.	53.9	17.90	3.46	2.08	11.2	27.3	19	19
γ-quench + age, 550°C, 4 h, in vac.	50.7	17.92	3.48	2.10	11.5	27.8	10	21
Isothermal quench, 500°C, 3 h, in Pb	58.0	17.88	3.41	2.04	10.8	26.4	-	-
			U-2.53 wt% Nb-1.28 wt% Ti					
γ-quench + age, 450°C, 4 h, in vac.	51.2	17.96	3.46	1.97	10.1	25.5	18	12
γ-quench + age, 550°C, 4 h, in vac.	48.9	17.95	3.51	2.12	11.7	28.4	8	16

[redacted]

TABLE C-1

(Continued)

Heat Treatment	Hardness (R_C)	Density (g/cm^3)	Longitudinal Sound Vel. (mm/μsec)	Shear Velocity (mm/μsec)	Shear Modulus (10^6 psi)	Young's Modulus (10^6 psi)	Hugoniot Elastic Limit (kbar)	Spall Strength (kbar)
				U-0.62 wt% Ti				
γ-quench + age, 450°C, 4 h, in vac.	51.2	18.70	3.40	2.05	11.4	27.6	24	27
γ-quench + age, 550°C, 4 h, in vac.	43.3	18.70	3.43	2.09	11.8	28.5	5	24
Isothermal quench, 500°C, 3 h, in Pb	50.0	18.70	3.42	2.07	11.6	28.0	5	26
γ-quench + age, 450°C, 4 h, in Pb	51.7	18.63	3.41	2.05	11.4	27.6	-	-
γ-quench + age, 550°C, 4 h, in salt	40.0	18.64	3.43	2.09	11.8	28.4	5	22
				U-0.75 wt% Ti				
γ-quench + age, 450°C, 4 h, in vac.	46.2	18.62	3.42	2.09	11.8	28.4	-	22.8
				U-0.77 wt% Ti				
γ-quench + age, 550°C, 4 h, in vac.	41.0	18.57	3.44	2.11	12.0	28.7	6	24
Isothermal quench, 500°C, 3 h, in Pb	49.1	18.49	3.43	2.08	11.6	28.0	7	23
				U-0.83 wt% Ti				
γ-quench only	40.4	18.46	3.32	1.96	10.3	25.3	9	36
γ-quench + age, 550°C, 4 h, in vac.	38.8	18.51	3.45	2.11	12.0	28.7	5	25
Isothermal quench, 500°C, 3 h, in Pb	50.8	18.61	3.43	2.08	11.7	28.2	9	22
γ-quench + age, 450°C, 4 h, in Pb	54.5	18.49	3.41	2.06	11.4	27.6	20	25

[redacted]

REFERENCES

1. M. M. Rottenberg, W. O. Davis, and R. G. Wishart, "Advancement of Uranium Penetrator Technology," Air Force Armament Laboratory report TR-TI-63 (June 1971).

2. H. P. Tardif, "A Study of Polynary U-Mo-Nb-V Alloys," Canadian Armament and Development Establishment, Carde 558/66 Project B105-10-19-11 (August 1966).

3. A. G. Harding and M. B. Waldron, "Transformations in Uranium Alloys with High Solute Solubility in the B. C. C. Gamma Phase. Part I - Preliminary Observations on the "Banded Structures" Produced by Non Equilibrium Transformations in Uranium Alloys," UKAEA Research Group, Atomic Energy Research Establishment report AERE M/R 2673 NPCC/FEWP/211 (September 1958).

4. A. G. Harding, M. B. Waldron, and C. Knight, "Transformation in Uranium Alloys with High Solute Solubility in the B. C. C. Gamma Phase. Part II - Transformation in Uranium Alloys of 5 at%, 10 at%, 15 at% and 20 at% Titanium on Quenching from the Gamma Phase," UKAEA Research Group, Atomic Energy Research Establishment report AERE M/R 2673A (December 1958).

5. "Uranium Alloys for Critical Ordnance Components," Watertown Arsenal Laboratories, Proceedings of a Conference Published as Watertown Arsenal Monograph Series AD 609896, June, 1960.

6. E. G. Zukas, "Transformation Kinetics and Mechanical Properties of 0.5 and 1.0 wt% Molybdenum-Uranium Alloys," The Second Nuclear Engineering and Science Conference, Mar. 11-14, 1957, Philadelphia, Pa. Published by ASME.

7. M. W. Burkart, I. Cohen, and R. K. McGeary, "The Corrosion of Uranium-Molybdenum Alloys in High-Temperature Water," The Second Nuclear Engineering and Science Conference, Mar. 11-14, 1957, Philadelphia, Pa. Published by ASME.

8. R. F. Hills, B. R. Butcher, and B. W. Howlett, "The Mechanical Properties of Quenched Uranium-Molybdenum Alloys. Part I: Tensile Tests on Polycrystalline Specimens," Nucl. Mater. 11, 2 (1964).

9. B. R. Butcher and B. A. Hatt, "The Mechanical Properties of Quenched Uranium-Molybdenum Alloys. Part II: A Preliminary Survey of the Deformation Mechaisms," Nucl. Mater. 11, 2 (1964).

10. R. V. London and R. E. Edelman, "Chill Effect on Cast Uranium-8.5 % Molybdenum Plates," Modern Castings, pp 233-237 (1964).

11. H. P. Tardif, "The Heat Treatability and Properties of Uranium Alloys," Trans. Inst. Mining Met. 68, p. 1167 (1965).

12. H. M. Skelly, C. F. Dixon, and N. S. Spence, "Uranium Alloy Development for Non-Nuclear Applications," Dept. of Mines and Technical Surveys, Ottawa, Mines Branch Investigation report IR65-75 (September 1965).

13 H. A. Saller, F. A. Rough, and A. A. Bauer, "Heat Treatment and Properties of the Uranium-5 wt% Zirconium Alloy," Battelle Memorial Institute report BMI-915 (May 1954).

14. R. D. Bland, J. E. McDonald, and D. M. Mattox, "Ion Plated Coatings for the Corrosion Protection of Uranium," Sandia Laboratories, Albuquerque report SC-DR-65-519 (October 1965).

15. K. G. Hage, "Some Mechanical Properties of Uranium-10 wt% Molybdenum Alloy Under Dynamic Tension Loads," Lawrence Livermore Laboratory report UCRL-12357 Rev. I (February 1965).

16. Jacob Greenspan and F. J. Rizzitano, "Development of a Structural Uranium Alloy," Materials Engineering Division, U. S. Army Materials Research Agency report AMRA TR-64-28 AD609554 (September 1964).

17. M. B. Waldron, R. C. Burnett, and S. F. Pugh, "The Mechanical Properties of Uranium-Molybdenum Alloys," UK AEA Research Group, Atomic Energy Research Establishment report AERE-M/R 2554.

18. E. G. Zukas, "Properties of As-Cast and Heat-Treated 2 wt% Molybdenum-Uranium," Trans. ASM 50, p. 752 (1959).

19. D. J. Murphy, "Some Properties of Uranium-Low Titanium Alloys," Am. Soc. Metals 50, 884-900 (1958).

20. R. J. Jackson and D. V. Niley, "Tensile Properties of Gamma Quenched and Aged Uranium-Base Niobium Alloys," Trans. ASM 61, p 336 (1968).

21. G. DuPont and A. Dube, "Study of the Mechanism of Tempering of a Quenched U-2Mo Alloy," Defense Research Establishment Valcartier (Canada), 1970. Project D97-01-19, AD-880241.

22. G. J. Irwin and W. H. Erickson, "The Effect of Heat-Treatment on the Mechanical Properties of U-2Mo and U-1Mo-.7Nb-.7Zr," Defense Research Establishment Valcartier (Canada), September 1970 Project D97-01-19, AD-880242.

23. Y-12 Plant Technical Data Sheets, Union Carbide, Oak Ridge, Tennessee.
No. 2.2.1 Uranium-10% Mo Alloy
No. 2.2.4 Uranium-1/2% W Alloy
No. 2.2.7 Uranium-Zirconium Alloys
No. 2.2.9 Uranium-Low Titanium Alloys
No. 2.2.10 Uranium-2% Mo Alloy
No. 2.2.11 Cast Uranium-2 to 4% Mo Alloys.

24. G. E. Jaynes, J. M. Taub, and D. T. Doll, "Development of Casting Techniques for Uranium and Uranium Alloys," Trans. AIME, Vol. IV, p. 1 (1957).

25. D. J. Sandstrom, "Some Mechanical and Physical Properties of Heat Treated Alloys of Uranium With Small Additions of Ti or Mo," Los Alamos Scientific Laboratory report LA-4781 (1971).

26. D. J. Sandstrom, R. E. Seegmiller, G. E. Jaynes, R. W. Keil, G. S. Hanks, and J. M. Taub, "Uranium Alloy Development at Los Alamos," Los Alamos Scientific Laboratory report LA-DC-11478 (1970).

27. W. C. Erickson, G. E. Jaynes, D. J. Sandstrom, R. E. Seegmiller, and J. M. Taub, "Evaluation of Uranium Alloys," Los Alamos Scientific Laboratory report LA-5002 (September 1972).

28. F. A. Rough and A. A. Bauer, "Constitution of Uranium and Thorium Alloys," Battelle Memorial Institute report BMI-1300 (June 1958).

29. M. Ammons, Y-12 Plant-UCC, personal communication, June, 1972.

30. G. S. Hanks, J. M. Taub, and D. T. Doll, "Effect of Annealing Media On the Mechanical Properties of Uranium," Los Alamos Scientific Laboratory report LA-1619 (August 1953).

31. K. Eckelmeyer and F. Zanner, Sandia Laboratories, Albuquerque, personal communication, May, 1972.

32. J. F. Heyda, S. R. Woodall, D. A. Wolfgang, and L. L. Wilson, "A Combined Theoretical and Experimental Investigation of Armor Penetration Mechanics," Air Force Armament Laboratory report AFATL-TR-70-78 (August 1970).

33. S. R. Woodall, J. F. Heyda, H. J. Galbraith, and L. L. Wilson, "Ballistic Impact Mechanics of Selected Metallic and Composite Materials," Air Force Armament Laboratory report AFATL-TR-70-112 (November 1970).

34. R. T. Sedgwick and L. J. Hagerman, "Numerical, Analytical and Experimental Investigation of Penetration by Kinetic Energy Projectiles," Air Force Armament Laboratory report AFATL-TR-72-48 (March 1972).

35. M. H. Rice, "Capacitor Technique for Measuring the Velocity of a Plane Conducting Surface," Rev. Sci. Inst. 32, 449 (1961).

36. M. H. Rice, J. M. Walsh, and R. G. McQueen, "Compression of Solids by Strong Shock Waves," in Solid State Physics, F. Seitz and D. Turnbull, Eds. (Academic Press, Inc., New York, 1958), Vol. VI.

37. J. Williams and J. Lamb, "On the Measurement of Ultrasonic Velocity in Solids," J. Acoust. Soc. Am., 30, 308 (1958).

UNCLASSIFIED

KT:150

 0000 0000 1143 1421